UNIVERSITÉ DE GRENOBLE

THÈSE

Pour obtenir le grade de

DOCTEUR DE L'UNIVERSITÉ DE GRENOBLE

Spécialité : **Chimie Physique Moléculaire et Structurale**

Arrêté ministériel : 7 août 2006

Présentée par

« Sudarsan TAMANG »

Thèse dirigée par **« Dr. Peter REISS »** et
codirigée par **« Dr. Isabelle TEXIER-NOGUES »**

préparée au sein du **Laboratoire d'Electronique Moléculaire, Oraganique et Hybride, CEA, Grenoble.**
dans **l'École Doctorale Chimie et et Sciences du Vivant, de l'Université Joseph Fourier, Grenoble, France**

Synthèse et fonctionalisation des nanocristaux émettant dans le proche infrarouge pour l'imagerie biologique

Thèse soutenue publiquement le **« 24 juin 2011 »**,
devant le jury composé de :

Prof. Valerie MARCHI-ARZNER
Directeur de rechercher, Université de Rennes (Rapporteur)
Dr. Benoit, DUBERTRET
Chargé de rechercher, ESPCI Paris (Rapporteur)
Prof. Pierre LABBE
Professeur, Université Joseph Fourier Grenoble (Président)
Prof. Adam PRON
Professeur, Université Joseph Fourier Grenoble, (Examinateur)
Dr. Fabien DELPECH
Maitre de conférence, INSA Toulouse (Examinateur)
Dr. Peter REISS
Chercher, CEA Grenoble (Directeur de thèse)
Dr. Isabelle TEXIER-NOGUES
Chercher, CEA Grenoble, (invitée)

Acknowledgement

Foremost, I would like to sincerely acknowledge Dr. Peter Reiss for supervising my PhD thesis for last three years-with patience, professionalism and at times even steadfastness. I have benefited a lot from his leadership quality, composed nature and sound knowledge of chemistry and nanoscience. Moreover, this manuscript in its final form would not have been possible without meticulous corrections and valuable suggestions from him. Dr. IsabelleTexier-Nogues has also been welcoming and supportive to me. I thank her for extending support to me in capacity of a co-supervisor as and when needed.

My deepest sense of gratitude to Angela, Antoine, Elsa, Chiara, Aurélie, Cécile, Grégory, Lucia, Anastasia, Thuy, Emanuela, Fleur, Axel and all other current as well as past members of our group at CEA for their support and love. I could not have wished for more congenial and healthy working environment than one I witnessed in the laboratory during my tenure from July 2008 to June 2011. I have been moved by the warmth my colleagues have bestowed upon me all these years. I will always be thankful to Antoine and Angela for their invaluable help when my days had been inundated with thesis related stuffs and had also to cope up with the chaos of moving back to India.

A project as interdisciplinary as this could not have been possible without a team work. Therefore, I would like to acknowledge collaborators Dr. Marco Giardiello, Dr. Graeme Stasiuk, Dr. Daniel Imbert and Dr. Marinella Mazzanti from SCIB/CEA; Dr. Cathy Poillot and Dr. Michael De Waard from Grenoble Institute of Neuroscience; and Dr. Samuel Clarke and Dr. Maxime Dahan from Laboratory Kastler Brossel (ENS Paris). Dr. Liang Li and Dr. Toufic Jean Daou are sincerely acknowledged for setting up a strong foundation for the project initially.

Thanks and appreciation to the people in the administration at CEA and University of Joseph Fourier for their support. Christian Lombard and Yann Kervella are thanked for their assistance with various types of laboratory related works.

I would like to thank Dr. Stéphanie Pouget for help with XRD, Dr. Julien Gravier for DLS measurements. Prof Adam Pron and other researchers of LEMOH are sincerely acknowledged for helping me at various times.

I also take this opportunity to thank some of the individuals who I have helped me to shape my life during formative years and other pre-PhD engagements. All the teachers who taught me at Rangli Primary School, Griffith's High School, St. Robert's Higher Secondary School, St. Joseph's College

Darjeeling and North Bengal University are sincerely acknowledged for helping me built a decent academic foundation needed for the PhD journey. I thank Dr. B.LV Prasad for his help and support during my tenure as a junior research fellow at National Chemical laboratory, Pune. I also thank Prof Mathias Brust for extending help during my short visit at University of Liverpool, UK.

Finally, I express heartfelt thanks to my parents for instilling in me positive values and right spirit to live. And big big thanks to my wife, Tshering for her love and support. Without her by my side, journey to PhD would have been perhaps akin to climbing a greased pole.

Table of contents

Chapter I

General Introduction & Motivation

1.1 Background

Semiconductor materials are at the core of modern civilisation. They can be found in most electronic devices, being the constituents of transistors, light emitting diodes, solar cells and so on. The earliest days of semiconductor research date back to 1833 when Michael Faraday published his observation on the electrical conduction by silver sulfide (Ag_2S) [1]. The latter part of the 19^{th} century and early years of 20^{th} century saw a sedate, yet relentless progress in the field. And then the invention of the transistor in 1947 set up a precedent which led to a technological revolution. Research on semiconductor nanocrystals was triggered in the early 1980s when Alexei Ekimov observed size dependent optical properties of CdS particles in a glass matrix and Louis Brus in *colloidal* CdS [2]. Initially there was scepticism on whether these materials chemically synthesised in flask could ever compete or even complement with what was being produced by physical techniques in vacuum chambers. But with the advent of high quality synthetic schemes over last two decades [3-8], colloidal semiconductor nanocrystals are being investigated to foster their use in various technologically and economically important fields such as photovoltaics, solid state lighting, biological labeling, etc.

1.2 Colloidal semiconductor nanocrystals: quantum dots

1.2.1 Definition

Colloidal semiconductor nanocrystals (NCs) also known as quantum dots (QD) [9] are crystalline particles of a diameter typically ranging from 1 to 10 nm. Due to their small size which approaches molecular dimensions they have discrete electronic energy levels and size-dependent optical and electrical properties. They are chemically synthesized in form of colloids by restricting the growth of the crystal at an early stage. Usually organic surfactants or ligands are used to stabilize the NCs in colloidal solution.

1.2.2 Properties of quantum dots

1.2.2.1 Quantum confinement effect

When an electron is excited from the valence band to the conduction band in a semicondutor, it leaves behind a positively charge vacancy known as hole. In bulk semiconductors, the electron-hole pair is bound within a characteristic length referred to as exciton Bohr radius (r_B), which is given by the equation 1.1

$$r_B = \frac{\hbar \varepsilon_r}{e^2}\left(\frac{1}{m_e^*} + \frac{1}{m_h^*}\right) \qquad 1.1$$

where m_e^* and m_h^* are the effective masses of electron and hole respectively and ε_r is the relative dielectric constant of the medium. When the size of the semiconductor particle approaches the exciton Bohr radius, spacial confinement of the electrons and holes occurs which results in discrete atomic like energy spectra (Fig.1.1). In quantum dots, which are nearly spherical semiconductor NCs, the confinement occurs in all three dimensions. One of the interesting consequences of this discretisation of energy levels is that semiconductor NCs exhibit size dependent electronic and optical properties properties.

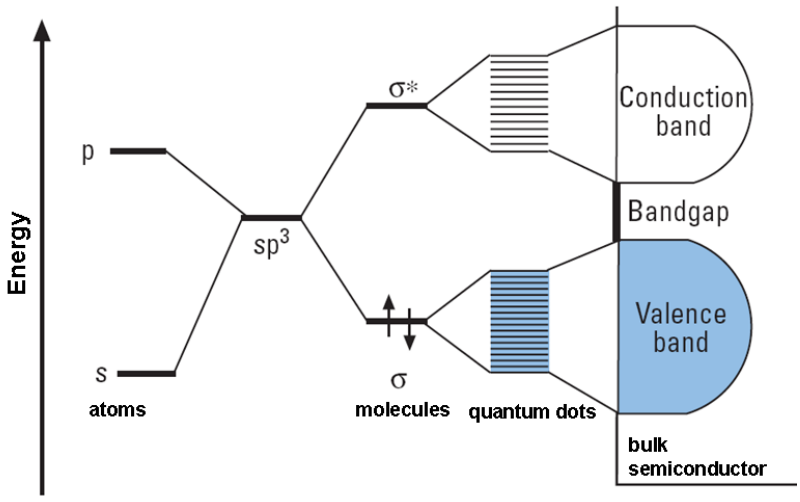

Fig 1.1 Scheme of the electronic levels in a single atom, a molecule, a quantum dot and a bulk semiconductor (example silicon) [10, 11].

The size dependency of the band gap is the most prominent effect of quantum confinement. To a first approximation, the band gap E_g of nanocrystals of radius *r* is given by the following equation 1.2 [12]

$$E_g = E_g^{bulk} + \frac{\hbar^2 \pi^2}{2r^2}\left(\frac{1}{m_e^*} + \frac{1}{m_h^*}\right) - \frac{1.786e^2}{\varepsilon_r \varepsilon_0}\frac{1}{r} \qquad 1.2$$

where the first term, E_g^{bulk} on left hand side of the equation is the band gap of the bulk material when *r* is infinitely large. The second term corresponds to the sum of the single particle ground state energies. When r is much smaller than r_B , the material is often said to be in "strong confinement regime" [13] as opposed to "weak confinement regime" when r slightly smaller than r_B. From equations 1.1 and 1.2, the correlation between the band gap, exciton Bohr radius and the radius of the NCs can be obtained (equation 1.3).

$$E_g = E_g^{bulk} + \frac{2.6}{\varepsilon_r \times r}\left(2.74\frac{r_B}{r} - 1\right) \qquad 1.3$$

Here E_g and E_g^{bulk} are expressed in eV and r_B and *r* in nm. It is thus evident that various semiconductor materials with a wide range of energy gaps cover a wide spectral range from the near infrared to the near ultraviolet. Therefore, for specific application the knowledge of the band gap as a function of particle size is important. Table 1.1 gives the parameters at room temperature for several II-VI, III-V and IV-VI semiconductors.

Material	**Structure (300K)**	**Type**	**E_{gap} (eV)**	**Lattice parameter (Å)**	**Density (kg/m^3)**
ZnS	Zinc-blende	II-VI	3.61	5.41	4084
ZnSe	Zinc-blende	II-VI	2.69	5.668	5266
ZnTe	Zinc-blende	II-VI	2.39	6.104	5636
CdS	Wurtzite	II-VI	2.49	4.136/6.714	4820
CdSe	Wurtzite	II-VI	1.74	4.3/7.01	5810
CdTe	Zinc-blende	II-VI	1.43	6.482	5870
GaN	Wurtzite	III-V	3.44	3.188/5.185	6095
GaP	Zinc-blende	III-V	2.27	5.45	4138
GaAs	Zinc-blende	III-V	1.42	5.653	5318
GaSb	Zinc-blende	III-V	0.75	6.096	5614
InN	Wurtzite	III-V	0.80	3.545/5.703	6810
InP	Zinc-blende	III-V	1.35	5.869	4787
InAs	Zinc-blende	III-V	0.35	6.058	5667
InSb	Zinc-blende	III-V	0.23	6.479	5774
PbS	Rocksalt	IV-VI	0.41	5.936	7597
PbSe	Rocksalt	IV-VI	0.28	6.117	8260
PbTe	Rocksalt	IV-VI	0.31	6.462	8219

Table 1.1 Parameters of selected semiconductors [14]

1.2.2.2 Optical properties

1.2.2.2.1 Absorption

In a direct band gap semiconductor, the absorption of a photon with energy greater than the band gap promotes an electron from the valence band to the conduction band, creating an electron hole pair (exciton). The exciton state with the lowest energy appears as a peak or distinct hump in an absorption spectrum of the NCs sample. This peak often referred to as first excitonic peak has an energy slightly lower energy than the band gap energy of the sample due to the contribution of coulomb attraction. The band gap is the energy required to create and electron (e-) and the hole (h+) at rest with the lattice and far apart enough so that the coulomb attraction is negligible [15]. The position of the excitonic peak depends on the band gap of the material as well as the size of the NCs. Due to quantum confinement the increase of NCs' size leads to the red-shift of the absorption onset. Another unique property of quantum dots is that their absorbance increases in the blue region. Consequently, the quantum dots can be excited in a wide range of wavelengths which give an advantage over organic dyes. Those generally have narrow absorption spectra and limited window of wavelength is available for the excitation of fluorescence.

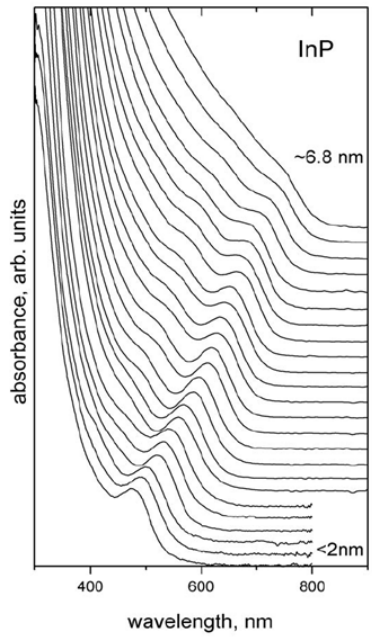

Figure 1.2 Size-dependent evolution of the UV-Vis absorption spectra of InP NCs [16].

1.2.2.2.2 Photoluminescence

After the absorption of a photon by the NC, leading to the formation of an exciton, the system can relax to the ground state by radiative recombination of the electron-hole pair. Radiative decay through emission of photons is called photoluminescence or more specifically in the case of QDs fluorescence. The emission efficiency of QDs is expressed

in terms of the fluorescence quantum yield (QY), which is the ratio between the number of absorbed photons and the number of emitted photons. The room temperature photoluminescence of the NCs is often poor due to the surface defects which cause non-radiative desexcitation channels [17]. The surface to volume ratio of NCs is much higher than in their bulk counterparts. For example, for 5 nm CdS, about 30% of the atoms are on the surface. Although surface passivation can be achieved to some extent using appropriate ligands [5], the most commonly employed and successful way of surface passivation is the epitaxial growth of another material around the NCs forming core/shell structure [14]. The shell plays a multiple role including surface passivation, protection of the core from oxidation and degradation. Due to the improved passivation of surface trap states, the fluorescence quantum yield is generally strongly increased by the shell growth.

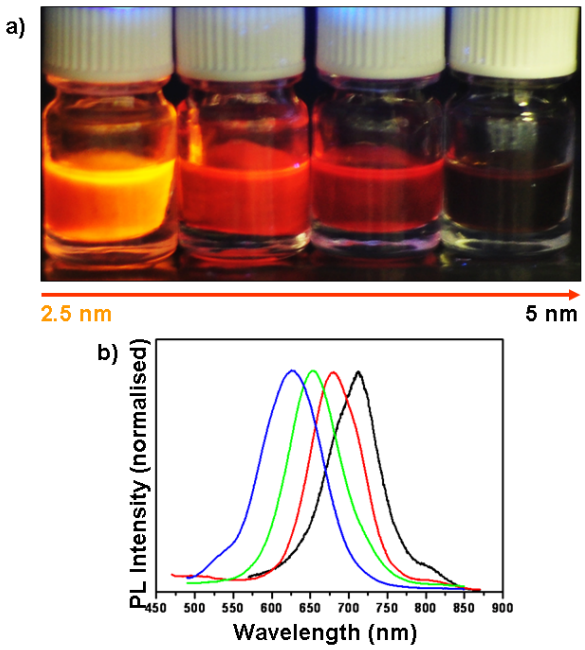

Figure 1.3 Size-dependent photoluminescence properties of InP NCs synthesised in thesis. A) Photograph showing different sized NCs under UV light B) corresponding PL spectra (self prepared samples).

1.2.2.3 Crystal structure

Zinc-blende and wurtzite are the most common crystal structuresrelized by bulk II-VI and III-V semiconductors (Figure 1.4). Zinc blende is based on a face centred cubic (FCC) lattice of anions whereas wurtzite is derived from hexagonal close packing (hcp) array of anions. Both structures have tetrahedrally coordinated atoms. Some semiconductors (e.g. ZnS, CdTe, ZnSe) are known to exhibit both types of crystals structures (known as polytypes) [18]. The general perception is that the semiconductor NCs exhibits the same crystal structure as in bulk. However, some reports suggest that the reaction parameters, nature of ligands and size of the NCs could well influence the crystalline nature and even the lattice structure of the NCs. For example, ZnS transforms from zinc-blende to a rocksalt phase at ~15.4 GPa. The transition pressure remains constant upon decreasing particle size to 15 nm. Below 15 nm, this phase transformation occurs at an elevated pressure [19]. A similar size dependent effect on the crystal structure has been observed in CdSe NCs [20].

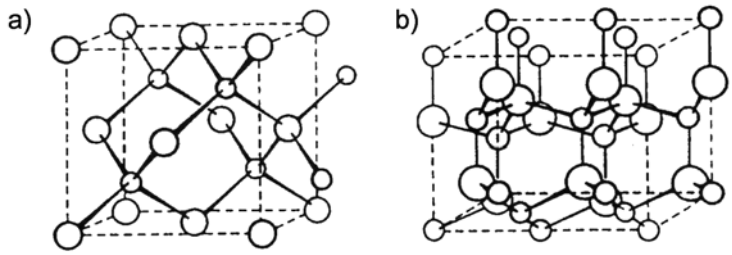

Figure 1.4: a) Zinc blende b) wurtzite crystal structure.

1.2.3 Synthesis of colloidal semiconductor NCs

The observation of the quantum size effect in nanometer sized colloidal CdS in the early 1980s [12, 15] gave the scientific community an impetus to synthesize and study colloidal NCs. Initially, these NCs were prepared in aqueous medium [21] as well as reverse micelles [22]. High boiling coordinating solvents were introduced for the synthesis of NCs in 1989 [23]. A real breakthrough came when Murray *et al.* reported highly crystalline and nearly monodiserse (size distributions of 8–11%) CdS, CdSe and CdTe NCs in 1993 [3]. They used a mixture of trioctylphosphine (TOP) and trioctyl phosphine oxide (TOPO) as high boiling point solvent/ligand. As demonstrated in classical studies by LaMer and

Dinegar [24], the synthesis of monodisperse colloids *via* homogeneous nucleation requires the temporal separation of nucleation and growth of the seeds. The mechanism and formation of mondispersed colloidal NCs can be explained using LaMer plot [24].

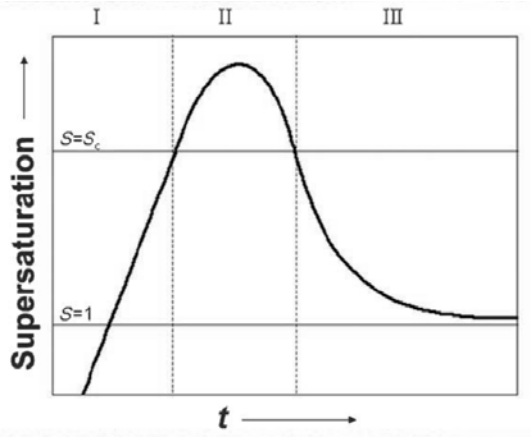

Fig. 1.5. LaMer plot depicting the degree of supersaturation as a function of reaction time

Initially the concentration of monomers, *i.e.* the minimum subunits of the crystal existing in solution, constantly increases by addition from exterior or by *in situ* generation within the reaction medium. It should be noted that in stage I no nucleation occurs even in supersaturated solution (S>1), due to the extremely high energy barrier for spontaneous homogeneous nucleation. The latter is overcome in Stage II for a yet higher degree of supersaturation ($S>S_c$), where nucleation and formation of stable nuclei take place. As the rate of monomer consumption induced by the nucleation and growth processes exceeds the rate of monomer supply, the monomer concentration and hence the supersaturation decreases below S_C, the level at which the nucleation rate becomes zero. In the following stage III, the particle growth continues under further monomer consumption as long as the system is in the supersaturated regime.

Experimentally, the separation of nucleation and growth can be achieved by rapid injection of the reagents into the hot solvent, which raises the precursor concentration in the reaction flask above the nucleation threshold ("hot-injection method") [25]. The hot injection leads to an instantaneous nucleation, which is quickly quenched by the fast cooling of the reaction mixture (the solution to be injected is at room temperature) and by the decreased supersaturation after the nucleation burst. Another possibility relies on attaining the degree of supersaturation necessary for homogeneous nucleation *via* the *in situ* formation of

reactive species upon supply of thermal energy (heating-up method) [26]. This method is widely used in the synthesis of metallic nanoparticles, but recently an increasing number of examples of semiconductor NCs prepared by this approach can be found. In an ideal case all crystallization nuclei are created at the same time and undergo identical growth. During the growth stage it is possible to carry out subsequent injections of precursors in order to increase the mean particle size without deterioration of the narrow size distribution as long as the concentration corresponding to the critical supersaturation S_c is not exceeded. Crystal growth from solution is in many cases followed by a second distinct growth process, which is referred to as Ostwald ripening [27]. It consists of the dissolution of the smallest particles because of their high surface energy and subsequent redeposition of the dissolved matter onto the bigger ones. Thereby the total number of NCs decreases, whereas their mean size increases. As shown in early studies [28], Ostwald ripening can lead to reduced size dispersions of micron-sized colloids. In the case of nanometer-sized particles, however, Ostwald ripening generally yields size dispersions of the order of 15-20%, and therefore the reaction should be stopped before this stage [29] .

1.2.4 Core/shell nanocrystals

The photoluminescence efficiency of the as-synthesized NCs is not sufficient for biological imaging application. This is true for all types of NCs including the highly studied CdSe systems. Generally, over-coating the nanocrystallites of one material with another inorganic material with larger band gap is a common mode of improving the PL efficiency of the material by passivating the surface related non-radiative recombination sites. They are commonly referred to as core/shell NCs. Some selected examples of such luminescent core/shell systems are CdSe/ZnS NCs [4, 30], CdSe/CdS NCs [31], CdSe/ZnSe [7], PbSe/PbS [32], InAs/ZnSe [33], InP/$ZnCdSe_2$ [34] and InP/ZnS [35]. Two important parameter for the synthesis of core/shell NCs are a) the band alignment which is the relative position of the conduction and valence band of the two materials in energy scale and b) the crystal structures or more precisely the lattice parameters of the core and shell materials. Depending on the band alignment of the core and shell materials, the NCs can be type I or type II [14]. In a type I core/shell system the conduction band edge of the shell (the higher band gap material) is of higher energy than that of the core (the lower band gap material), and the valence band edge of the shell has lower energy than that of the core.

Consequently, both electrons and holes are confined in the core. In a type-II QD in contrast, both the valence and conduction band edges in the core are situated below or above lower (or higher) than in the shell. As the only one carrier is confined to the core, while the other is confined to the shell, the photoluminescence emission of the type II systems are red shifted. As a result, much longer emission wavelengths are accessible with materials which otherwise emit in the shorter wavelengths. Some examples of such system are CdTe/CdSe [36], CdSe/ZnTe [36], ZnTe/ZnSe [37].

1.3 Quantum dots in biology

1.3.1 Aqueous solubility

The possibility to disperse NCs in aqueous medium is a fundamental criterion for application of these NCs in biology. QDs prepared in organic solvents have no intrinsic aqueous solubility as they are stabilised by ligands containing long hydrophobic alkyl chains. Usually a phase transfer step is involved before these NCs are solubilized in aqueous medium. A large number of methods for phase transfer involve the exchange of surface ligands on the NCs by hydrophilic molecules. One of the first reported methods involves exchange of surface ligands with hydrosoluble mercaptoacetic acid [38]. The thiol group and even more its deprotonated thiolate form, has high affinity for atoms like Zn in the ZnS shell resulting in strong binding. Consequently, thiol containing ligands have been widely used for the preparation of hydrophilic QDs. Some commonly used thiol group containing ligands include mercaptocarboxylic acids, amino acids such as cysteine [39], dihydrolipoic acid derivatives [40] and peptides [41, 42]. In addition, phospholipid micelles [43] and amphiphilic polymers [44] have also been used as phase transfer agents. In this case, no exchange of the original surface ligands is carried out, but the amphiphilic molecules “stick” to the surface by hydrophobic interactions involving their apolar groups. Their polar moieties point to the exterior, giving hydrosolubility and stability to the QDs. On the other hand, the hydrodynamic diameter is strongly increased to around 15-25 nm upon encapsulation with amphiphilic molecules. For *in vivo* studies such large hydrodynamic diameters are obstacle for renal clearance [45]. In the case of ligand exchange, however, the loss of fluorescence is a major concern. In this thesis the problem of fluorescence reduction during the aqueous transfer processes of NCs using ligand exchange will be addressed.

1.3.2 Bioconjugation

Since the first studies in 1998 showing that organically prepared quantum dots can be solubilised in water and then be used as fluorescent labels in biology [38, 46], a large number of functional molecules such as proteins, nucleotides, peptides, small molecules, drugs, genes etc. have been bioconjugated with QDs and various studies performed. There are various ways of attaching biomoleucles to NCs. Some of them include direct ligand exchange with thiol group containing biomolecules, the use of cross-linkers, use of coupling agents and electrostatic. Thiol groups containing biomolecules such cysteine rich peptides rely on the affinity of thiols to cationic sites on the NPs surface and are directly attached to the surface of the QDs [47, 48]. Bifunctional cross linkers such as 4-(N-maleimidomethyl) cyclohexane-1-carboxylate (SMCC), which contain both thiol reactive maleimide group and amino reactive N-hydrosuccinimide can be used if the quantum dots have free thiols or amines on the surface. Coupling agents such as carbodiimide are used to covalently link free carboxylic groups on the surface of conjugation and the amine group on of the biomolecules. Conjugation has also been achieved by means of electrostatic attraction between positively charged proteins and negatively charged lipoic acid capped CdSe/ZnS QDs [49].

1.3.3 Cellular labeling

One of the current interests of QDs lies in developing probes for imaging inside living cells. Intracellular application can be more challenging than extracellular target recognition. The first challenge is to cross the plasma membrane without being engulfed by living cells through a nonspecific uptake mechanism. Second, reaching the specific intracellular targets may be complicated by the presence of a variety of proteins, nucleic acids and other molecules in cytoplasm that may potentially bind to the QDs or the biomolecules on their surface, resulting in aggregation. Some reported methods used for intracellular delivery of quantum dots are a) Transfection – QDs are delivered into cells via artificially prepared vesicles made of lipid bilayers (called liposomes) [50, 51] b) Electroporation – QDs are delivered by increasing the electrical conductivity and the permeability of the cell membrane using an external electrical field [52] c) Microinjections [43, 51] d) Using cell penetrating peptides –peptides which can translocate into the cell carrying a cargo [53]. This cargo may vary from small drug molecules to QDs.

1.3.4 *In vivo* near infrared (NIR) fluorescence imaging

Given the versatility of the QDs surface for bioconjugation, the possibility of application is enormous. For example, QDs can be labeled with tumour-targetting antibodies and traced with fluorescence imaging techniques or can be employed in tracking cancer cells in metastasis [54, 55]. However, the efficiency of a fluorescence based probe in biomedical imaging highly depends on the fate of the photons propagating in and out of the living tissue. The loss of photon signal occurs through absorption and scattering by living tissues. In addition, the tissue auto-fluorescence (which can result from the absorption of photons by tissue components) substantially decreases the contrast between the target and the background. While scattering is either inversely proportional to a certain power of wavelength (e.g. 2.8 for rat skin) or nearly independent of the wavelength (e.g. 0.6 human breast) [56], the absorption by living tissues are relatively low in near infrared region (650-900 nm) of the spectrum [57]. This includes even the major absorbers of visible and NIR light, haemoglobin and water (Fig. 1.6). In fact, this window is bordered by increasing absorbance of blood (haemoglobin) on one side (<650nm), and by high absorbance of water on the other (>900nm) [58]. This makes an NIR (650-900 nm) emitting fluorescent probes ideal candidates for use in tissue imaging with increased penetration depth.

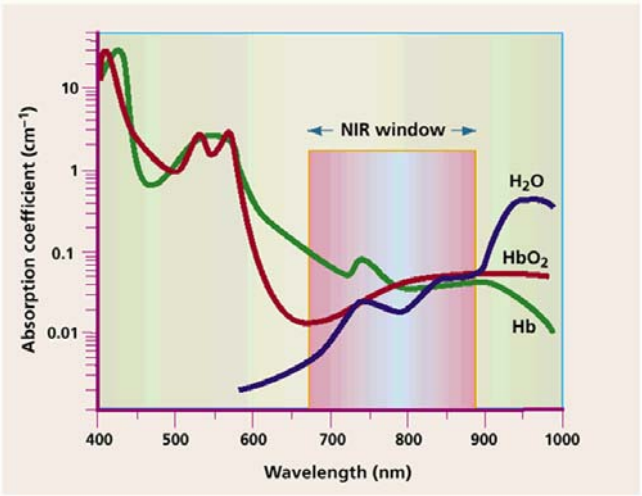

Fig 1.6 Absorption coefficient of two major light absorbers depending on wavelengths [57].

1.4 NIR emitting quantum dots

CdSe based NCs have been the most widely studied colloidal NCs. High crystallinity, shape and size control, and fluorescence quantum yields close to 100 % in organic solvents have been achieved [7, 31, 59]. However, due to relatively large band gap (bulk band gap: 1.74 eV at 300°K), the maximum PL emission achieved for CdSe NCs is around 650 nm. For *in vivo* imaging application in NIR, this might not be sufficient. Many other semiconductor NCs with smaller band gaps have been successfully synthesized to access NIR emission (Fig. 1.7). Recently in addition to II-IV and III-V, II-V semiconductor NCs emitting in NIR wavelengths have also been reported (e.g. Cd_3P_2 and Cd_3As_2) [60, 61]. In addition, the type II core/shell structures have also been synthesized to get access to NIR wavelengths. For example, NIR emitting CdTe/CdSe type II core/shelll NCs have been successfully applied to image lymph nodes present deep (up to 1 cm) in tissues [62]. Another example of NIR emitting NCs in biology is the use of InAs NCs for successful imaging tumor vasculature [63]. However, most of these NCs involve elements of highly restricted use like Cd, As, Hg (cf. Table 1.2). As an alternative InP based NCs (bulk band gap: 1.35 eV) are seen as a promising candidate for *in vivo* NIR imaging.

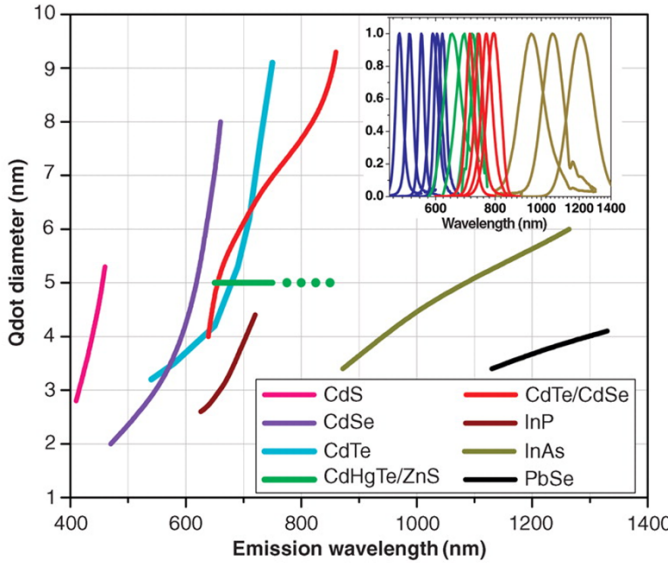

Figure 1.7 Emission wavelengths as a function of QD diameter for various semiconductors. Inset: normalized PL spectra [64].

Details	**Type I**							**Type II**
QD	CdTe	InP	Cd_3P_2	PbS	InAs	Cd_3As_2	HgTe	CdTe/CdSe
Bulk band gap (eV)	1.43	1.35	0.55	0.41	0.35	0.19	0*	NA
Reference	[65, 66]	[6, 67, 68]	[60]	[69]	[63]	[61]	[70, 71]	[36, 72]

Table 1.2 Various types of NIR emitting NCs. *Bulk HgTe is a semimetal.

1.4.1 Indium phosphide (InP) NCs

InP is a low band gap (bulk value: 1.35 eV) III-V semiconductor with a exciton Bohr's radius of 11.5 nm. In the strong quantum confinement regime its photoluminescence can be tuned from blue to the near infrared (NIR) by varying the size. As discussed in the previous section, NIR emitting QDs are particularly interesting for *in vivo* imaging, due to the better transparency of tissues in this region of the electromagnetic spectrum [57]. In addition, the absence of highly toxic elements like cadmium, arsenic, lead and mercury makes InP based luminescent probes highly attractive for biological imaging applications. To realise the full potential of InP NCs in biotechnonology the first requirement is to develop a robust method for synthesising larger sized InP NCs with emission >700 nm. The InP NCs can then be processed into core/shell systems [34] to improve their PL QY, photo- and chemical stability. Traditionally, the synthesis of III-V semiconductor QDs is considered more difficult than their II-VI counterparts (e.g. CdSe, CdTe, ZnS) due to the more covalent nature of bonds [73]. The majority of the existing routes for the synthesis of InP colloidal nanocrystals (NCs) found in literature are based on Well's dehalosilylation reaction [74] first adapted by Micic *et al* [75] for colloidal InP NCs. In this reaction $[(CH_3)_3Si]_3P$ is reacted with an indium (III) precursor at elevated temperatures (180-300°C) in a high boiling solvent and invariably in presence of a stabilising ligand (e.g. fatty acids [8], amines [6, 68] and/or the alkyl phosphine [73]). This synthetic approach has brought a major success in recent times in the synthesis of high quality InP/ZnS NCs with quantum yields nearly comparable to CdSe based NCs [6, 76]. However, as far as red or NIR emitting (>700 nm) InP NCs or related core/shell structures (e.g. InP/ZnS) are concerned although the successful preparation of emitting QDs is acclaimed, no experimental details

are given [6, 68]. Larger sized NCs are typically synthesised *via* multiple injections of precursor solutions to the solution of smaller InP NCs at high temperatures [6, 67], often followed by a size selective precipitation step [67]. The longest emission reported for InP NCs by this method is ~750 nm [6, 67]. Another way of synthesising InP NCs is using phosphine gas as the phosphorous precursor [77]. In this method, the *in situ* generated phosphine gas is reacted with the indium precursor in the presence of a ligand at high temperature (210°C to 290°C). Since the PH_3 gas is slowly and continuously bubbled into the flask containing the precursor solutions, similar to the aforementioned multiple injection method, the overall size is expected to be larger. In the frame of this thesis, we focus on exploring this last method with the goal to push the emission wavelength as far as possible to the NIR.

1.5 Motivation

As summarized above in the state-of-the-art (**Chapter I**), QDs are promising fluorescent labels for biological imaging, due to their size-dependent emission properties, pure emission colors, high absorption coefficient and fluorescence quantum yield (resulting in high brightness), and long term resistance against photobleaching. Furthermore, the possibility of exciting several NCs emitting at different wavelengths with the same light source facilitates multiplexing. However, most of the literature results concern cadmium-related NCs, in particular CdSe and CdTe QDs, whose applicability is strongly limited because of their intrinsic toxicity. InP based NCs, on the other hand, hold the promise of being acceptable in both *in vitro* and *in vivo* applications, as confirmed by several tests of their toxicity [78, 79, 90]. Up till now, only very few reports concern their use in biology, as their synthesis is less mastered than in the case of II-VI semiconductor NCs.

The goal of this PhD thesis is to develop the synthesis and aqueous phase transfer of NIR-emitting InP/ZnS core/shell NCs and to evaluate their potential as fluorescent probes in different biological applications. Therefore, first of all a robust synthesis method for producing InP NCs emitting as far as possible in the NIR has to be developed. In a second step, the InP NCs will be overcoated with a ZnS shell. The thickness and quality of the shell have important consequences on the fluorescence quantum yield (QY) and on the photostability of the obtained InP/ZnS core/shell NCs. **Chapter II** describes this part of the thesis.

Being hydrophobic after synthesis, the NCs will then be transferred to the aqueous phase by means of surface ligand exchange, described in **Chapter III**. We opt for this approach instead of using the encapsulation by amphiphilic molecules with the goal to obtain compact NCs (*i.e.* of low hydrodynamic diameter) with high colloidal stability in aqueous medium. Several thiol-containing molecules are being explored, with special emphasis on zwitterionic compounds such as cysteine, known for their low non-specific binding. An important point to be addressed is the ubiquitously observed reduction of fluorescence efficiency upon phase transfer by ligand exchange, This problem risks to be even more critical in the case of InP based NCs due to their lower initial QY as compared to CdSe or CdTe based NCs.

Finally, the use of the obtained water-solubilized InP/ZnS NCs in biology will be explored, (**Chapter IV**). We will first evaluate their cytotoxicity in cell culture. Due to the compact nature of the phase transfer ligands, the ZnS surface of the NCs is still available for the grafting of other types of molecules of biological interest. Such direct grafting will be used to functionalize the NCs with the cell penetrating peptide maurocalcine. The preparation of bimodal fluorescent/MRI probes will be explored by grafting gadolinium picolinate complexes on the surface of the QDs. Finally, the use of functional peptides as phase transfer agents will be investigated, and the grafting of streptavidin proteins. Owing to their high molecular weight and similar size as the NCs, QDs with one, two or more proteins per particle can be separated and isolated using gel electrophoresis.

Each chapter contains its corresponding experimental section and references. Following the general conclusion, the used characterization methods are summarized in the **Annex**.

The research described in this thesis was carried out in close collaboration with CEA/Leti/DTBS (Grégory Beaune, Isabelle Texier) and with INSERM U836 (Cathy Poillot, Michel De Waard) with financial support from ANR (project PNANO 2007 “SYNERGIE”) and CEA (program Technologies pour la Santé, project TIMOMA2).

1.6 References

1. Orton, J., *Story of semiconductor*. 2004, New York: Oxford University Press.
2. Rossetti, R., S. Nakahara, and L.E. Brus, *Quantum size effects in the redox potentials, resonance Raman spectra, and electronic spectra of CdS crystallites in aqueous solution.* The Journal of Chemical Physics,1983. **79**(2): p. 1086-1088.
3. Murray, C.B., D.J. Norris, and M.G. Bawendi, *Synthesis and characterization of nearly monodisperse CdE (E = sulfur, selenium, tellurium) semiconductor nanocrystallites.* Journal of the American Chemical Society, 1993. **115**(19): p. 8706-8715.
4. Hines, M.A. and P. Guyot-Sionnest, *Synthesis and Characterization of Strongly Luminescing ZnS-Capped CdSe Nanocrystals.* The Journal of Physical Chemistry, 1996. **100**(2): p. 468-471.
5. Talapin, D.V., A.L. Rogach, A. Kornowski, M. Haase, and H. Weller, *Highly Luminescent Monodisperse CdSe and CdSe/ZnS Nanocrystals Synthesized in Hexadecylamine−Trioctylphosphine Oxide−Trioctylphospine Mixture.* Nano Letters, 2001. **1**(4): p. 207-211.
6. Xu, S., J. Ziegler, and T. Nann, *Rapid synthesis of highly luminescent InP and InP/ZnS nanocrystals.* Journal of Materials Chemistry, 2008. **18**(23): p. 2653-2656.
7. Reiss, P., J.l. Bleuse, and A. Pron, *Highly Luminescent CdSe/ZnSe Core/Shell Nanocrystals of Low Size Dispersion.* Nano Letters, 2002. **2**(7): p. 781-784.
8. Battaglia, D. and X. Peng, *Formation of High Quality InP and InAs Nanocrystals in a Noncoordinating Solvent.* Nano Letters, 2002. **2**(9): p. 1027-1030.
9. *Theory of resonant tunneling through a quantum wire.* Physical Review B, 1995. **51**(3): p. 1735.
10. Murphy, C.J., *Peer Reviewed: Optical Sensing with Quantum Dots.* Analytical Chemistry, 2002. **74**(19): p. 520 A-526 A.
11. Alivisatos, A.P., *Nanocrystals: Building blocks for modern materials design.* Endeavour, 1997. **21**(2): p. 56-60.
12. Brus, L., *Electronic wave functions in semiconductor clusters: experiment and theory.* The Journal of Physical Chemistry, 1986. **90**(12): p. 2555-2560.
13. Einevoll, G.T., *Confinement of excitons in quantum dots.* Physical Review B, 1992. **45**(7): p. 3410.
14. Reiss, P., M. Protière, and L. Li, *Core/Shell Semiconductor Nanocrystals.* Small, 2009. **5**(2): p. 154-168.
15. Brus, L.E., *Electron--electron and electron-hole interactions in small semiconductor crystallites: The size dependence of the lowest excited electronic state.* The Journal of Chemical Physics, 1984. **80**(9): p. 4403-4409.

16. Adam, S., D.V. Talapin, H. Borchert, A. Lobo, C. McGinley, A.R.B. de Castro, M. Haase, H. Weller, and T. Moller, *The effect of nanocrystal surface structure on the luminescence properties: Photoemission study of HF-etched InP nanocrystals.* The Journal of Chemical Physics, 2005. **123**(8): p. 084706-10.
17. Klimov, V.I., D.W. McBranch, C.A. Leatherdale, and M.G. Bawendi, *Electron and hole relaxation pathways in semiconductor quantum dots.* Physical Review B, 1999. **60**(19): p. 13740.
18. Yeh, C.-Y., Z.W. Lu, S. Froyen, and A. Zunger, *Zinc-blende-wurtzite polytypism in semiconductors.* Physical Review B, 1992. **46**(16): p. 10086.
19. Wang, Z. and Q. Guo, *Size-Dependent Structural Stability and Tuning Mechanism: A Case of Zinc Sulfide.* The Journal of Physical Chemistry C, 2009. **113**(11): p. 4286-4295.
20. Jacobs, K., J. Wickham, and A.P. Alivisatos, *Threshold Size for Ambient Metastability of Rocksalt CdSe Nanocrystals.* The Journal of Physical Chemistry B, 2002. **106**(15): p. 3759-3762.
21. Henglein, A., *Photo-Degradation and Fluorescence of Colloidal-Cadmium Sulfide in Aqueous Solution.* Berichte der Bunsengesellschaft für physikalische Chemie, 1982. **86**(4): p. 301-305.
22. Steigerwald, M.L., A.P. Alivisatos, J.M. Gibson, T.D. Harris, R. Kortan, A.J. Muller, A.M. Thayer, T.M. Duncan, D.C. Douglass, and L.E. Brus, *Surface derivatization and isolation of semiconductor cluster molecules.* Journal of the American Chemical Society, 1988. **110**(10): p. 3046-3050.
23. Bawendi, M.G., A.R. Kortan, M.L. Steigerwald, and L.E. Brus, *X-ray structural characterization of larger CdSe semiconductor clusters.* The Journal of Chemical Physics, 1989. **91**(11): p. 7282-7290.
24. LaMer, V.K. and R.H. Dinegar, *Theory, Production and Mechanism of Formation of Monodispersed Hydrosols.* Journal of the American Chemical Society, 1950. **72**(11): p. 4847-4854.
25. de Mello Donegá, C., P. Liljeroth, and D. Vanmaekelbergh, *Physicochemical Evaluation of the Hot-Injection Method, a Synthesis Route for Monodisperse Nanocrystals.* Small, 2005. **1**(12): p. 1152-1162.
26. Park, J., J. Joo, S.G. Kwon, Y. Jang, and T. Hyeon, *Synthesis of Monodisperse Spherical Nanocrystals.* Angewandte Chemie International Edition, 2007. **46**(25): p. 4630-4660.
27. Voorhees, P.W., *The theory of Ostwald ripening.* Journal of statistical physics, 1985. **38**: p. 231-252.
28. Reiss, H., *The Growth of Uniform Colloidal Dispersions.* The Journal of Chemical Physics, 1951. **19**(4): p. 482-487.
29. Rogach, A.L., D.V. Talapin, E.V. Shevchenko, A. Kornowski, M. Haase, and H. Weller, *Organization of Matter on Different Size Scales: Monodisperse Nanocrystals and Their Superstructures.* Advanced Functional Materials, 2002. **12**(10): p. 653-664.
30. Dabbousi, B.O., J. Rodriguez-Viejo, F.V. Mikulec, J.R. Heine, H. Mattoussi, R. Ober, K.F. Jensen, and M.G. Bawendi, *(CdSe)ZnS Core-Shell Quantum Dots: Synthesis and Characterization of a Size Series of Highly*

Luminescent Nanocrystallites. The Journal of Physical Chemistry B, 1997. **101**(46): p. 9463-9475.

31. Peng, X., M.C. Schlamp, A.V. Kadavanich, and A.P. Alivisatos, *Epitaxial Growth of Highly Luminescent CdSe/CdS Core/Shell Nanocrystals with Photostability and Electronic Accessibility.* Journal of the American Chemical Society, 1997. **119**(30): p. 7019-7029.
32. Sashchiuk, A., L. Langof, R. Chaim, and E. Lifshitz, *Synthesis and characterization of PbSe and PbSe/PbS core-shell colloidal nanocrystals.* Journal of Crystal Growth, 2002. **240**(3-4): p. 431-438.
33. Cao, Y.-W. and U. Banin, *ChemInform Abstract: Synthesis and Characterization of InAs/InP and InAs/CdSe Core/Shell Nanocrystals.* ChemInform, 2000. **31**(13):
34. Micic, O.I., B.B. Smith, and A.J. Nozik, *Core-Shell Quantum Dots of Lattice-Matched ZnCdSe2 Shells on InP Cores: Experiment and Theory.* The Journal of Physical Chemistry B, 2000. **104**(51): p. 12149-12156.
35. Haubold, S., M. Haase, A. Kornowski, and H. Weller, *Strongly Luminescent InP/ZnS Core–Shell Nanoparticles.* ChemPhysChem, 2001. **2**(5): p. 331-334.
36. Kim, S., B. Fisher, H.-J.r. Eisler, and M. Bawendi, *Type-II Quantum Dots: CdTe/CdSe(Core/Shell) and CdSe/ZnTe(Core/Shell) Heterostructures.* Journal of the American Chemical Society, 2003. **125**(38): p. 11466-11467.
37. Bang, J., J. Park, J.H. Lee, N. Won, J. Nam, J. Lim, B.Y. Chang, H.J. Lee, B. Chon, J. Shin, J.B. Park, J.H. Choi, K. Cho, S.M. Park, T. Joo, and S. Kim, *ZnTe/ZnSe (Core/Shell) Type-II Quantum Dots: Their Optical and Photovoltaic Properties.* Chemistry of Materials, 2009. **22**(1): p. 233-240.
38. Chan, W.C.W. and S. Nie, *Quantum Dot Bioconjugates for Ultrasensitive Nonisotopic Detection.* Science, 1998. **281**(5385): p. 2016-2018.
39. Liu, W., H.S. Choi, J.P. Zimmer, E. Tanaka, J.V. Frangioni, and M. Bawendi, *Compact Cysteine-Coated CdSe(ZnCdS) Quantum Dots for in Vivo Applications.* Journal of the American Chemical Society, 2007. **129**(47): p. 14530-14531.
40. Susumu, K., H.T. Uyeda, I.L. Medintz, T. Pons, J.B. Delehanty, and H. Mattoussi, *Enhancing the Stability and Biological Functionalities of Quantum Dots via Compact Multifunctional Ligands.* Journal of the American Chemical Society, 2007. **129**(45): p. 13987-13996.
41. Roullier, V., S. Clarke, C. You, F. Pinaud, G.r. Gouzer, D. Schaible, V.r. Marchi-Artzner, J. Piehler, and M. Dahan, *High-Affinity Labeling and Tracking of Individual Histidine-Tagged Proteins in Live Cells Using Ni2+ Tris-nitrilotriacetic Acid Quantum Dot Conjugates.* Nano Letters, 2009. **9**(3): p. 1228-1234.
42. Lévy, R.l., N.T.K. Thanh, R.C. Doty, I. Hussain, R.J. Nichols, D.J. Schiffrin, M. Brust, and D.G. Fernig, *Rational and Combinatorial Design of Peptide Capping Ligands for Gold Nanoparticles.* Journal of the American Chemical Society, 2004. **126**(32): p. 10076-10084.

43. Dubertret, B., P. Skourides, D.J. Norris, V. Noireaux, A.H. Brivanlou, and A. Libchaber, *In Vivo Imaging of Quantum Dots Encapsulated in Phospholipid Micelles.* Science, 2002. **298**(5599): p. 1759-1762.
44. Pellegrino, T., L. Manna, S. Kudera, T. Liedl, D. Koktysh, A.L. Rogach, S. Keller, J. RÃ¤dler, G. Natile, and W.J. Parak, *Hydrophobic Nanocrystals Coated with an Amphiphilic Polymer Shell: A General Route to Water Soluble Nanocrystals.* Nano Letters, 2004. **4**(4): p. 703-707.
45. Soo Choi, H., W. Liu, P. Misra, E. Tanaka, J.P. Zimmer, B. Itty Ipe, M.G. Bawendi, and J.V. Frangioni, *Renal clearance of quantum dots.* Nat Biotech, 2007. **25**(10): p. 1165-1170.
46. Bruchez, M., M. Moronne, P. Gin, S. Weiss, and A.P. Alivisatos, *Semiconductor Nanocrystals as Fluorescent Biological Labels.* Science, 1998. **281**(5385): p. 2013-2016.
47. Pinaud, F., D. King, H.-P. Moore, and S. Weiss, *Bioactivation and Cell Targeting of Semiconductor CdSe/ZnS Nanocrystals with Phytochelatin-Related Peptides.* Journal of the American Chemical Society, 2004. **126**(19): p. 6115-6123.
48. Clarke, S., F. Pinaud, O. Beutel, C. You, J. Piehler, and M. Dahan, *Covalent Monofunctionalization of Peptide-Coated Quantum Dots for Single-Molecule Assays.* Nano Letters. **10**(6): p. 2147-2154.
49. Mattoussi, H., J.M. Mauro, E.R. Goldman, G.P. Anderson, V.C. Sundar, F.V. Mikulec, and M.G. Bawendi, *Self-Assembly of CdSe-ZnS Quantum Dot Bioconjugates Using an Engineered Recombinant Protein.* Journal of the American Chemical Society, 2000. **122**(49): p. 12142-12150.
50. Hui, L. and et al., *Transfection of aqueous CdS quantum dots using polyethylenimine.* Nanotechnology, 2008. **19**(47): p. 475101.
51. Derfus, A.M., W.C.W. Chan, and S.N. Bhatia, *Intracellular Delivery of Quantum Dots for Live Cell Labeling and Organelle Tracking.* Advanced Materials, 2004. **16**(12): p. 961-966.
52. Y Yoo, J. S.; Won, N.; Kim, H. B.; Bang, J.; Kim, S.; Ahn, S.; Soh, K.-S., *In vivo imaging of cancer cells with electroporation of quantum dots and multispectral imaging*. Journal of Applied Physics, 2010; **107**: p 124702-124710.
53. Delehanty, J.B., I.L. Medintz, T. Pons, F.M. Brunel, P.E. Dawson, and H. Mattoussi, *Self-Assembled Quantum Dot−Peptide Bioconjugates for Selective Intracellular Delivery.* Bioconjugate Chemistry, 2006. **17**(4): p. 920-927.
54. Gao, X., Y. Cui, R.M. Levenson, L.W.K. Chung, and S. Nie, *In vivo cancer targeting and imaging with semiconductor quantum dots.* Nat Biotech, 2004. **22**(8): p. 969-976.
55. Hoshino, A., K.-i. Hanaki, K. Suzuki, and K. Yamamoto, *Applications of T-lymphoma labeled with fluorescent quantum dots to cell tracing markers in mouse body.* Biochemical and Biophysical Research Communications, 2004. **314**(1): p. 46-53.
56. Lim, Y.T.K., S. ; Nakayama, A. ; Stott, N. E.; Bawendi, M. G.; Frangioni, J. V. , *Selection of Quantum Dot Wavelengths for biomedical Assays and Imagining* Mol. Imaging, 2003. **2**: p. 50-64.

57. Weissleder, R., *A clearer vision for in vivo imaging.* Nat Biotech, 2001. **19**(4): p. 316-317.
58. Chance, B., *Near-Infrared Images Using Continuous, Phase-Modulated, and Pulsed Light with Quantitation of Blood and Blood Oxygenationa.* Annals of the New York Academy of Sciences, 1998. **838**(1): p. 29-45.
59. Mekis, I., D.V. Talapin, A. Kornowski, M. Haase, and H. Weller, *One-Pot Synthesis of Highly Luminescent CdSe/CdS Core-Shell Nanocrystals via Organometallic and "Greener" Chemical Approaches* The Journal of Physical Chemistry B, 2003. **107**(30): p. 7454-7462.
60. Miao, S., S.G. Hickey, B. Rellinghaus, C. Waurisch, and A. Eychmüller, *Synthesis and Characterization of Cadmium Phosphide Quantum Dots Emitting in the Visible Red to Near-Infrared.* Journal of the American Chemical Society, 2010. **132**(16): p. 5613-5615.
61. Harris, D.K., P.M. Allen, H.-S. Han, B.J. Walker, J. Lee, and M.G. Bawendi, *Synthesis of Cadmium Arsenide Quantum Dots Luminescent in the Infrared.* Journal of the American Chemical Society, 2011. **133**(13): p. 4676-4679.
62. Frangioni, J. V., S-W. Kim, Shunsuke Ohnishi, S. Kim, and M. G. Bawendi, *Sentinel Lymph Node Mapping with Type II Quantum Dots*, 2007, **374**, 147-159
63. Allen, P.M., W. Liu, V.P. Chauhan, J. Lee, A.Y. Ting, D. Fukumura, R.K. Jain, and M.G. Bawendi, *InAs(ZnCdS) Quantum Dots Optimized for Biological Imaging in the Near-Infrared.* Journal of the American Chemical Society, 2009. **132**(2): p. 470-471.
64. Michalet, X., F.F. Pinaud, L.A. Bentolila, J.M. Tsay, S. Doose, J.J. Li, G. Sundaresan, A.M. Wu, S.S. Gambhir, and S. Weiss, *Quantum Dots for Live Cells, in Vivo Imaging, and Diagnostics.* Science, 2005. **307**(5709): p. 538-544.
65. Gaponik, N., I.L. Radtchenko, G.B. Sukhorukov, H. Weller, and A.L. Rogach, *Toward Encoding Combinatorial Libraries: Charge-Driven Microencapsulation of Semiconductor Nanocrystals Luminescing in the Visible and Near IR.* Advanced Materials, 2002. **14**(12): p. 879-882.
66. Zintchenko, A., A.S. Susha, M. Concia, J. Feldmann, E. Wagner, A.L. Rogach, and M. Ogris, *Drug Nanocarriers Labeled With Near-infrared-emitting Quantum Dots (Quantoplexes): Imaging Fast Dynamics of Distribution in Living Animals.* Mol Ther, 2009. **17**(11): p. 1849-1856.
67. Talapin, D.V., N. Gaponik, H. Borchert, A.L. Rogach, M. Haase, and H. Weller, *Etching of Colloidal InP Nanocrystals with Fluorides: Photochemical Nature of the Process Resulting in High Photoluminescence Efficiency.* The Journal of Physical Chemistry B, 2002. **106**(49): p. 12659-12663.
68. Xie, R., D. Battaglia, and X. Peng, *Colloidal InP Nanocrystals as Efficient Emitters Covering Blue to Near-Infrared.* Journal of the American Chemical Society, 2007. **129**(50): p. 15432-15433.
69. Hinds, S., S. Myrskog, L. Levina, G. Koleilat, J. Yang, S.O. Kelley, and E.H. Sargent, *NIR-Emitting Colloidal Quantum Dots Having 26%*

Luminescence Quantum Yield in Buffer Solution. Journal of the American Chemical Society, 2007. **129**(23): p. 7218-7219.

70. Kovalenko, M.V., E. Kaufmann, D. Pachinger, J.r. Roither, M. Huber, J. Stangl, G.n. Hesser, F. Schäffler, and W. Heiss, *Colloidal HgTe Nanocrystals with Widely Tunable Narrow Band Gap Energies: From Telecommunications to Molecular Vibrations.* Journal of the American Chemical Society, 2006. **128**(11): p. 3516-3517.
71. Gaponik, N., I.L. Radtchenko, M.R. Gerstenberger, Y.A. Fedutik, G.B. Sukhorukov, and A.L. Rogach, *Labeling of Biocompatible Polymer Microcapsules with Near-Infrared Emitting Nanocrystals.* Nano Letters, 2003. **3**(3): p. 369-372.
72. Zhang, Y., Y. Li, and X.-P. Yan, *Aqueous Layer-by-Layer Epitaxy of Type-II CdTe/CdSe Quantum Dots with Near-Infrared Fluorescence for Bioimaging Applications.* Small, 2009. **5**(2): p. 185-189.
73. Guzelian, A.A., J.E.B. Katari, A.V. Kadavanich, U. Banin, K. Hamad, E. Juban, A.P. Alivisatos, R.H. Wolters, C.C. Arnold, and J.R. Heath, *Synthesis of Size-Selected, Surface-Passivated InP Nanocrystals.* The Journal of Physical Chemistry, 1996. **100**(17): p. 7212-7219.
74. Wells, R.L., C.G. Pitt, A.T. McPhail, A.P. Purdy, S. Shafieezad, and R.B. Hallock, *The use of tris(trimethylsilyl)arsine to prepare gallium arsenide and indium arsenide.* Chemistry of Materials, 1989. **1**(1): p. 4-6.
75. Micic, O.I., C.J. Curtis, K.M. Jones, J.R. Sprague, and A.J. Nozik, *Synthesis and Characterization of InP Quantum Dots.* The Journal of Physical Chemistry, 1994. **98**(19): p. 4966-4969.
76. Li, L. and P. Reiss, *One-pot Synthesis of Highly Luminescent InP/ZnS Nanocrystals without Precursor Injection.* Journal of the American Chemical Society, 2008. **130**(35): p. 11588-11589.
77. Li, L., M. Protière, and P. Reiss, *Economic Synthesis of High Quality InP Nanocrystals Using Calcium Phosphide as the Phosphorus Precursor.* Chemistry of Materials, 2008. **20**(8): p. 2621-2623.
78. Yong, K.-T.; Ding, H.; Roy, I.; Law, W.-C.; Bergey, E. J.; Maitra, A.; Prasad, P. N., *Imaging Pancreatic Cancer Using Bioconjugated InP Quantum Dots.* ACS Nano **2009,** 3 (3), 502-510.
79. Tanaka, A., Hisanaga, A.; Hirata, M.; Omura, M.; Inoue, N and Ishinish, N, *Pulmonary toxicity of indium arsenide and arsenic selenide following repeated intratracheal instillations to the lungs of hamsters.* Applied Organometallic Chemistry, 1994. **8**(3): p. 265-271.
80. Chibli, H.; Carlini, L.; Park, S.; Dimitrijevic, N. M.; Nadeau, J. L., *Cytotoxicity of InP/ZnS quantum dots related to reactive oxygen species generation*. Nanoscale. 2011, **3**:p. 2552-2559

Chapter II

Synthesis of NIR emitting InP and InP/ZnS NCs

2.1 Introduction

Due to greater transparency of living tissues in the near infrared window (650-900) [1], NIR emitting InP based nanocrystals have great potential in biological imaging applications. Although, accessibility of the NIR emission with InP NCs have been shown by various research groups [2, 3], detailed work exclusively focused on synthesis of NIR emitting InP NCs is still missing. It has been shown that bigger InP NCs with longer emission wavelengths (extending to near infrared region) could be synthesised *via* multiple injections of precursor solutions [2, 4] to the dispersion of smaller InP NCs at high temperatures, often followed by a size selective precipitation step [4]. Recently, our group has introduced an alternative method for synthesis of InP NCs via phosphine gas [5]. Considering the size of the NCs, one of the important aspects of this synthetic scheme is that the PH_3 is slowly and continuously bubbled into the NCs solution similar to multiple injections of precursors. Therefore, the system is well suited for synthesis of larger sized NCs. While the influence of different parameters (e.g. reaction temperature, precursor concentrations, ratio of the different reactants etc.) on the size evolution of nanocrystals was studied with this synthetic approach, the NIR emission from InP and InP/ZnS NCs have not been fully explored. This synthetic scheme has been adapted here with special goals synthesizing NIR emitting InP NCs for biological application. Section 2.2 of this chapter deals with the synthesis and characterisation of the NIR emitting core InP NCs while the section 2.3 focuses on the preparation of NIR emitting InP/ZnS core/shell nanostructures with high quantum yield in organic medium. Finally, experimental details are provided in the last section (cf. 2.4)

2.2 InP nanocrystals

2.2.1 Synthesis of InP NCs using PH_3 gas a phosphorous precursor

Synthesis of NIR emitting InP NCs is based on the reaction of *in situ* generated PH_3 gas with indium acetate in presence of myristic acid in 1-octadecene reported by our group [5]. The two steps of the chemical reactions leading to InP formation are shown in a simplified way in equations 2.1a and 2.1b:

$$\text{Step I: } 3H_2SO_4 + Zn_3P_2 \rightarrow 2\ PH_3 + 3Zn^{2+} + 3\ SO_4^{2-} \quad (2.1a)$$

$$\text{Step II: } PH_3 + In(CH_3COO)_3 \rightarrow InP + 3\ CH_3CO_2H \quad (2.1b)$$

The reaction has been slightly modified from its original reported form. First, the reaction was optimized by replacing highly air-sensitive Ca_3P_2 with Zn_3P_2 as the phosphorous source. Second, zinc stearate is added in the Indium precursor solution. Indeed, the InP NCs synthesized without zinc carboxylates have extremely poor photoluminescence efficiency and the band edge emission is often not detectable at room temperature. The reaction setup for synthesis of NIR emitting InP NCs is shown in Figure 2.1. The phosphine gas was generated by addition of 1M sulfuric acid into flask A containing certain amount of Zn_3P_2 powder. The evolved gas is subsequently bubbled into flask B containing a mixture of Indium acetate and myristic acid (MA) in 1-octadecene (ODE) with the help of the carrier gas Argon. The molar ratio of In:MA is fixed to 1:3 based on earlier studies [5]. The temperature inside the flask during the course of the reaction was monitored with a sensor.

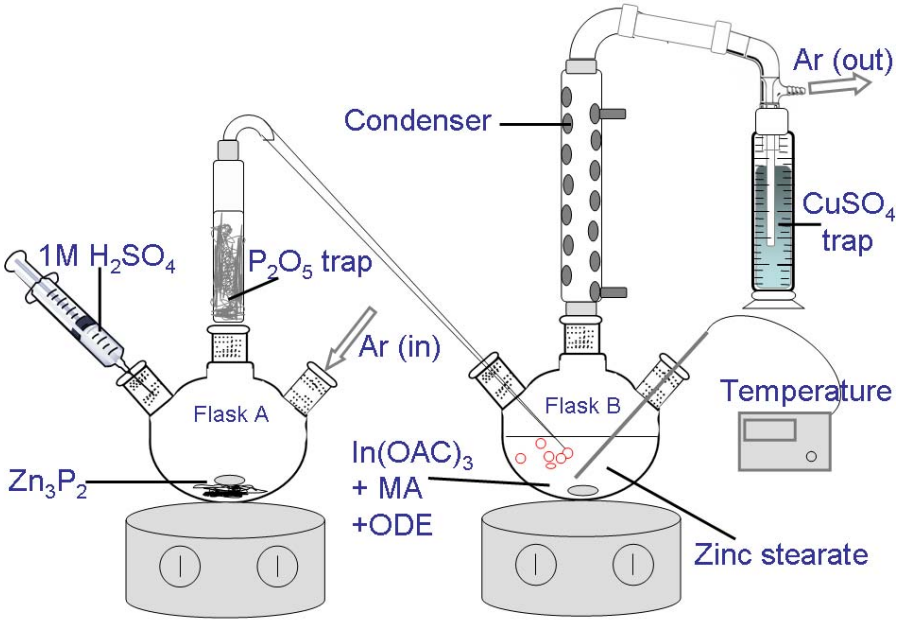

Figure 2.1 Set up for synthesis of InP NCs based on the reaction of *in situ* generated PH_3 gas with indium myristate.

PH_3 gas is dried on a P_2O_5 column before injecting to the Indium precursor solution in flask B. Another trap containing a saturated aqueous solution of $CuSO_4$ was connected via a condenser to flask B in order to neutralize unreacted phosphine gas. Cu^{2+} ions react with PH_3 gas to form Cu_3P_2 evidenced as a black precipitate. Within 2 minutes of phosphine gas introduction the solution in flask B changed from transparent to red and became darker with growing size of the NCs. The reaction is stopped after 60 minutes as no further change of the absorption and emission spectra could be detected for longer heating times.

2.2.2 Study of different reaction parameters

2.2.2.1 P:In molar ratio

Larger sized InP NCs (>4 nm) were obtained using an excess of the phosphine precursor (Zn_3P_2 in flask A). As shown in Figure 2.2a, the first excitonic peak approaches 700 nm as the P: In molar ratio is increased from 1.6 to 5.8. The corresponding PL spectra with emission maximum at 660, 715 and 747 nm are shown in Figure 2.2.b.

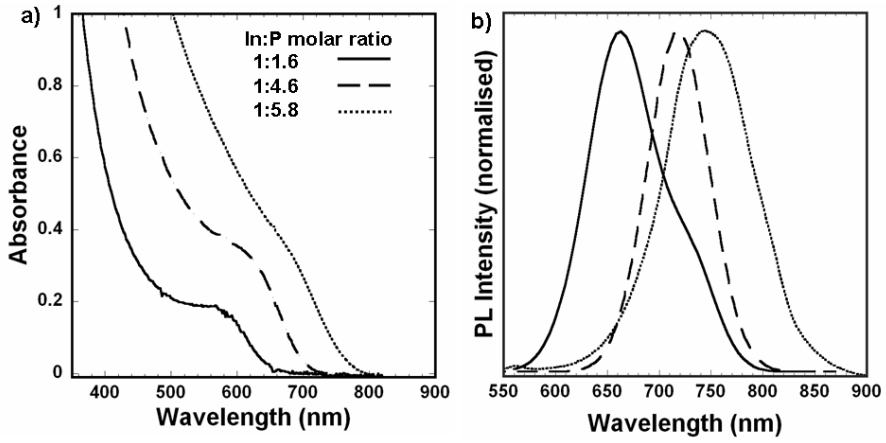

Figure 2.2 (a) Absorption and (b) emission spectra of InP NCs showing the influence of In: P molar ratio on the size of the InP NCs. The In:MA:Zn molar ratio (1:3:0.4) and the reaction temperature are kept constant.

The high amount of Zn_3P_2 (5.8 molar equivalents) increases the concentration of the precursor in the flask above the nucleation threshold and also ensures the continuous supply of phosphine precursor for the growth of the InP NCs, similar to the multiple injections of

precursor solution. In a conventional multiple injection method, the additional injections of precursor are carried out at certain time intervals to promote further growth. This approach, however, bears the risk of new nucleation events when the concentration of the added precursor exceeds nucleation threshold.

2.2.2.2 Addition of zinc stearate

The beneficial effect of zinc carboxylates (e.g. zinc undecylenate [2], zinc stearate [6] and zinc acetate [7]) on InP NCs has been reported by several groups. Nann and co-workers have shown that synthesizing InP nanocrystals in the presence of zinc undecylenate and hexadecylamine dramatically increased the PL efficiency (~30%). They have hypothesized that zinc carboxylate (in combination with hexadecylamine) improves the surface passivation of the InP NCs [2]. A similar observation was reported with zinc acetate and the authors have attributed the PL enhancement to surface etching of InP NCs by the acetic acid originated *in situ* from zinc acetate. On the other hand, recent studies by Thuy *et al.* provide a strong evidence of the formation of In(Zn)P alloy structure through lattice doping of InP by zinc leading to the PL enhancement [6]. In the experiments carried out here with the phosphine gas precursor, the PL efficiency of the InP NCs synthesized without zinc stearate was extremely low (< 0.02 %). The addition of zinc stearate during the synthesis results in a slight improvement of the room temperature PL NCs (up to a QY of ~ 0.5%). Figure 2.3 shows the absorption and emission spectra of the InP NCs synthesised with three different concentrations of zinc stearate. The PL maxima of the NCs synthesized with lower (In:Zn 1:0.4) and higher (In:Zn 1:1) concentration of zinc stearate after 60 minutes of reaction were the same (~747±3 nm). This reveals that there is little effect of zinc stearate on the final size of the NCs, which is in contrast to the observations using single injection methods [2], where $P(TMS)_3$ is injected to the indium precursor solution containing different amounts of zinc carboxylates. The increase in the zinc carboxylate concentrations was found to decrease the NCs size, resulting in the blue shift of the emission wavelength. However, a careful analysis of the absorption and emission spectra of the NCs from the aliquots taken at shorter reaction times reveal that the reaction kinetics seems to be faster in case of a lower amount of the zinc stearate. The PL maxima of the two samples synthesized with In:Zn 1:0.4 and 1:1 at different times of the reaction (2 to 60 minutes) are provided in the table 2.1. Concluding, addition of zinc stearate during the synthesis increased the PL of the InP NCs was by a factor of 25. The red shift of the

emission peak with time is slower for higher zinc stearate concentration, while the same final PL wavelength is attained after 60 minutes.

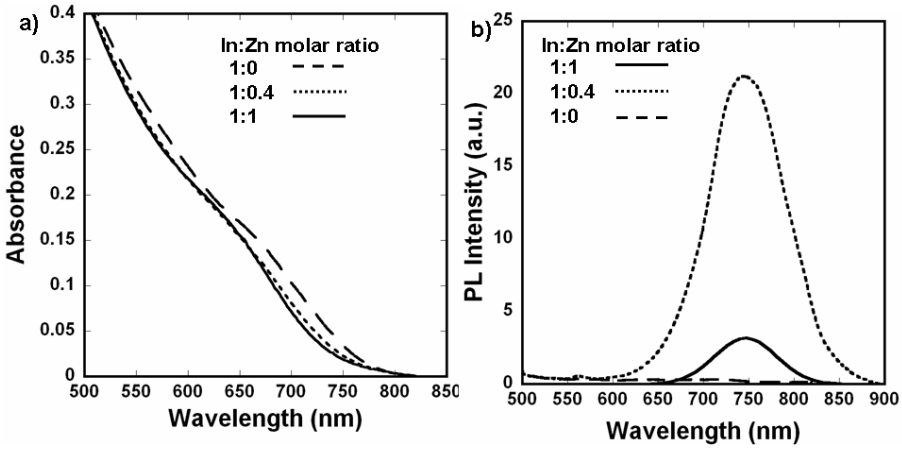

Figure 2.3 (a) UV-Vis and (b) the PL spectra (Excitation: 480 nm) of the three InP NCs samples synthesized using different concentrations of zinc stearate. Reaction time: 60 minutes. The In:MA molar ratio is 1:3 and the In:P ratio is 1:5.8.

In:Zn molar ratio	PL emission (nm)				
	2 min	7 min	15 min	30 min	60 min
1:04	611	691	735	743	747
1:1	538	665	723	736	748

Table 2. 1 Effect of zinc stearate on the PL emission of the InP NCs at different reaction time

2.2.2.3 Addition of hexadecyl amine (HDA)

The use of hexadecylamine during the InP NCs synthesis in combination with Zinc carboxylate is known to increase the PL efficiency of the InP NCs [2]. QY of the InP NCs up to 30% have been reported. While these results were reproducible if performed under same conditions with the reported precursors, similar attempts with the phosphine gas precursor did not improve the PL of the NCs. Figure 2.4 shows the absorption and emission

spectra of the InP NCs synthesised with different combinations of HDA and zinc carboxylate. No PL was detected when only HDA was used (in absence of zinc stearate). Even with combination with zinc stearate the PL QY of the samples were below 1%.

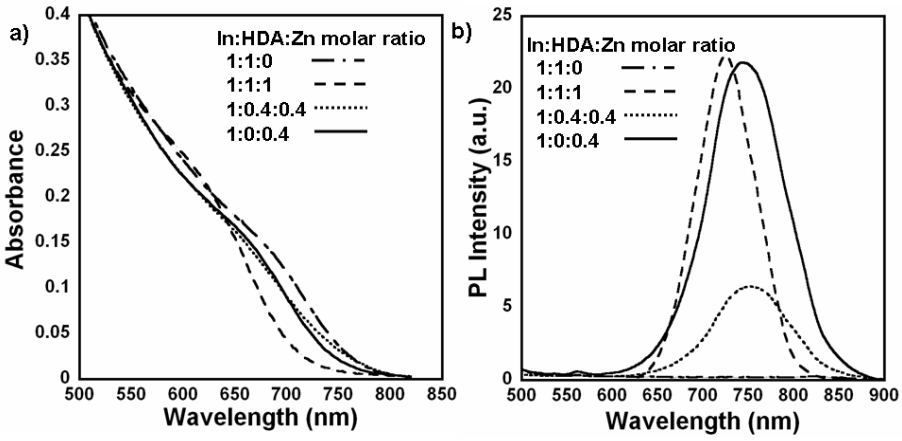

Figure 2.4 (a) UV and (b) PL spectra of the InP NCs samples synthesized under different In:Zn:HDA ratio. Reaction time: 60 minutes.

2.2.2.4 Effect of the temperature to modulate the diffusion rate of the monomers and the reaction between PH_3 and In^{3+}

Figure 2.5a shows the influence of the reaction temperature on the absorption and emission spectra of the NCs. With increase of the reaction temperature a red shift of the first excitonic band was observed. This implies that the larger sized NCs were obtained at higher temperatures. The two factors that are central to the growth process are diffusion of the monomers towards the NCs and the chemical reaction of these monomers with the already formed crystals. High temperatures promote both the rate of diffusion and the reaction of phosphine gas with the indium precursor as predicted by the Gibbs-Thomson and Arrhenius equations respectively. Figure 2.5b shows the corresponding PL spectra. At the highest temperature investigated (285^{o}C) the PL intensity was extremely low. Moreover, a too high temperature leads to Ostwald ripening characterized by poor size distribution and decrease in total concentrations of the nanocrystals.

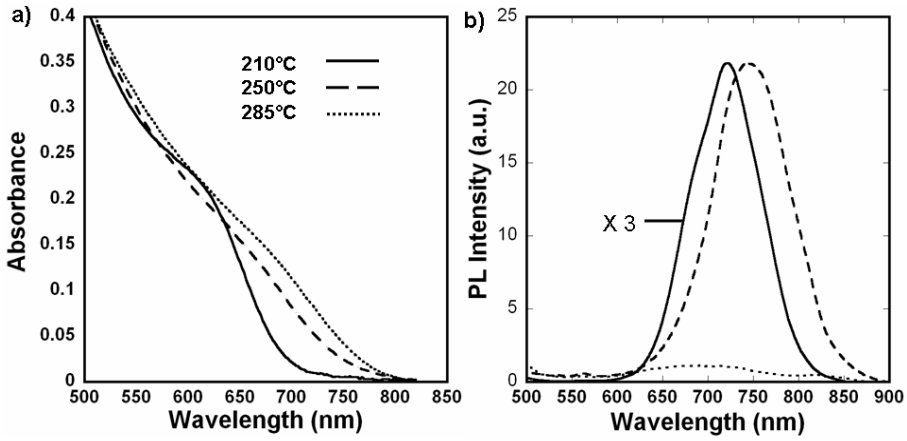

Figure 2.5 (a) Influence of reaction temperature on a) the absorption and (b) PL spectra of the InP NCs synthesised with the molar ratio In:MA:P:Zn of 1:3:5.8:0.4

2.2.2.5 Conclusion

Based on the influence of the different reaction parameters studied above, it was clear that the major factor for the growth of the larger sized NCs was the amount of phosphorus precursor. A certain amount of zinc stearate is important to obtain a detectable PL of the InP NCs core. The optimized synthesis of NIR emitting InP NCs involves the use of In:P:Zn molar ratio of 1:5.8:0.4 without HDA and at the reaction temperature of 250^{o}C. These InP NCs were thoroughly characterized by various physical techniques. The details are presented in the following section.

2.2.3 Characterization of the NIR emitting InP NCs

2.2.3.1 Optical characterization

Figure 2.6a displays the absorption spectrum of the InP NCs after 60 minutes. The absorption spectrum shows the hump around 700 nm, which is attributed to the characteristic first excitonic transition. However, the peak is rather broad compared to the first excitonic peak observed for CdSe NCs or smaller InP NCs [5, 8-10]. Usually polydispersity of the NCs is implicated in the broadening of the absorption and emission peaks. However, for larger sized NCs, especially InP, the absorption peak becomes featureless as the size of the NCs is increased even for the size selected samples of low size dispersion [4]. This is attributed to the overlap of electronic transitions with similar

intensities, which has been observed experimentally [4]. It arises from the narrowing of the spacing of the electronic levels in the conduction and valence band of the NCs with increasing size. The full width at half maximum (FWHM) of the PL spectrum of InP NCs after 60 minutes is 84 nm. The reported FWHM of the PL spectra of InP-based NCs emitting are in the range of 50–100 nm [11]. The growth of the NCs was followed by measuring PL spectra of the aliquots taken at different reaction times. The band edge emission shifts from 615 nm at 2 minutes to 747 nm at 60 minutes.

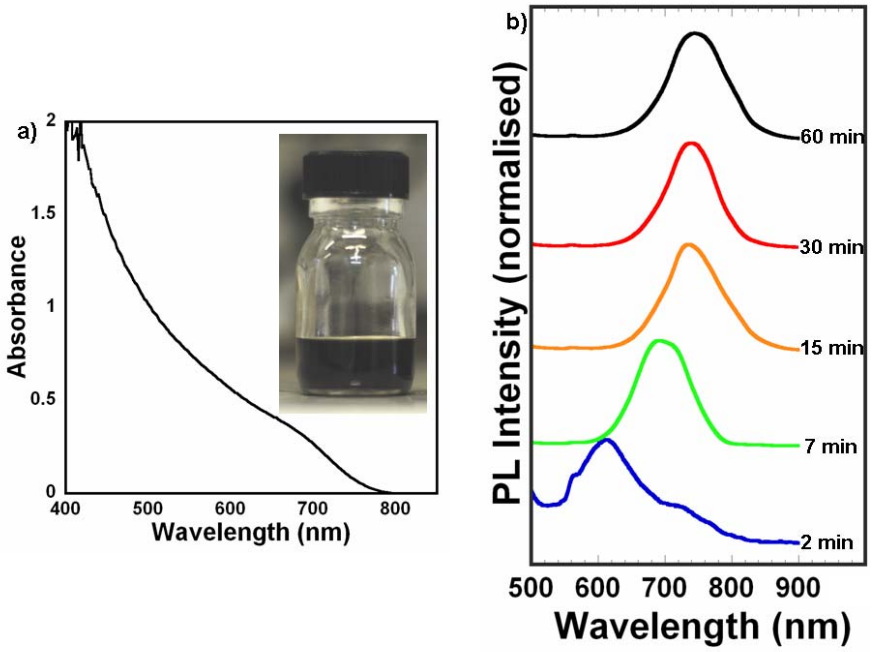

Figure 2.6 (a) UV-Vis spectrum of the 747 nm emitting InP NCs. The inset shows a photograph of the colloidal solution in hexane. (b) Evolution of the PL spectra of the InP NCs with time (vertically shifted for clarity).

2.2.3.2 Structural characterization

The mean size of the 747 nm emitting InP NCs obtained from transmission electron microscope is 4.7± 0.85 nm with size dispersion of ~18% (Figure 2.7a). No size selective precipitation step was performed prior to size measurements. For the size determination (Figure 2.7b) higher resolution images were used to clearly see the border of the NCs

obtained. The values obtained were in agreement with the data reported in the literature correlating the size with the excitonic peak [12]. Lattice fringes arising from zinc blende (111) InP crystal planes are observable in high resolution TEM images (Figure 2.7 c).

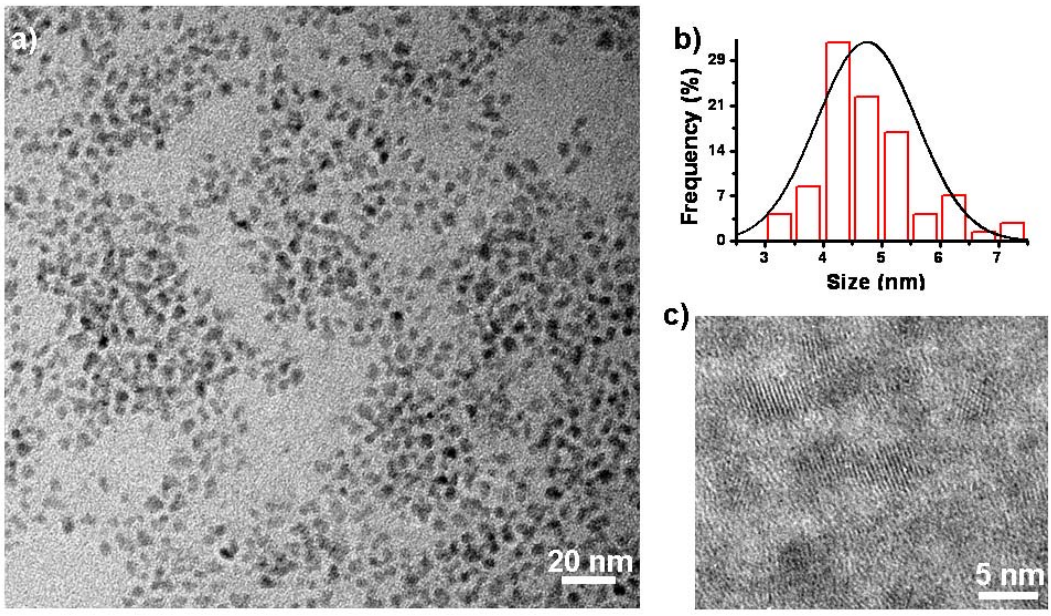

Figure 2.7 (a) TEM micrograph of 4.70± 0.85 nm InP NCs (b) The size distribution curve c) HRTEM image of the same sample of InP NCs.

X-ray diffraction measurements confirm the structure of the InP NCs to be zinc blende. The crystallite size calculated with Scherrer's equation is 3.6 nm, which is lower than the particle size (~4.7 nm) obtained from TEM. The Scherrer's equation estimates the crystallite size (D) (< 100 nm) using equation 2.2:

$$D = \frac{K\lambda}{B\cos\theta} \qquad 2.2$$

where K is the shape factor, λ is the wavelength of the X-ray, B is the full width at half maximum (FWHM) in radians, and θ is the Bragg angle. For our calculation, we use the shape factor of 1.1 which is a theoretical value estimated under the assumption that the crystal is a perfect sphere [13]. Even with the accurate shape factor the Scherrer formula still provides a lower bound on the crystallite size due to contribution of other factors (e.g.

inhomogeneous strain and instrumental effects) to the width of a diffraction peak besides crystallite size. In addition, in our case the significant distribution of size and shape of the NCs contribute to the discrepancy of the crystallite size obtained from XRD and the particle size obtained from TEM. Figure 2.8 (a) compares the XRD spectra of the 747 nm emitting InP NCs with InP NCs synthesized under the same conditions except that no zinc stearate was used during the synthesis. Both of the spectra can be perfectly indexed to zinc blende InP. There is no evidence of the structural modification on the sample when zinc stearate was used during the synthesis. However, this does not rule out the possibility of Zn diffusion into InP lattice. It has been previously reported that, even with dopant concentration as high as 20%, the peak positions in the XRD spectra of the InP NCs still remain unchanged [14]. The Rietveld method was used to fit the measured profile with a theoretical line profile. This technique is usually helpful in resolving the overlapping reflections and phase identification.

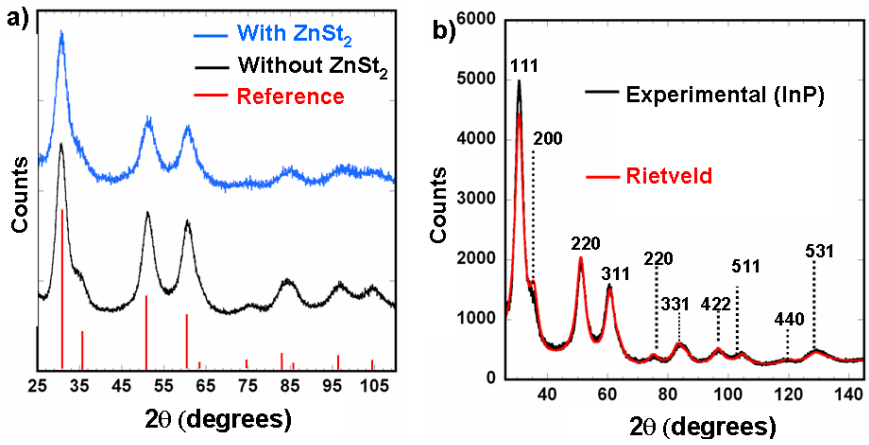

Figure 2.8 (a) Comparison between the X-ray spectra of pure InP NCs (sample 1) and of the InP NCs synthesized in the presence of zinc stearate (sample 2). Red bars indicate the peak positions of reference InP (PDF database number: 04-004-1833). (b) Rietveld refinement and indexation of the diffraction peaks.

2.2.3.3 Elemental composition

The elemental composition of the InP NCs synthesized under various zinc stearate and HDA concentrations was determined by energy dispersive X-ray spectroscopy (EDX). The mean atomic percentages of P and In in InP NCs synthesized without zinc stearate were 48.4 and 51.6 respectively. The sample synthesized under zinc stearate contained about 5 %

of zinc. It should be noted that the samples have to be purified very carefully prior to these measurements (cf. experimental section) in order to remove the adsorbed or free zinc stearate from the NCs. The data indicate that zinc replaces indium as we observe a concomitant decrease of the In content with increasing Zn content. The lattice doping of InP NCs by Zn stearate in situ has already been put into evidence by our group for the colloidal InP synthesized by reaction of indium myristate with $P(TMS)_3$ at elevated temperature (250-300°C) in the presence of Zinc stearate [6] i.e. under similar experimental conditions. Both *ex situ* [15] and *in situ* [16] doping of Zn into InP are known in the literature. However, further studies such as for example XPS are required to conclude about possible lattice doping in our case.

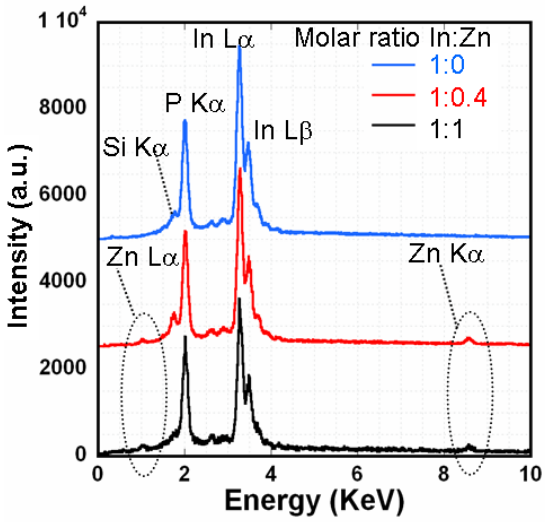

Figure 2.9 EDX spectra of the samples 1, 2 and 3 (Table 2.2)

Sample	In:Zn molar ratio	Atomic percent		
		P % (SD)	In % (SD)	Zn % (SD)
1	1:0	48.4(0.9)	51.6(0.9)	-
2	1:0.4	47.4 (2.4)	47.5(4.4)	5.1(2.6)
3	1:1	48.7(1.5)	46.1(1.3)	5.2 (1.4)

Table 2.2 The elemental composition of the InP NCs synthesized under various ratio of In and Zn. The values are expressed as mean value of atomic percentages obtained with >10 measurements for each sample. SD is the standard deviation of the measurements. Other reaction parameters are same for all the samples.

2.2.4 Conclusion

By using phosphine gas as a precursor InP NCs with band edge emission > 700 nm were synthesized. A high P:In molar ratio is crucial for forming larger sized NCs with longer emission wavelengths. The reaction temperature also has a direct influence on the size and the photoluminescence of the NCs. Within the investigated temperature range (210°C to 285°C) the best results in terms of both size of the NCs and photoluminescence were obtained at 250°C. The room temperature PL could only be detected when the NCs were synthesized in the presence of zinc stearate. The NIR emission wavelengths of the NCs synthesized under various conditions are summarized in Table 2.3:

Sample	**In:Zn:HDA molar ratio**	**Reaction Temperature (°C)**	**PL emission (nm)**
1	1:0:0	250	-
2	1:0.4:0	250	747
3	1:1:0	250	748
4	1:1:1	250	725
5	1:0.4:0.4	250	750
6	1:0:1	250	-
7	1:0.4:0	210	722
8	1:0.4:0	285	-

Table 2.3 Emission wavelength of the InP NCs synthesized under various conditions. For sample 1, 6 and 8 PL could not be measured.

While an emission wavelength up to 750 nm is reproducibly achieved using the phosphine gas route, for application in biological imaging the obtained fluorescence quantum yield below 1% is insufficient. One way to improve the fluorescence efficiencies of InP NCs is treating with HF. However, in view of biological application, growing a shell of another material is desirable. The reason for this is a) an inorganic shell around the core is known to dramatically increase the PL quantum efficiency of the core NCs b) imparts both chemical

and photo stability to the core material by acting as a protective shell around it. In the following section, growth of ZnS shell growth on NIR emitting InP NCs will be addressed.

2.3 NIR emiting InP/ZnS NCs

2.3.1 Introduction

Zinc sulfide (ZnS) was chosen as the shell material for the following reasons: (a) it is a larger band gap material (bulk: 3.6 eV) with type I band alignment (b) the lattice mismatch is not too high (InP/ZnS: 7.6 % compared to CdSe/ZnS: 10.6%) c) chemically stable and (c) it does not contain toxic elements like Cd, Se etc. Haubold and coworkers first reported the growth of ZnS shell on the InP NCs resulting in a PL increase to 15% after 3 days and to 23% after 3 weeks [17]. Recent developments in InP/ZnS core/shell NCs have led to much shorter reaction time with high PL quantum efficiencies [2, 3].

2.3.2 Calculation of the precursor concentration for ZnS shell growth

The amount of precursors needed for desired ZnS thickness was estimated using the correlation between molar extinction coefficient (ε/L mol^{-1}cm^{-1}), diameter of the NCs (D/nm), the bulk crystal parameters such as the density (ρ/kg m^{-3}) and molar mass (m/kgmol^{-1}) and the thickness of one monolayer (d/nm) of ZnS as summarized in the literature. The correlation between size of the NCs and the molar extinction coefficient is given by the following equation 2.3 [12]:

2.3

Once the molar extinction coefficient is calculated, the concentration (C/ mol L^{-1}) of the InP NCs could be determined by UV-Vis spectroscopy using Lambert-Beer's law:

2.4

Where A is the dispersion absorbance (dimensionless) and l is the path length of the used cuvette (cm). Assuming that the InP core NCs to be a sphere of radius (r/nm), the volume

(Vs/nm^{-3}) of the ZnS shell of thickness d (nm) around the core is given by the difference of the volume of the InP/ZnS core/shell and the volume InP core spheres.

$$Vs = \frac{4}{3} \times \pi \times (r + x \times d)^3 - \frac{4}{3} \times \pi \times r^3 \qquad 2.5$$

Where thickness of the ZnS shell is x.d , where x being the number of ZnS monolayers. From this we can calculate the number (Ns) of ZnS monomer units per NC

$$Ns = \frac{\rho \times Vs \times 10^{-27}}{m} \qquad 2.6$$

Finally, the molar quantity of the precursor needed to grow the shell of desired monolayers (ns/mmol) can be calculated using equation 2.8

$$ns = nc \times Ns \qquad 2.8$$

Where nc (mmol) is the molar quantity of the InP NCs core used for the synthesis given by $nc = C \times V$, V being the volume of the colloidal solution (nm^3).

2.3.3 Growth of the ZnS shell on the as-prepared InP NCs

A literature method [3] for preparation of InP/ZnS based on injection of zinc and sulfur precursor at low temperatures (150-220°C) did not yield any substantial PL increase in the case of the obtained NIR emitting InP NCs. Figure 2.10 (a/b) studies the absorption and PL spectra of the as synthesized InP NCs (sample 2) upon addition of appropriate amount of ZnS (zinc stearate and sulfur in ODE) precursors. The zinc stearate and sulfur solution corresponding to 3 monolayer of ZnS shell was slowly injected stepwise (one monolayer at a time) at 150°C and heated at 220°C for 30 minutes before the precursor solution for the next monolayer was injected. However, even after third cycle of injection, the PL QY of the NCs was still below 1% (Fig. 2.10b). In another experiment, zinc ethyl xanthate and zinc stearate were chosen as the precursors for the shell growth [18]. Due to low decomposition temperature of zinc ethylxanthate, it is highly effective for ZnS shell

synthesis. The ratio of Zn:S in zinc ethyl xanthate is 1:4 and therefore zinc stearate is usually added to compensate the shortage of zinc. A calculated amount of ZnS shell precursor corresponding to about 5 monolayers of ZnS was slowly injected to the InP NCs at 230°C over a period of 1h. However, as in the previous case, no substantial improvement of the PL efficiency could be achieved as visible in Fig. 2.10d.

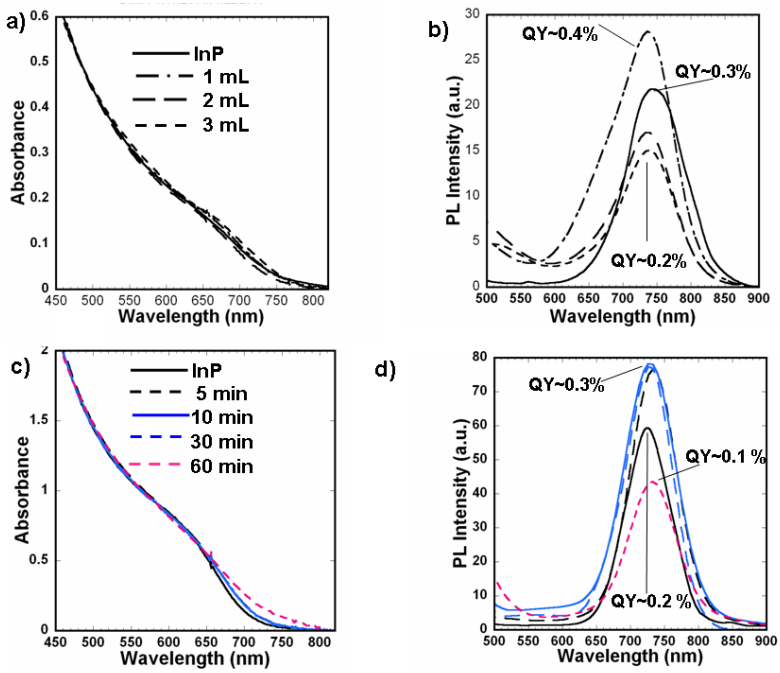

Figure 2.10 Absorption and PL spectra (a and b) of InP NCs (sample 2) after the injection of ZnS precursors (equivalent to 1 to 3 monolayers) performed at 220°C according to a reported protocol [3]. Absorption and PL (c and d) spectra of the InP NCs (sample 4) after the slow injection of ZnS precursor (equivalent to 5 monolayers) at 230^{O}C during 1h. (PL Excitation: 480 nm)

2.3.4Growth of a ZnS shell on InP NCs treated with zinc stearate

The two step synthesis reported by our group was adapted to prepare luminescent InP/ZnS NCs[5]. In the first step, the as synthesized InP NCs was heated with zinc stearate at 280°C, followed by heating with $Zn(EX)_2$ at 210°C. Figure 2.11 shows the absorption and emission spectra of the 747 nm emitting InP NCs (sample 2) during the two step ZnS growth process. Consistent with the earlier reports [5, 7], heating with zinc stearate in the first step already results in dramatic PL increase of the quantum dots (QY~16.5% for sample 2).

Interestingly, a blue shift of the peak maximum to 680 nm was observed while the base of the peak remained stable. The introduction of the sulfur precursor (equivalent to ~5 monolayers of ZnS) led to a slight increase in (QY ~18.5%) accompanied by a red shift (~50 nm) of the peak maximum yielding a final PL wavelength of 730 nm.

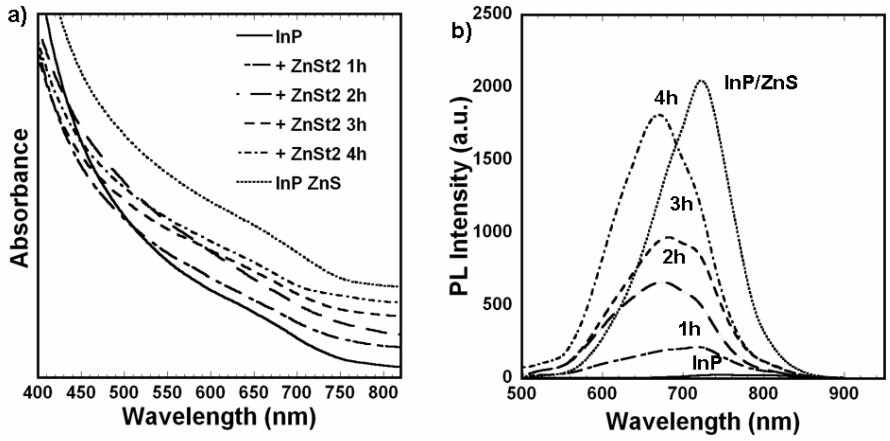

Figure 2.11 a) UV-Vis and b) PL spectra of the InP NCs during the two step ZnS shell growth (excitation: 480 nm). UV-Vis spectra vertically shifted for clarity.

The PL enhancement by addition of zinc stearate was accompanied by a blue shift of peak maximum. Under the prevailing conditions (i.e. high temperature, presence of zinc stearate), the blue shift can result from various factors, including: (a) alloy formation [6, 15] (at 280^{O}C) (b) Surface etching and decrease in NCs size [4, 7] or (c) the dielectric change of the medium [19, 20]. Similar observations were made by Ryu and co workers on heating InP NCs with Zinc acetate [7]. The authors have attributed the blue shift to surface etching by acetic acid, which originates from zinc acetate. They have also drawn an analogy of the role of acetic acid to the etching of InP nanocrystals by HF [4]. An alternative explanation could be the diffusion of ZnS material into InP lattice at 280°C similar to the formation of CdSe/ZnS "interfused" nanocrystals at 300°C reported in the literature [21]. In our case, we attribute the spectra shift upon heating with zinc stearate to a change of the dielectric environment due to the coordination of zinc stearate. A proof for this and against size reduction (*via* etching) comes from the fact that a) after ZnS shell growth the initial emission wavelength in reached again b) no broadening of reflections in XRD diffractogram of the InP NCs treated with zinc stearate was observed and. Moreover, prolonged heating of InP NCs in the presence of ZnS precursor at lower temperature

(200°C) did not lead to a significant PL increase. In accordance with Xu and Nann[2], we propose that the increase of PL intensity originates from the passivation of surface P atoms dangling bonds by zinc stearate.

2.3.5 Characterization of NIR emitting InP/ZnS NCs

2.3.5.1 Optical characterization

Figure 2.12 shows the absorption and emission spectra of the as synthesized and size selected fraction of InP/ZnS NCs. The FWHM the as prepared InP/ZnS NCs is 95 nm with emission maximum at 730 nm and fluorescence quantum yield of 18%. A low intensity shoulder in the red region of the spectrum (~700 nm) was observed (Fig. 2.12b). This hump disappears upon size selective precipitation indicating that it may have come from size distribution. The size selective precipitation is performed by adding a non-solvent (methanol) into the InP NCs dispersed in chloroform (cf. experimental section). Figure 2.14 compares the InP/ZnS NCs before and after the size selection step. The FWHM the size selected InP/ZnS NCs with emission maximum at 742 nm is 72 nm.

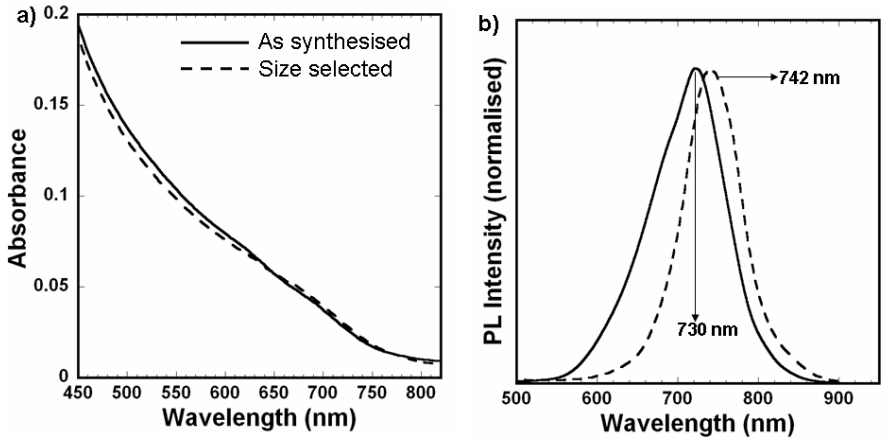

Figure 2.12 Absorption (a) and emission spectra (b) of the NCs before and after the size selective precipitation step.

2.3.5.2 Structural characterization

In TEM (Fig. 2.13) a small increase of the mean size was observed between the core (4.70±0.85 nm) and the core/shell NCs (5.16±0.86 nm). This increase of size corresponds to 1-2 monolayer(s) of ZnS shell (thickness of a monolayer: 0.31 nm) [22]. Calculation for the InP NCs (5.7 nm) coated with two monolayers of ZnS, results in In:P:Zn:S atomic ratio of 1:1:1.3:1.3. The EDX measurements (Fig 2.14b) reveal that atomic percentages of In, P, Zn and S are respectively 18.69, 23.79, 28.12 and 29.4 which means Zn/In and S/P ratio in the sample are respectively 1.5 and 1.23. Taking into account the size and shape distribution of the NCs these results are in fair agreement with the expected values from the TEM results.

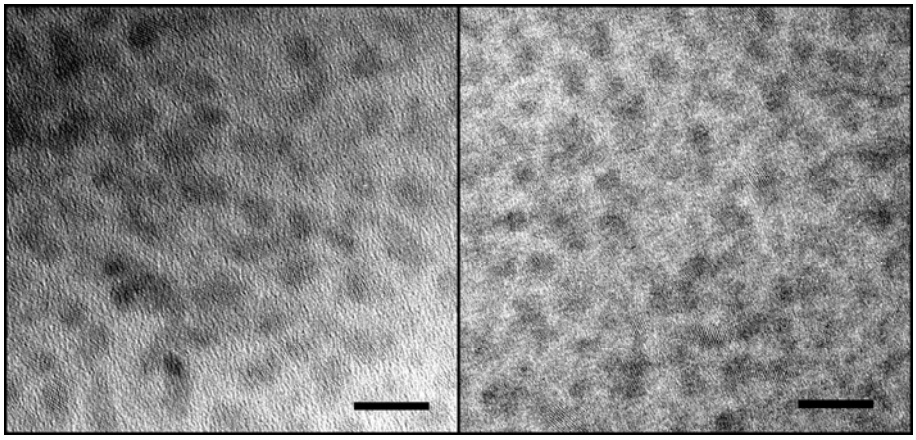

Figure 2.13 TEM micrograph of the 4.70±0.85 nm emitting InP core (right) and the corresponding 5.16±0.86 nm InP/ZnS core/shell (left) NCs. The scale bar is 10 nm for both the images.

The InP/ZnS NCs were further characterized using powder X-ray diffraction. Figure 2.13a shows the X-ray diffractogram of purified InP/ZnS NCs compared with the corresponding core InP NCs. A clear shift of the peaks for characteristic zinc-blende InP towards those of cubic ZnS is observed. The major peaks (e.g. 111 at 33.3°, 220 at 55.8° and 331 at 66.5°) arising from ZnS can easily be identified.

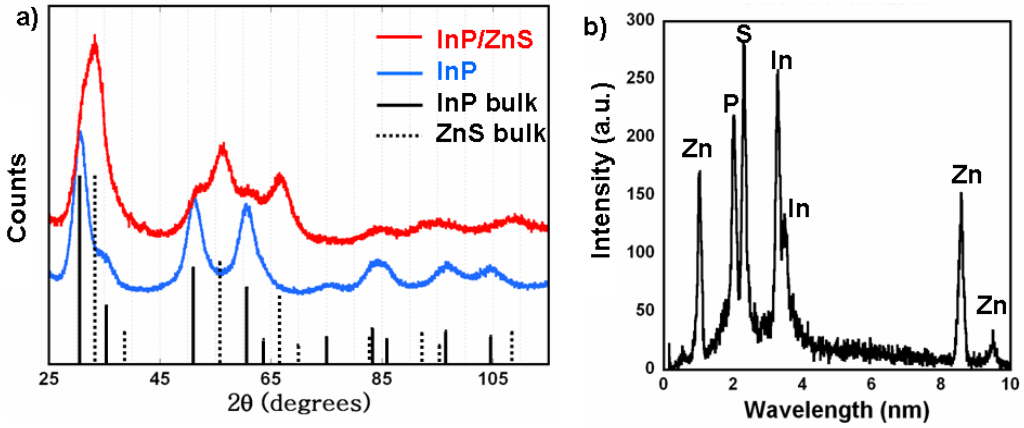

Figure 2.14 (a) X-ray diffractogram of InP/ZnS core/shell NCs compared with core InP NCs (same sample as in Fig 2.11). (b) EDX spectrum of the InP/ZnS NCs.

2.3.6 Conclusion

In the case of NIR emitting InP NCs synthesized using the phosphine precursor the adaptation of usual routes for the ZnS shell growth were not successful in terms of increase of PL quantum yield. As an alternative, a two step process first by heating the as synthesized InP NCs with zinc stearate and then introducing the sulfur precursor was developed. NIR emitting InP/ZnS NCs (720-750 nm) with quantum yield up to ~18% at room temperature were obtained using this approach. The samples are suitable for the aimed biological applications. In the next chapter, their transfer to the aqueous phase will be described.

2.4 Experimental section

2.4.1 Chemicals

Except for zinc stearate (90%, Riedel de Haën), zinc phosphide (≥19.4 % active phosphor, Riedel de Haën) and zinc ethyl xanthate (>90%, synthesized following reference 13), all reagents and solvents were purchased from Sigma Aldrich and used as received: indium acatate (99.99%), myristic acid (>99%), 1-octadecene (90%), hexadecyl amine (98%), stearic acid (>99%), N,N-dimethylformamide (anhydrous, 99.8%) and dioctylamine (≥97%).

2.4.2 InP NCs synthesis

Sample 2

0.072 g (0.248 mmol) of Indium acetate, 0.069 g (0.1 mmol) of Zn stearate and 0.17 g (0.75 mmol) of myristic acid were mixed in 20 g (80 mmol/25 mL) of 1-octadecene (ODE) in a 50 mL three necked flask (B). The mixture is heated to ~120°C to obtain a clear solution. The flask is then degassed for 1 h under vacuum (~3. 10^{-2} mbar). During this step the solution is stirred magnetically at 600 rpm. Simultaneously, in another flask (A) as shown in the Figure 2.1, 0.45 g (1.74 mmol) of fine powdered Zn_3P_2 is weighed and degassed. Both the flasks are backfilled with Argon. The temperature of flask B is increased to 250°C. 10 mL of 1M H_2SO_4 solution is injected to the flask A to generate phosphine gas and the gas is carried to the flask B by a strong flow of Argon. Within 2 minutes, the solution turns reddish black. Under constant Ar flux, the reaction was continued for 1h.
PL: 747 nm, QY: 0.3 %

Sample 1

Synthesized as above (sample 2), except no zinc stearate is used.
PL: no emission was detectable.

Sample 3

Synthesized as above (sample 2), except 0.158 g (0.2 mmol) of zinc stearate was used instead of 0.069 g (0.1 mmol).
PL emission: 748 nm, QY: 0.04 %

Sample 4

0.0720 g (0.248 mmol) of indium acetate, 0.1074 g (0.25 mmol) of zinc undecynelate, 0.120 g (0.5 mmol) of hexadecylamine and 0.0712 g (0.75 mmol) of stearic acid are mixed in 20 g (80 mmol) of 1-Octadecene (ODE) in a 50 mL three necked flask (B). The rest of the reaction is the same as for sample 2.
PL: 725 nm, QY: 0.2 %

Sample 5

Synthesized as above (sample 2), except 0.158 g (0.2 mmol) of zinc stearate is used instead of 0.069 g (0.1 mmol).

PL: 753 nm, QY: 0.06 %

Sample 6

Synthesized as sample 2, except that 0.072 g (0.2 mmol) of hexadecylamine is used instead of 0.069 g (0.1 mmol) zinc stearate.

PL: no emission detectable

Sample 7

Synthesized as above (sample 2), except that the reaction was performed at 210°C for 1h.

PL: 722 nm, QY: 0.1%

Sample 8

Synthesized as sample 2, except that the reaction is performed at 285°C for 1h.

PL: no emission detectable

2.4.3 InP/ZnS NCs synthesis

2.4.3.1 Growth of ZnS shell on the as-prepared InP NCs

Method 1

10 mL of 0.1 M zinc stearate and 0.1 M sulfur solution (precursor solution) was prepared in degassed ODE. 5 mL (~0.3 µmol) of the as-synthesized 747 nm emitting InP NCs (sample 2) are degassed for 30 minutes under vacuum (~3. 10^{-2} mbar) in a 50 mL three-neck flask connected to the Schlenk line. 0.7 ml of the precursor solution was injected at 150°C and then heated at 220°C with constant stirring at 600 rpm for 30 minutes. This is followed by a second (1 mL) and third injection (1.2 mL) after 30 minutes of interval.

PL: 737 nm, QY: 0.18%

Method 2

11 mL (~0.3 µmol) of the as-synthesized 725 nm emitting InP NCs (sample 4) were degassed for 30 minutes under vacuum (~3. 10^{-2} mbar) in a 50 mL three neck flask connected to the Schlenk line. 0.79 g (1.25 mmol) of zinc stearate and 0.095 g (0.31 mmol)

of zinc ethylxanthate are dissolved in 6 mL dioctylamine and injected into the flask containing InP NCs at 230°C. Rate of injection: 6 mL/hr
PL: 731 nm, QY: 0.1%

2.4.3.2 Growth of ZnS shell on the InP NCs treated with zinc stearate

11 mL (~0.3 µmol) of the as-synthesized InP NCs (sample 2) were mixed with 0.79 g (1.25 mmol) of zinc stearate (in 3 mL ODE) and the mixture is degassed for 30 minutes under vacuum (~3. 10^{-2} mbar). The mixture is then heated to 280°C with constant stirring at 600 rpm for 4hrs. 0.095 g (0.31 mmol) of zinc ethylxanthate (in a mixture of 0.2 mL dimethylformamide (DMF), 1 mL of ODE and 1 mL of toluene) is slowly injected into the solution slowly (rate of injection: 4.4 mL/h) at 210°C.
PL: 730 nm, QY: 18%, FWHM: 96 nm

2.4.4 Work up

Method 1 (Fig. 2.15)

10 mL of as synthesized InP/ZnS NCs in ODE are precipitated by adding an excess of acetone (30 mL). The precipitate is filtered through a filtration column with a glass filter 63. The solution is heated during the filtration (40-50°C) to dissolve the excess of zinc stearate in acetone.

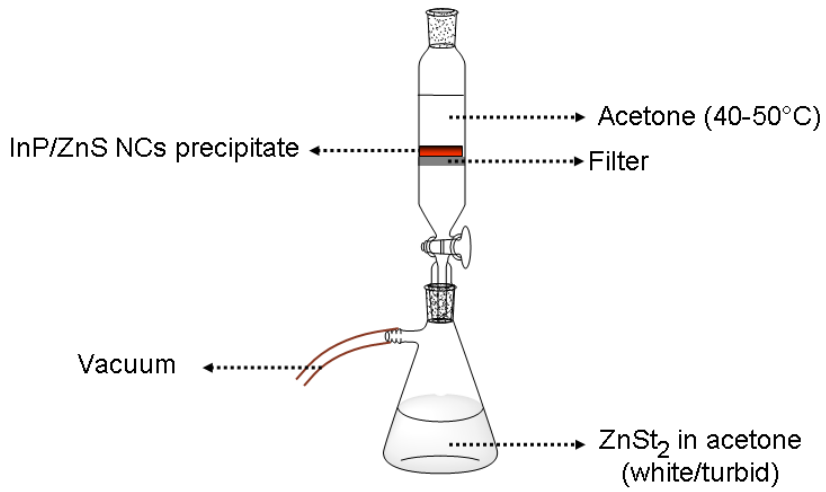

Figure 2.15: Diagram of filtration set-up using suction.

Method 2 (Fig. 2.16)

5 mL of InP/ZnS NCs are mixed with 15 mL of anhydrous acetone and the mixture is centrifuged at 1000 rpm for 5 minutes. The precipitate is dispersed in 5mL of anhydrous hexane and centrifuged at 2800 g for 1 minute. The excess of zinc stearate, which is insoluble in hexane precipitates, while InP/ZnS NCs remain in the solvent as a stable sol. A fraction of bigger NCs may settle down along with zinc stearate in this step. Therefore, the last step is repeated 2-3 times until the precipitate is free of NCs (indicated by the white color of zinc stearate).

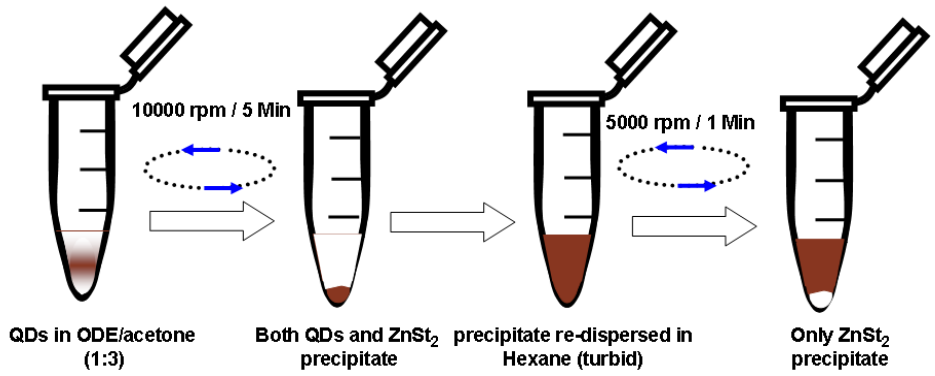

Figure 2.16: Scheme depicting the purification by centrifugation.

2.4.5 Size selective precipitation

Around 3 mg of purified 730 nm emitting InP/ZnS QDs are dissolved in 2 mL of chloroform, subsequently anhydrous methanol is added dropwise under stirring until the solution becomes slightly turbid. The fraction of precipitated QDs is collected by centrifugation (4 min, 1792 g). This procedure is repeated 3 times to collect fraction containing the larger sized NCs.

2.5 References

1. Weissleder, R., *A clearer vision for in vivo imaging.* Nature Biotechnology, 2001. **19**(4): p. 316-317.
2. Xu, S., J. Ziegler, and T. Nann, *Rapid synthesis of highly luminescent InP and InP/ZnS nanocrystals.* Journal of Materials Chemistry, 2008. **18**(23): p. 2653-2656.
3. Xie, R., D. Battaglia, and X. Peng, *Colloidal InP Nanocrystals as Efficient Emitters Covering Blue to Near-Infrared.* Journal of the American Chemical Society, 2007. **129**(50): p. 15432-15433.
4. Talapin, D.V., N. Gaponik, H. Borchert, A.L. Rogach, M. Haase, and H. Weller, *Etching of Colloidal InP Nanocrystals with Fluorides: Photochemical Nature of the Process Resulting in High Photoluminescence Efficiency.* The Journal of Physical Chemistry B, 2002. **106**(49): p. 12659-12663.
5. Li, L., M. Protière, and P. Reiss, *Economic Synthesis of High Quality InP Nanocrystals Using Calcium Phosphide as the Phosphorus Precursor.* Chemistry of Materials, 2008. **20**(8): p. 2621-2623.
6. Thuy, U.T.D., P. Reiss, and N.Q. Liem, *Luminescence properties of In(Zn)P alloy core/ZnS shell quantum dots.* Applied Physics Letters. **97**(19): p. 193104-3.
7. Ryu, E., S. Kim, E. Jang, S. Jun, H. Jang, B. Kim, and S.-W. Kim, *Step-Wise Synthesis of InP/ZnS Core-Shell Quantum Dots and the Role of Zinc Acetate.* Chemistry of Materials, 2009. **21**(4): p. 573-575.
8. Li, L. and P. Reiss, *One-pot Synthesis of Highly Luminescent InP/ZnS Nanocrystals without Precursor Injection.* Journal of the American Chemical Society, 2008. **130**(35): p. 11588-11589.
9. Xu, S., S. Kumar, and T. Nann, *Rapid Synthesis of High-Quality InP Nanocrystals.* Journal of the American Chemical Society, 2006. **128**(4): p. 1054-1055.
10. Battaglia, D. and X. Peng, *Formation of High Quality InP and InAs Nanocrystals in a Noncoordinating Solvent.* Nano Letters, 2002. **2**(9): p. 1027-1030.
11. Dieu,U. T., T. P. Thi, L. N. Quang, L. Liang, and P. Reiss, *Comparative photoluminescence study of close-packed and colloidal InP/ZnS quantum dots.* Applied Physics Letters. **96**(7): p. 073102.
12. Reiss, P., M. Protière, and L. Li, *Core/Shell Semiconductor Nanocrystals.* Small, 2009. **5**(2): p. 154-168.
13. Patterson, A.L., *The Diffraction of X-Rays by Small Crystalline Particles.* Physical Review, 1939. **56**(10): p. 972.
14. Xie, R. and X. Peng, *Synthesis of Cu-Doped InP Nanocrystals (d-dots) with ZnSe Diffusion Barrier as Efficient and Color-Tunable NIR Emitters.* Journal of the American Chemical Society, 2009. **131**(30): p. 10645-10651.
15. Yoon, K., Y. Lee, D. Yeo, and S. Kim, *The characteristics of Zn-doped InP using spin-on dopant as a diffusion source.* Journal of Electronic Materials, 2002. **31**(4): p. 244-247.
16. Montie, E.A. and G.J. van Gurp, *Photoluminescence of Zn-diffused and annealed InP.* Journal of Applied Physics, 1989. **66**(11): p. 5549-5553.
17. Haubold, S., M. Haase, A. Kornowski, and H. Weller, *Strongly Luminescent InP/ZnS Core–Shell Nanoparticles.* ChemPhysChem, 2001. **2**(5): p. 331-334.
18. Protière, M. and P. Reiss, *Facile synthesis of monodisperse ZnS capped CdS nanocrystals exhibiting efficient blue emission.* Nanoscale Research Letters, 2006. **1**(1): p. 62-67.

19. Thuy, U.T.D., N.Q. Liem, D.X. Thanh, M. Protiere, and P. Reiss, *Optical transitions in polarized CdSe, CdSe/ZnSe, and CdSe/CdS/ZnS quantum dots dispersed in various polar solvents.* Applied Physics Letters, 2007. **91**(24): p. 241908-3.
20. Wang, W., G.K. Liu, H.S. Cho, Y. Guo, D. Shi, J. Lian, and R.C. Ewing, *Surface charge induced Stark effect on luminescence of quantum dots conjugated on functionalized carbon nanotubes.* Chemical Physics Letters, 2009. **469**(1-3): p. 149-152.
21. Jun, S. and E. Jang, *Interfused semiconductor nanocrystals: brilliant blue photoluminescence and electroluminescence.* Chemical Communications, 2005(36): p. 4616-4618.
22. Xie, R., U. Kolb, J. Li, T. Basché, and A. Mews, *Synthesis and Characterization of Highly Luminescent CdSe-Core CdS/Zn0.5Cd0.5S/ZnS Multishell Nanocrystals.* Journal of the American Chemical Society, 2005. **127**(20): p. 7480-7488.

Chapter III

Phase transfer of InP/ZnS nanocrystals from organic solvent to aqueous medium

3.1 Introduction

In view of their application in biological imaging, the basic requirements for quantum dots are: a) water solubility b) colloidal stability in physiological pH over an extended period of time c) good fluorescence efficiency d) small hydrodynamic diameter and d) and low non-specific binding in biological environment. The transfer of semiconductor NCs prepared in organic solvents have no intrinsic aqueous solubility and therefore their phase transfer to aqueous medium is an essential step for benefiting from the progress of nanoscience in biotechnology [1-3]. One way to address the issue of colloidal stability is the use of specially designed organic ligands — a strategy that has been extensively applied to gold and silver nanoparticles (NPs). Mono- as well as dithioalkylated polyethylene glycols [4, 5], peptide based ligands [6, 7, 50, 51], phospholipid micelles [8] and amphiphilic polymers[9] have been used with the goal to prevent from particle aggregation after phase transfer. Despite remarkable stability in aqueous environment of various NCs and NPs capped with these engineered ligands, the small amino acid cysteine has recently also drawn strong attention, mainly due to its zwitterionic nature, compact size and commercial availability [10, 11]. Both cationic and anionic ligands exhibit non-specific interactions with serum proteins, resulting in an increased hydrodynamic diameter (D_h). In contrast, NCs coated with these small ligands (e.g. cysteine) have been shown to produce small hydrodynamic diameters (~5-10nm) [10, 11]. For *in vitro* and *in vivo* studies, the compact size of the fluorescent probe can be mandatory. Examples are monitoring the traffic within synapses [12], extravagation of QDs from vasculature[13] and renal clearance observed in mice [11]. In the latter case, very compact (D_h~6nm) cysteine-capped CdSe/CdZnS NCs have been applied [11]. However, these NCs obtained by phase transfer with cysteine at physiological pH (7.4), were found to be stable only 24 hours at 4°C before their precipitation. The colloidal stability could be increased to one week by adding sodium borohydroxide and dithiothreitol (DTT), reducing agents that prevent ligand desorption under disulfide formation [11].

In addition to colloidal stability, phase transferring fluorescent semiconductor NCs into water should also maintain the fluorescence quantum yield (QY) during the transfer reaction. The decrease of QY is commonly reported from both core semiconductor NCs as well as core/shell NCs such as CdSe/ZnS [5, 14], CdSe/ZnCdS [11] and InP/ZnS [15], implying that despite the inorganic shell, the fluorescence properties of the core could still

be influenced by the surrounding environment in solution (e.g. nature of organic capping ligands, pH etc.). Quenching in presence of a protective inorganic shell can be attributed to defects in the shell or to its insufficient thickness [14]. The loss of fluorescence becomes a major issue when dealing with new classes of cadmium-free semiconductor NCs that are not as fluorescent as Cd based NCs, whose QY has been reported to reach almost 100% in organic medium [16-18]. InP/ZnS core/shell nanocrystals, for example, have attracted much attention as alternative to Cd chalcogenide QDs. In this chapter we investigate the phase transfer of InP/ZnS QDs using commercially available small thiolated ligands. In particular the emphasis will be given on colloidal stability, conservation of fluorescence and anti-fouling surface to reduce nonspecific interaction with cells. For all phase transfer agents studied, the deprotonation of the thiol function by appropriately adjusting the pH of the aqueous phase is of prime importance to obtain strong ligand binding to the NCs' surface. The versatility of the approach is demonstrated by successfully phase transferring CdSe nanospheres and nanorods as well as CdSe/CdS nanorods, $CuInSe_2$, $CuInS_2$/ZnS core/shell and CdSe/CdS/ZnS nanocrystals in addition to InP and InP/ZnS NCs. Finally, we elucidate the origin of fluorescence quenching of cysteine-capped QDs, which is related to cysteine dimer (cystine) formation. We further show that penicillamine, a molecule less prone to dimerization than cysteine, constitutes a more suitable transfer agent in view of biological applications.

3.2 Phase transfer

The transfer of NCs synthesized in organic medium to aqueous medium involves exchanging a hydrophobic surface ligand with a hydrophilic molecule containing an appropriate anchor functional group. The ligand exchange of InP/ZnS NCs is achieved by vigorously stirring a biphasic mixture of QDs in chloroform and of the thiol containing ligand in basic aqueous solution (Figure 3.1). Thiol containing molecules are widely used for capping the NCs surface. The driving force of the reaction is the high binding energy of the thiols with ZnS surface as compared to carboxylic acids. Strong bonds between ligand and the NCs surface also provide colloidal stability to the NCs in aqueous medium. The calculated binding energy for thiolated ions to cations at the NCs' surface is much higher than the binding energy of the protonated thiol group. For example, in the case of CdSe, the calculated binding energies in vacuum for the thiolate and the thiol group are 1283 and 34.7 kJ/mol, respectively [19]. Similarly, in case of the shell material zinc sulfide, a relatively

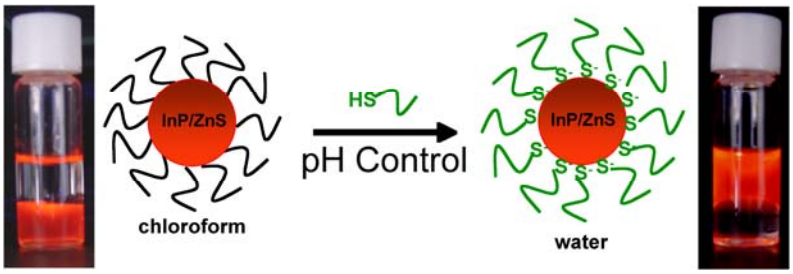

Figure 3.1: Phase transfer of InP/ZnS NCs in presence of a hydrophilic thiolated ligand at a pH conducive for the deprotonation of the thiol group. The photographs show the NCs in chloroform and water respectively before and after the phase transfer under UV light.

high binding energy has been reported for Zn-$S_{thiolate}$ (194.7 kJ/mol) while Zn-S_{thiol} account only for 31,8 kJ/mol, respectively [20]. Since thiolate formation is pH dependent, the control of the pH during the phase transfer is of primary importance. The reaction pH should be chosen high enough (typically 8-11) for the deprotonation of the thiol group. On the other hand basic pH values favour undesired disulfide formation. To determine the optimal pH for the phase transfer reaction, acid-base titration curves were acquired by titrating a 0.2 M solution of various ligands with 0.5 M tetramethylammonium hydroxide, TMAH. The titration curves for the following thiol group containing ligands were measured (Scheme 3.1 and Fig. 3.2): cysteine (Cys), dihydrolipoic acid (DHLA), penicillamine (Pen), thioglycolic acid (TGA), 3-mercaptopropanoic acid (MPA), 11-mercaptoundecanoic acid (MUA). These ligands behave as polyprotic acids due to the presence of multiple acid functionalities. The strongly acidic carboxylic group (-COOH) already dissociates at acidic to neutral pH, where as a sufficiently high pH (8-11) is required to dissociate the –SH group. This simple acid-base titration gives us a direct correlation between thiol dissociation and the pH of the solution. As seen in the titration curves (Fig. 3.2), the successive addition of the strong base TMAH leads to steady increase in the pH of the solution. However, in the pH range where the carboxylic acid group (<pH 4) or the thiol group (>pH 8) of the ligand starts dissociating, the rate of pH increase as a function of base addition is slowed down. As for example, thiol dissociation of TGA starts at ~8.7 resulting in the slowing of pH increase due to the release of protons which

neutralize the added base until ~10.5 when the dissociation is complete and the further addition of TMAH effectively increases the pH. By analyzing the titration curves we determined the pH used for the phase transfer reactions (Table 3.1). The NCs phase transferred with MUA, MPA and DHLA capped NCs were very stable in basic pH (~8-11) i.e. no increase of the hydrodynamic diameter observed for at least 10 weeks while the stability decreased to just a few hours when stored in neutral to acidic pH. On the other hand cysteine, penicillamine and thioglycolic capped NCs were stable in wider range of pHs (~6-10). The NCs transferred with these ligands have negative zeta potential in PBS buffer (pH 7.4).

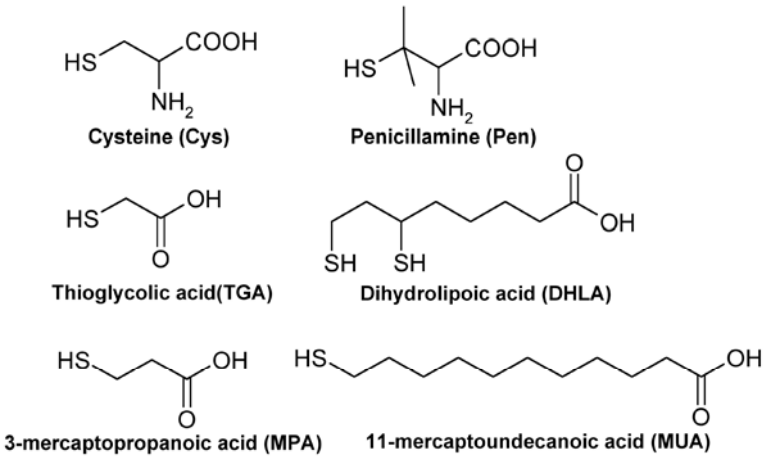

Scheme 3.1: Structures and abbreviations of the used ligands for aqueous phase transfer.

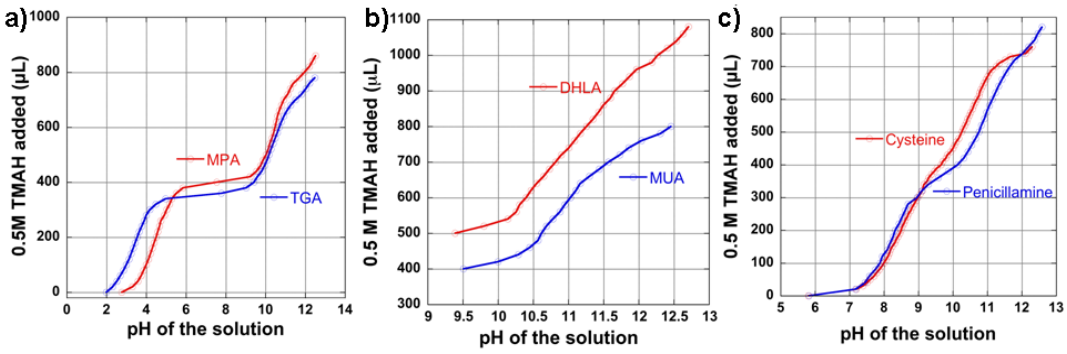

Figure 3.2: Titration curves of (a) 3-mercaptopropanoic acid (MPA) and thioglycolic acid acid (TGA); (b) 11-mercaptoundecanoic acid (MUA) and dihydrolipoic acid (DHLA); (c) L-cysteine (Cys) and D-penicillamine (Pen). A 0.5 M aqueous solution of tetramethylammonium hydroxide

(TMAH) is used as the base during the titration. N.B.: MUA and DHLA are not soluble in acidic or neutral pH range.

An unusually low zeta potential was observed for thioglycolic acid in 1 X PBS. This could be due to the complete degradation of surface thioglycolic acid in basic pH [21]. The breaking of intra ligand –C-S bond of thioglycolic acid on CdTe NCs has been shown experimentally [22]. We also note that cysteine yields significantly lower zeta potential (-22.3 mV) than other ligands whose values are in the range of -32 to -41 mV. The typical ligand: QD ratio during the transfer reaction was ~10^4 to 10^5. Lower ligand: QD ratios (10^3 or 10^2) produced a marked increase of the mean D_h. For example, with 660 nm emitting InP/ZnS NCs, mean hydrodynamic diameter (D_h) values obtained from dynamic light scattering (DLS) measurements were 7.9, 7.5, 9.6, and 10.7 nm respectively, for the ligand:QD ratios of 10^5, 10^4, 10^3 and 10^2 (Table 3.2). Also, the QDs transferred with lower ligand concentration (samples 1 and 2) aggregated during the purification process, indicating incomplete ligand exchange. The simple law of mass action could explain the inefficiencies of the phase transfer process at low ligand concentration. Using a ligand: QD ratio $\geq 10^4$ during the phase transfer reaction, the QDs moved quantitatively from the organic to the aqueous phase within two hours, as could be judged from the colour change of both phases. To assess the efficiency of the transfer process, the transfer yield was calculated for the QDs *after purification*. In fact, the fraction of QDs having an insufficient

Ligand	Thiol pKa	Reaction pH	Transfer Yield (%)	Zeta potential (mV)
DHLA	10.7	11.9	89	-32.4±4.3
Cys	8.35	9.3	60	-22.3 ±0.7
Pen	7.9	9	58	-32.7 ±2.3
TGA	9.78	10.3	74	-10.7 ±1.0
MPA	10.8	11	78	-40.9 ±1.7
MUA	~11	11.6	98	-36.5 ±0.7

Table 3.1: Thiol pK_a values for each ligand, reaction pH used for the phase transfer, transfer yield (amount of QDs in water/amount of QDs in chloroform) and zeta potential measured in in 1X PBS buffer for the phase transferred QDs.

surface coverage with the new hydrophilic ligands could not be redispersed in water of buffer solution. Therefore the transfer yield is always below 100% and depends on the nature of the transfer ligand. More generally it also depends on the bond strength of the original ligands on the NCs' surface which in our case is the same for all the samples. To calculate the transfer yield, the concentration of the sample before and after phase transfer is estimated from the first excitonic peak in the UV-Vis spectra using the empirical correlations between the excitonic peak, size and molar extinction coefficient[23]. The obtained values varied from 58% to 98% for the different ligands (Table 3.1).

Sample No.	[Ligand]/[QD]	Hydrodynamic diameter (nm)
1	100	10.7±1.7
2	1000	9.6±0.8
3	10000	7.5±2.6
4	100000	7.9±1.3

Table 3.2: Hydrodynamic diameter of the NCs transferred using different ligand (penicillamine): QD ratios (TEM diameter ~4 nm).

3.3 Photoluminescence of the phase transferred InP/ZnS NCs

Consistent with earlier reports [1, 5, 11, 24, 25], the phase transfer by means of surface ligand exchange is generally accompanied by a significant decrease of the fluorescence intensity. In Fig. 3.3a the integrated photoluminescence is plotted against absorbance, which gives a direct comparison of the QY by comparing the slopes of the different curves.

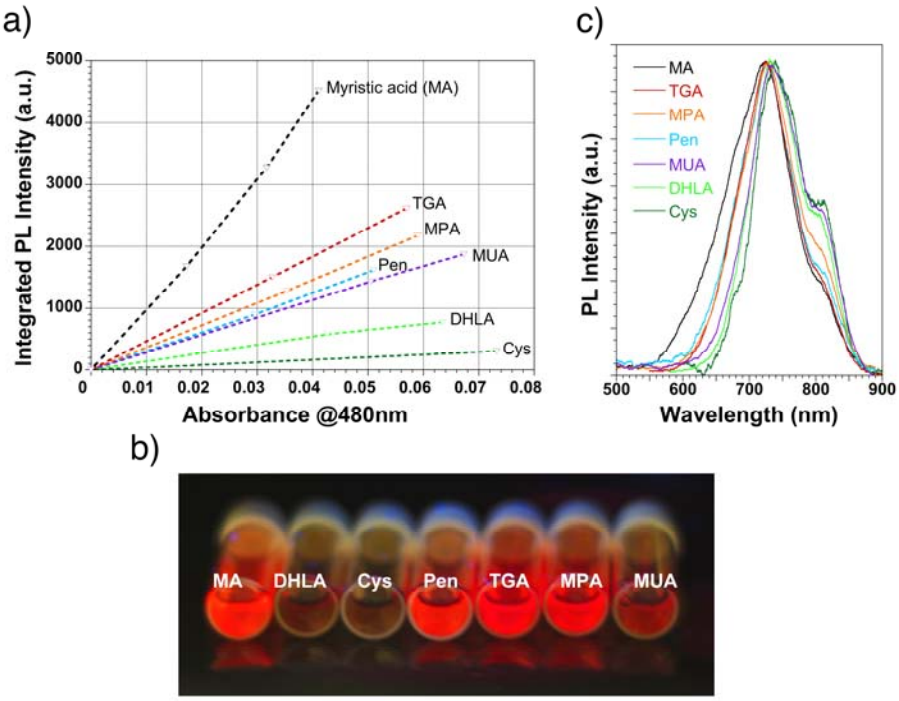

Figure 3.3: (a) Integrated photoluminescence *vs.* absorbance plot for NCs capped with the different ligands in water (TGA, MPA, Pen, MUA, DHLA, Cys) and in hexanes (MA). Absorbance is measured at 480 nm. Straight lines are added to guide the eye. (b) Photograph showing the obtained colloidal solutions under UV light (365 nm). (c) Normalized PL spectra of these samples (λ_{ex} = 480 nm).

In our studies an unusually pronounced quenching was seen in the case of cysteine and DHLA, retaining only around 4% and 10%, respectively. The possible source of this quenching and prevention will be discussed in section 3.4. Penicillamine (retained PL ~30%), TGA (~42 %), MPA (~34%), and MUA (~26%) capped NCs were comparably brighter as can be directly seen when the samples are put under a UV lamp (Fig. 3.3b). Fig. 3.3c shows the normalized PL of the QDs with different ligands in water. A slight red shift was observed (9 nm for MUA, 6 nm for DHLA, 15 nm for cysteine, 3 nm for MPA and 1 nm for TGA), which is attributed to the change of the dielectric environment of the NCs' surface charge [26] and eventually on solvatochromic effects.

3.4 Zwitterionic ligands

Reducing non-specific binding of NCs in biological medium is a major challenge when bio-applications of quantum dots are aimed. Adsorption of serum proteins leads to increase in hydrodynamic diameter of the NCs, complicating the transport and clearance processes. Initially, surfaces coated with self assembled monolayers (SAMs) of polyethylene ethylene glycols have been shown to strongly reduces the adsorption of proteins [27]. Holmlin et al. first showed that the zwitterionic SAMs were equally efficient against nonspecific adsorption of proteins [28]. This concept has been recently extended to quantum dots with enormous success [10, 11, 28]. It has been shown that NCs capped zwitterionic ligands provide an antibiofouling surface [28], making quantum dots averse to non-specific adhesion with cells and serum proteins. Successful renal clearances of the zwitterionic cysteine capped quantum dots have been reported [11]. In addition, the zwitterionic ligand coated NCs have better colloidal stability in neutral to basic pH range due to the presence of positively and negatively charged groups [29]. For these reasons we focused our study in the following two zwitterionic ligands: L-cysteine and D-penicillamine. Both of them are commercially available and share the following features: a) non-toxic b) small size and c) zwitterionic.

3.4.1 Cysteine coated InP/ZnS NCs

Fig.3.4 shows the hydrodynamic diameter of the cysteine capped NCs in 1X PBS buffer at ~pH 7.4 plotted as a function of time. Within the experimental error, during three months no size increase was observed. It is interesting to note that no additional reducing agents such as dithiothereitol (DTT) are added to protect from cysteine oxidation, which has been attributed to trigger NCs' aggregation in earlier reports [11]. The samples have been thoroughly purified by centrifugation method (cf. experimental section) to ensure removal of free ligands.

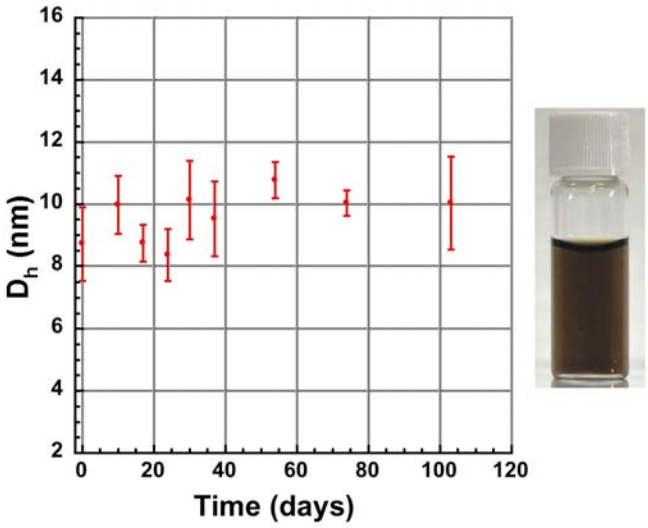

Figure 3.4: Stability of cysteine capped InP/ZnS NCs in 1X PBS buffer illustrated by the evolution of their hydrodynamic diameter as a function of time (TEM diameter 5.1±0.7 nm). Right: photograph of the colloidal solution after three months. The hydrodynamic diameters are measured in number distribution.

However, the dramatic PL quenching of cysteine capped InP/ZnS NCs is a major drawback as far as their bio-applications are concerned. We consistently observed the discussed behaviour for different sized InP/ZnS NCs. As seen in Figure 3.3a, a similar quenching effect was observed with dihydrolipoic acid (DHLA) another transfer ligand [3]. Therefore, it is necessary to identify and eliminate the source of PL quenching at the NC's surface. Seen alone, these results imply that the thickness (~1 nm) and/or quality of the ZnS shell are not sufficient. Both Cys and DHLA are susceptible to oxidation under disulphide formation in a solution of basic pH: in the case of DHLA an intermolecular reaction yielding thioactic acid takes place; in the case of cysteine, its dimer (cystine) is formed. Disulfides, especially cystine, are well known to quench the fluorescence of organic molecules such as tryptophan[30] and tyrosine[31]. Moreover, cysteine efficiently quenches the fluorescence of MPA-capped CdTe QDs at pH > 9.6[32]. The observed quenching has been attributed to hole transfer from the band edge (HOMO) of the QDs to the cysteine/cystine redox energy level. To understand the quenching mechanism in our case, we performed the phase transfer of InP/ZnS NCs with cysteine in presence and absence of tris(2-carboxyethyl) phosphine hydrochloride (TCEP) [33] — a molecule which is used for the selective reduction of disulfide bonds within a wide pH range. Remarkably, in presence of TCEP, 72% of the initial PL QY was retained (Fig. 3.5a/b) with 730 nm

emitting InP/ZnS NCs. The beneficial effect of TCEP on the QY was also observed when the quenched quantum dots (QY<0.5%) were *subsequently* treated with TCEP. Within 2 hours, the fluorescence already increased 5 fold and the maximum increase was 13 fold when the solution was kept in dark at room temperature for 72 hours (Fig. 3.5c). In other words, a substantial fraction of the PL intensity lost during the phase transfer using cysteine at pH ~9, could be recovered by means of the addition of the disulfide reducing agent TCEP. Similarly, the fluorescence efficiency of the "quenched" DHLA capped NCs could be recovered. In all experiments,

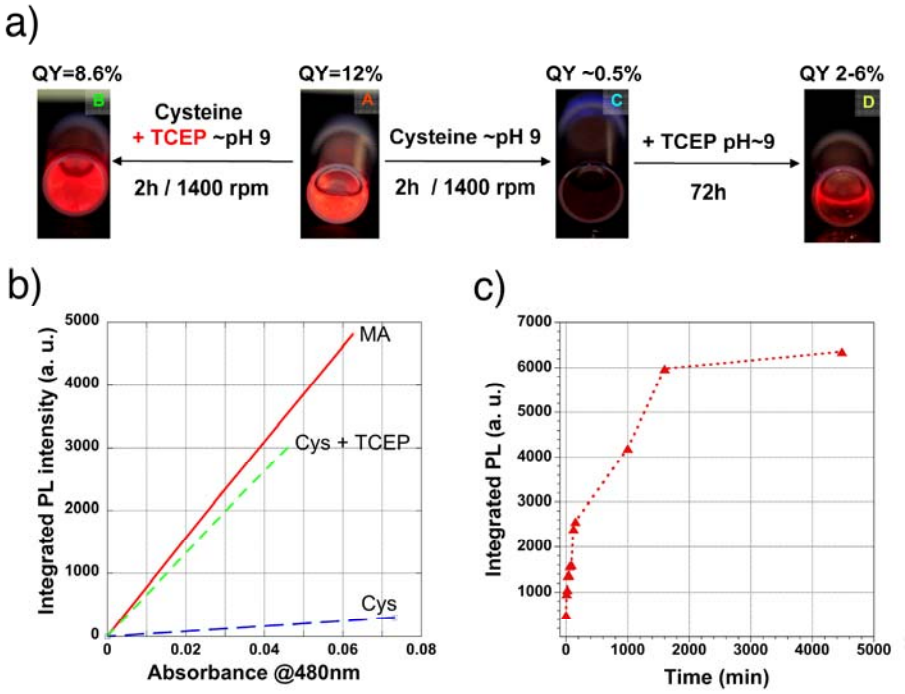

Figure 3.5: a) Phase transfer of InP/ZnS NCs (A) at pH~9 with cysteine in presence (B) and in absence (C) of TCEP; (D) fluorescence recovery by addition of 0.5 equivalents of TCEP (with respect to cysteine). b) Integrated PL intensities as a function of absorbance for the samples A, B and C. c) Evolution of the relative PL intensity with time after TCEP addition (sample D).

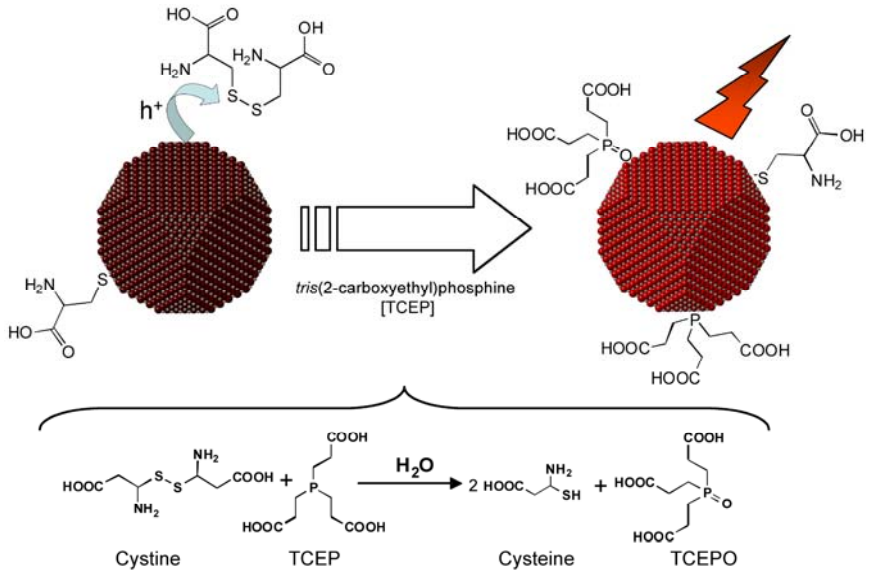

Scheme 3.2: Possible mechanisms taking place in the fluorescence quenching induced by hole (h+) transfer from the QD to cystine and the PL recovery in presence of *tris*(2-carboxyethyl)phosphine (TCEP). In addition of being a reducing agent for cystine, TCEP and its oxidized form TCEPO can also act as nanocrystals' surface ligands.

the pH was kept constant (~9) in order to rule out any pH related changes in the PL emission. The amount of TCEP with respect to cysteine-capped QDs was chosen in a way that even if there was 100% disulfide bond formation, still sufficient TCEP would be present to reduce them. The hypothetical mechanisms occurring during PL quenching and recovery are illustrated in Scheme 3.2: (1) hole transfer from the valence band of InP/ZnS NCs to cystine bound or in proximity to the surface, leading to fluorescence quenching; (2) cystine reduction by TCEP, while TCEP itself gets oxidised to TCEPO [33]. Both TCEP and TCEPO have functionalities (phosphine and phosphine oxide) that are known to passivate the surface of various types of semiconductor NCs, including InP[34] and to improve their photoluminescence efficiency. Depending on the nature of QDs, different ligands show different quenching properties. For example, thiols such as amino ethanethiol or hexanethiol give high quantum yields with CdTe NCs while they quench almost completely the fluorescence of CdSe NCs[35]. This behaviour was attributed to the difference in the energetic position of the valence band of CdTe and CdSe with respect to the thiol redox level – in the case of CdSe, the lower lying valence band edge leads to hole trapping on the thiols. In the other example cited earlier, at pH > 9.6 the addition of cysteine to MPA-capped CdTe NCs led to a pronounced drop in fluorescence [32]. In contrast, no such quenching was observed with homocysteine, a homologue of cysteine

with an additional methylene group. The observed behaviour has been explained by the different energetic position of the HOMO levels of both molecules, lying higher (cysteine) or lower (homocysteine) than the valence band of CdTe [32]. To date, no biological studies with cysteine-capped InP/ZnS NCs have been reported despite the cited advantages of cysteine as a capping ligand of CdSe-based QDs [11]. One of the reasons could be the strong PL quenching of InP/ZnS NCs by cystine, which we have put into evidence here. Although the phase transfer reaction carried out at ~pH 9 with cysteine leads to stable NCs in water, it also favours cystine generation. We propose a twofold solution to this problem: a) the use of TCEP during the transfer with cysteine; b) the use of penicillamine, providing similar properties as cysteine as being bio-compatible, compact and zwitterionic but being less prone to dimerization.

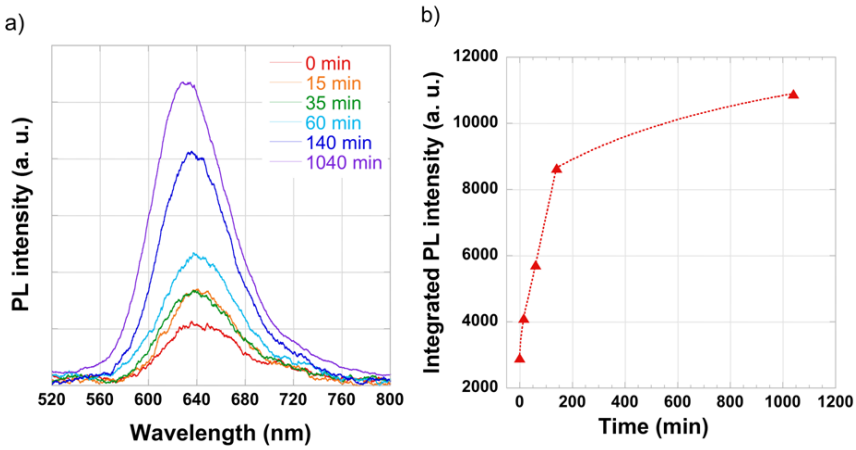

Figure 3.6: Evolution of DHLA-capped ~640 nm emitting InP/ZnS NCs (200 µL, ~5 µM, pH~9) upon addition of 40 µL of a 0.5 M aqueous solution of TCEP (tris(2-carboxyethyl) phosphine) (a) Photoluminescence spectra recorded at different times after TCEP addition (excitation wavelength 480 nm); (b) evolution of the integrated emission intensity with time

We observed the formation of small white crystals on the bottom of the vial when the as transferred NCs were kept for 24 hours without purification and removal of excess cysteine (Fig. 3.7). Interestingly, the NCs themselves had not precipitated. As expected for cystine, the crystals were insoluble in water, alcohol, chloroform and acetone and could only be solubilized in water at higher pH (> 12). ^{1}H NMR analysis unambiguously confirms the cystine formation (Figure 3.7). Cystine is responsible for up to 4% of all kidney stones due to its insolubility at the pH prevalent in the kidneys. Therefore, *in vivo* studies using

InP/ZnS QDs capped with cysteine could possibly result in side effects related to insoluble cystine. Penicillamine, on the other hand, is used in the treatment of cystinurea, a genetic disease caused by accumulation of cystine in the kidneys [36]. In fact, penicillamine-cysteine disulfide has a much higher solubility at near-neutral pH values than cystine.

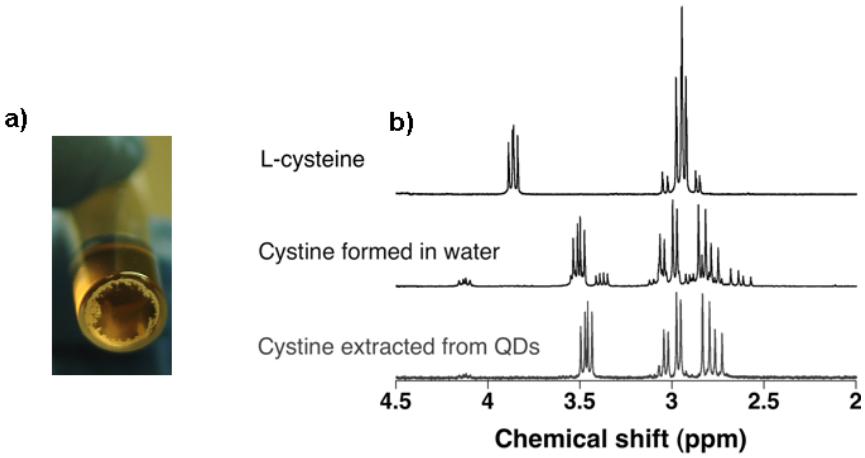

Figure 3.7: a) Cystine formation during 24 hrs storage of cysteine-capped InP/ZnS NCs. b) ^{1}H-NMR spectra of commercial L-cysteine, of cystine formed when keeping a solution of L-cysteine at pH~9 for 24 hrs at room temperature and of cystine recovered from NCs solution after 24hrs. Due to the insolubility of cystine in water at neutral pH, the spectra have been recorded in a D_2O/NaOH mixture at pH 11. The chemical shifts of the methine and methylene protons in L-cysteine account for 3.9 and 2.95 ppm, respectively. In cystine, the signal of the methine protons is shifted to 3.45 ppm and the methylene protons split into two multiplets at 3.0 and 2.78 ppm, respectively, owing to the molecular chirality.

3.4.2 Penicillamine coated InP/ZnS NCs

In contrast to cysteine, penicillamine contains two methyl groups (instead of protons) at the carbon atom in α position to the thiol group. This structural difference has a strong influence on the reactivity of both molecules. In particular, the sterically hindered thiol group in penicillamine makes it less susceptible to oxidation as compared to cysteine. In literature, penicillamine has been used as a capping ligand in the aqueous synthesis of QDs [37] and also as a phase transfer agent at pH 7.4 (PBS buffer) [29]. While the stability of the CdSe/ZnS NCs phase transferred with penicillamine at pH 7.4 was high, a rather

long reaction time (18h) has been reported [29]. On the other hand, by adjusting the pH to 9 we have seen that the phase transfer reaction takes place within 2h or less and after purification and transfer to 1X PBS buffer the product is stable for approximately ten weeks (Fig. 3.8a) before an increase of the hydrodynamic diameter is observed. The typical hydrodynamic diameter obtained for 610 nm (orange), 660 nm (red) and 730 nm (near infrared) emitting InP/ZnS NCs in water were respectively 6.9±1.3, 7.9±1 and 8±0.5 nm (Fig. 3.8b).

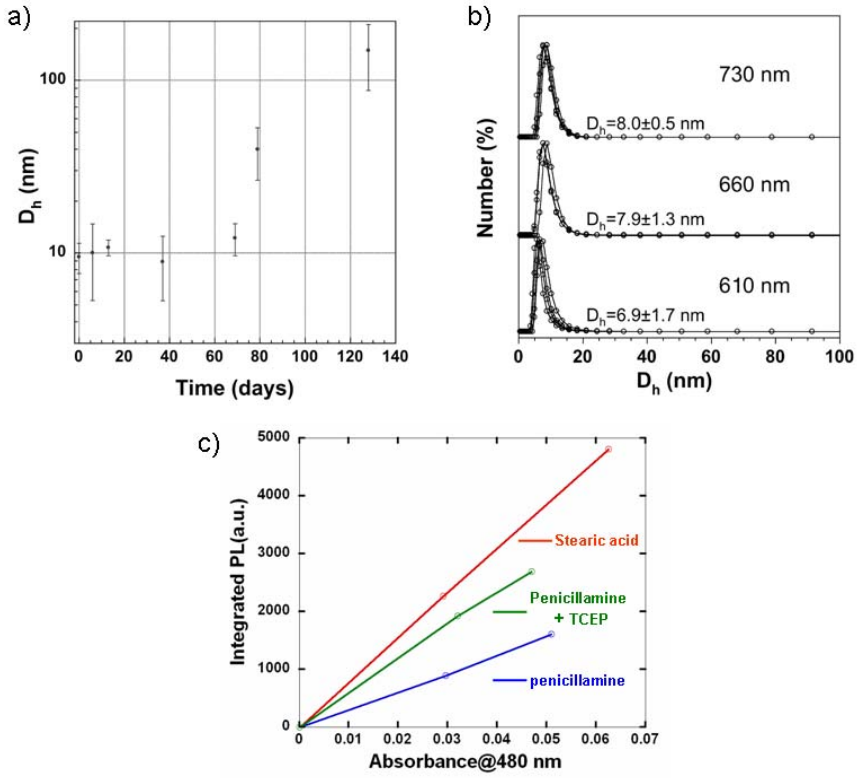

Figure 3.8: a) Hydrodynamic diameter of penicillamine-capped InP/ZnS NCs (emission: 730 nm) in 1X PBS buffer as a function of time. b) Hydrodynamic diameter measurements of 610 nm, 660 nm and 730 nm emitting NCs in water directly after the phase transfer. Multiple runs (> 3) were performed for each sample. C) Integrated photoluminescence *vs.* absorbance plot for the 730-nm emitting NCs in the presence (green) and absence (blue) of TCEP during the phase transfer.

In comparison to cysteine (retained QY 4%), with penicillamine as the phase transfer ligand the retained QY of the same InP/ZnS NCs is around 30-40%. The retained PL quantum yield of the aqueous InP/ZnS NCs could further be improved to ~65% by adding TCEP during the transfer (Fig 3.9c). The maximum retained integrated PL intensities are 45% (emission at 610 nm), 63% (660 nm) and 65 % (730 nm) for the Pen-capped InP/ZnS QDs. In addition to the florescence properties, chirality in QDs induced by optically active ligands such as D-penicillamine (or L-penicillamine) recently has attracted interest. Besides chiral gold [38] and silver nanoparticles [39], the first chiral QDs were reported by Moloney *et. al.* through microwave heating of Cd and Se precursors in the presence of the optically active enantiomers of penicillamine in water [37]. This concept has more recently been enlarged to the aqueous synthesis of chiral CdS nano-tetrapods [40]. The chiral NCs have a high potential for the development of chiral nanosensors and chirooptical devices [41].The purified D-pencillamine capped NCs showed circular dichroism in 1X PBS buffer with a maximum and minimum at 244 nm and 266 nm, respectively, in addition to a peak at 228 nm. The latter one is close to 234 nm, the characteristic peak of D-penicillamine (Fig. 39a/b). Three different models have been proposed to account for circular diochroism (chirality) in NCs: first, inherently chiral cores; second, inherently achiral cores with thiol head groups adsorbed on the surface in a chiral pattern and third, with only chiral adsorbates [42, 43]. In our case we do not know which model applies at the present stage. Obtaining chiral QDs without having to use chiral stabilizing ligands during synthesis has advantages in terms of the ability to choose the NCs' nature, size, and shape.

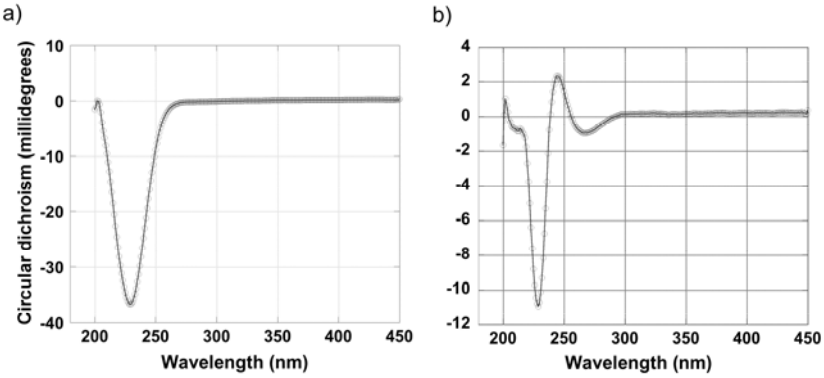

Figure 3.9: Circular dichroism (CD) spectra of (a) D-penicillamine, b) D-pencillamine- capped InP/ZnS QDs in 1X PBS buffer. The QDs are passed through a Nap5 size selective column prior to the measurement.

3.5 Versatility of the phase transfer protocol

In addition to different sized InP/ZnS NCs, the protocol could be successfully applied to InP core NCs, CdSe and CdSe/CdS nanorods, triangular shaped $CuInSe_2$ NCs, and spherical CdSe/CdS/ZnS as well as $CuInS_2$/ZnS core/shell structures without any modification of the procedure (Fig 3.10). The transfer yield was strongly dependent on the initial surface ligands. In the case of NCs already capped with thiols (e.g. $CuInS_2$/ZnS) it was much lower (<30%) than in the case of fatty acid (myristic acid or stearic acid) or amine (hexadecylamine or oleylamine) capped QDs (50-98%).

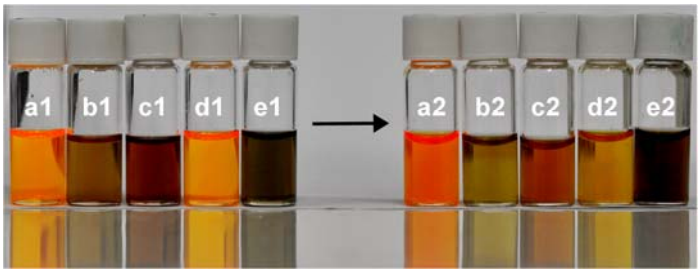

Figure 3.10: Photograph of (a) 6 nm CdSe/CdS/ZnS cores/shell/shell NCs transferred with penicillamine; (b) 7 nm $CuInS_2$ NCs transferred with MUA; (c) 3.5 x 15 nm CdSe nanorods transferred with cysteine; (d) 4 x 32 nm CdSe/CdS nanorods transferred with penicillamine and (e) $CuInSe_2$ (edge length 18 nm) triangles transferred with penicillamine. "1" indicates the samples in chloroform and "2" the corresponding samples in water.

Fig. 3.11 shows the UV-Vis and PL spectra of some samples before and after the phase transfer using different ligands. While in the case of the CdSe based systems the transfer is accompanied by a decrease of the PL intensity without spectral shift, in the case of CIS/ZnS NCs a red shift of ~50 nm was observed. This shift is attributed to the higher sensitivity of the photoluminescence properties of CIS/ZnS to surface modification than the CdSe based NCs. In fact, the emission of the CIS/ZnS NCs is not excitonic recombination but to donor-acceptor pair recombination implying surface related defect states [44].

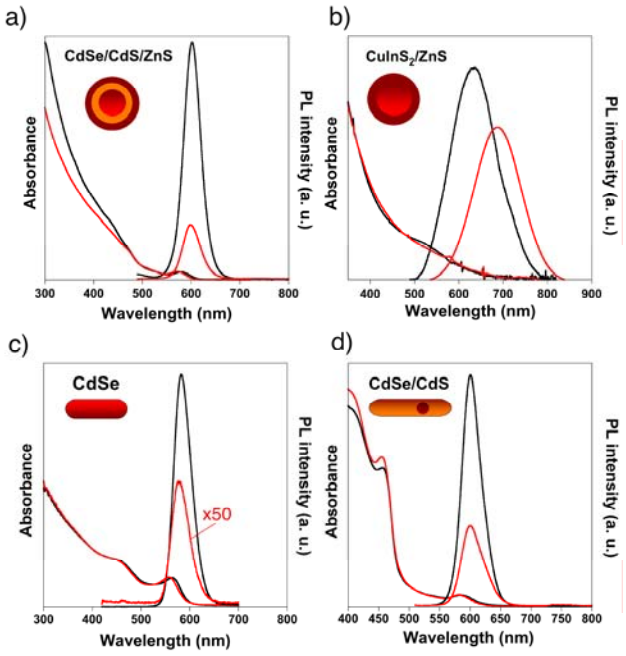

Figure 3.10: UV-Vis and PL spectra of a) ~6 nm CdSe/CdS/ZnS cores/shell/shell NCs capped with penicillamine; b) ~7 nm $CuInS_2$/ZnS core/shell NCs capped with MUA; c) ~3.5x15 nm CdSe nanorods capped with cysteine and d) ~4x32 nm CdSe/CdS nanorods with penicillamine. Red lines: spectra recorded in water, black lines: spectra in organic phase (hexane or chloroform).

3.6 Conclusion

The aqueous phase transfer of colloidal InP/ZnS quantum dots using small hydrosoluble thiols was studied. The deprotonation of the thiol function by an appropriate adjustment of the pH of the aqueous phase to slightly basic values is important to obtain strong binding of the ligand molecules to the NCs' surface. Using this approach cysteine and penicllamine-capped InP/ZnS NCs with a colloidal stability of several weeks in water or buffer solution have been obtained. They combine a low hydrodynamic diameter (<10nm) and potentially low non-specific binding in biological environment due to their zwitterionic coating. The developed strategy can be applied for a large variety of QDs and NPs whose surface atoms have an affinity for thiolates. The formation of cysteine dimer, cystine, has been shown to be at the origin of the significant decrease of the PL efficiency of phase-transferred cysteine-capped InP/ZnS QDs. This phenomenon can be avoided by addition of the reducing agent TCEP during the transfer reaction, and in the best cases more

than 90% of the initial fluorescence intensity can be retained. The obtained hydrosoluble InP/ZnS NCs have a high potential for biological labeling in both *in vitro* and *in vivo* experiments.

3.7 Experimental Section

3.7.1 Materials

D-penicillamine, L-cysteine, thioglycolic acid (98%), 11-mercaptoundecanoic acid (95%), tetramethylammonium hydroxide (97%), phosphate buffered saline solution (1X PBS), 3-mercaptopropanoic acid (99+%), and *tris*(2-carboxyethyl)phosphine hydrochloride solution (0.5M), were purchased from Sigma-Aldrich and used as received. Dihydrolipoic acid was synthesized from thioactic acid following a literature procedure.

3.7.2 Titration of ligands

3.269 g of tetramethylammonium hydroxide pentahydrate was dissolved in 35 mL of degassed MilliQ water (18 MΩ) to prepare a 0.5 M base solution. In a clean glass vial (with cap) 0.2 mmol (Table 3.3) of the ligand is dissolved in 1 mL degassed MilliQ water and the solution is titrated by slowly adding the base solution (10 μL steps) and measuring the pH by a pH meter each time. During the titration, the ligand solution is constantly stirred (at ~200 rpm).

Ligand	**Exact weight (mg[μL])**
DHLA	43.1
Cys	23.9
Pen	30.0
TGA	18.0[13.9]
MPA	21.2[17.4]
MUA	43.6

Table 3.3: Amount of ligand used during the titration. The same quantities of ligand in 1 mL of water (0.2 M solution) have been used for the phase transfer

3.7.3 Phase transfer of QDs

3.7.3.1 Purification

Thorough purification of the initial QDs, enabling the removal of excess hydrophobic ligands is crucial for successful phase transfer. 5 mL of the QDs in organic solvent are mixed with anhydrous ethanol (1:3) and centrifuged at 11200 g (g-force) for 2 minutes. The clear solution of supernatant is discarded and the precipitate is redispersed in 15 mL of 1:3 chloroform:ethanol mixture and centrifuged again. The precipitate is dispersed in a minimum amount of chloroform. The concentration is estimated from the first excitonic peak in the UV-Vis spectrum.

3.7.3.2 Phase transfer

A 0.2 M solution of the ligand is prepared in 1 mL of degassed MilliQ water (18 MΩ) (cf. Table 3.3) and the pH is adjusted to the value specified in Table 3.1 by drop-wise addition of 0.5 M tetramethylammonium hydroxide. This solution is mixed with 1.5 mL (~5 μM) dispersion of QDs in chloroform. The biphasic mixture is stirred vigorously at ~1400 rpm for 2 h.

3.7.3.3 Phase transfer in presence of TCEP

The same procedure as before is applied with the difference that the ligand solution is constituted of 500 μL of a 0.2 M solution of the transfer ligand and 100 μL of a 0.5 M TCEP solution, mixed with 1 mL of ~5 μM dispersion of QDs in chloroform.

3.7.3.4 Work up

Depending on the nature of the initial ligands on the QDs surface in organic media, at the end of the reaction the biphasic mixture can result in the clear separation of two phases or in an emulsion. In the latter case, the mixture is centrifuged at lower speed (4,032 g) for 1 min to obtain a clear phase separation. The QDs in the (upper) aqueous phase are separated from the (lower) organic phase.

3.7.3.5 Purification and storage

Method A

200 µL of the QDs in water are centrifuged in a Millipore centrifugal filter from VWR (MWCO 30k) at 11,200 g for 2 min. 200 µL of 1X PBS buffer (pH 7.4) or MilliQ water are added to the pellet and the QDs are redispersed in 200 µL 1X PBS buffer or MilliQ water (pH ~7) and stored in a fridge (~4°C). The typical storage concentration is ~10 µM.

Method B

A Nap5 size exclusion column from GE-Biosciences is vertically clamped. It is equilibrated by running ~10 mL of 1X PBS buffer which corresponds to the three refills of the column. The buffer is allowed to completely enter the gel bed by gravity flow. 500 µL of QDs in water are added to the equilibrated column the allowed them be absorbed by the gel bed. ~900 µL of 1X PBS buffer is added from the top of the column and the QDs coming out from the bottom as drips are collected in a vial.

3.7.3 Recovery of fluorescence by addition of TCEP

600 µL of a ~6 µM dispersion of freshly transferred cysteine-capped InP/ZnS NCs at pH 9 are mixed with 100 µL of a 0.5 M TCEP solution.

3.7.4 Synthesis of InP/ZnS NCs

730 nm emitting

The synthesis of 730 nm emitting InP/ZnS NCs is discussed in chapter II.

610 nm emitting

The 610-nm emitting InP QDs were synthesized following the procedure of Xu et. al. [45] with slight modification. Precisely, 0.087 g (0.3 mmol) of indium acetate, 0.130 g (0.3 mmol) of zinc undecynelate, 0.144 g (0.6 mmol) of hexadecylamine and 0.088 g (0.3 mmol) of stearic acid are mixed in 9 ml (36 mmol) of 1-Octadecene (ODE) in a 50 mL three necked flask. The mixture is heated to ~120°C to obtain a clear solution. The flask is then degassed for 1 h under vacuum (~3. 10^{-2} mbar). During this step the solution is stirred magnetically at 600 rpm. Separately, 0.154 g (1.74 mmol) of $P(TMS)_3$ in 0.5 mL of ODE is prepared in glove box. The flasks containing Indium precursor is backfilled with Argon and the $P(TMS)_3$ solution is injected at 280°C and kept 240°C for 20 minutes. For ZnS shell growth: 0.95 g (1.5 mmol) of zinc stearate and 0.012 g (0.37 mmol) of zinc stearate in 3

mL of ODE are added to the solution. The flask is degassed for 30 minutes and backfilled with argon and then the solution is heated at 230°C for 20 minutes. QY: 30% in hexane.

660 nm emitting

660-nm emitting QDs were prepared using the same protocol as 610 nm emitting InP/ZnS, except that *in situ* generated PH_3 gas was used instead of $P(TMS)_3$ as the phosphorous precursor. 0.087 g (0.3 mmol) of indium acetate, 0.130 g (0.3 mmol) of zinc undecynelate, 0.144 g (0.6 mmol) of hexadecylamine and 0.088 g (0.3 mmol) of stearic acid are mixed in 9 ml (36 mmol) of 1-Octadecene (ODE) in a 50 mL three necked flask. The mixture is heated to ~120°C to obtain a clear solution. The flask is then degassed for 1 h under vacuum (~3. 10^{-2} mbar). During this step the solution is stirred magnetically at 600 rpm. Separately, Separately, 0.19 g (0.6 mmol) of fine powdered Zn_3P_2 is weighed and degassed. Both the flasks are backfilled with Argon. The temperature of flask B is increased to 250°C. 10 mL of 1M H_2SO_4 solution is injected to the flask A to generate phosphine gas and the gas is carried to the flask B by a strong flow of Argon. Within 2 minutes, the solution turns reddish black. Under constant Ar flux, the reaction was continued for 1h. QY in hexane: 12%.

3.7.5 Synthesis of other types of QDs.

The synthesis of other types of QDs followed reported protocols and were carried out by other members of the laboratory: CdSe/CdS core/shell nanorods [46], CdSe rods [47], CdSe/CdS/ZnS core/shell/shell NCs [48], tetragonal $CuInSe_2$ [49] and $CuInS_2$/ZnS core/shell NCs [44].

3.8 Reference

1. Bruchez, M., M. Moronne, P. Gin, S. Weiss, and A.P. Alivisatos, *Semiconductor Nanocrystals as Fluorescent Biological Labels.* Science, 1998. **281**(5385): p. 2013-2016.
2. Chan, W.C.W. and S. Nie, *Quantum Dot Bioconjugates for Ultrasensitive Nonisotopic Detection.* Science, 1998. **281**(5385): p. 2016-2018.
3. Medintz, I.L., H.T. Uyeda, E.R. Goldman, and H. Mattoussi, *Quantum dot bioconjugates for imaging, labelling and sensing.* Nature Material, 2005. **4**(6): p. 435-446.
4. Doty, R.C., T.R. Tshikhudo, M. Brust, and D.G. Fernig, *Extremely Stable Water-Soluble Ag Nanoparticles.* Chemistry of Materials, 2005. **17**(18): p. 4630-4635.

5. Susumu, K., H.T. Uyeda, I.L. Medintz, T. Pons, J.B. Delehanty, and H. Mattoussi, *Enhancing the Stability and Biological Functionalities of Quantum Dots via Compact Multifunctional Ligands.* Journal of the American Chemical Society, 2007. **129**(45): p. 13987-13996.
6. Roullier, V., S. Clarke, C. You, F. Pinaud, G.r. Gouzer, D. Schaible, V.r. Marchi-Artzner, J. Piehler, and M. Dahan, *High-Affinity Labeling and Tracking of Individual Histidine-Tagged Proteins in Live Cells Using Ni2+ Tris-nitrilotriacetic Acid Quantum Dot Conjugates.* Nano Letters, 2009. **9**(3): p. 1228-1234.
7. Lévy, R.l., N.T.K. Thanh, R.C. Doty, I. Hussain, R.J. Nichols, D.J. Schiffrin, M. Brust, and D.G. Fernig, *Rational and Combinatorial Design of Peptide Capping Ligands for Gold Nanoparticles.* Journal of the American Chemical Society, 2004. **126**(32): p. 10076-10084.
8. Dubertret, B., P. Skourides, D.J. Norris, V. Noireaux, A.H. Brivanlou, and A. Libchaber, *In Vivo Imaging of Quantum Dots Encapsulated in Phospholipid Micelles.* Science, 2002. **298**(5599): p. 1759-1762.
9. Pellegrino, T., L. Manna, S. Kudera, T. Liedl, D. Koktysh, A.L. Rogach, S. Keller, J. RÃ¤dler, G. Natile, and W.J. Parak, *Hydrophobic Nanocrystals Coated with an Amphiphilic Polymer Shell: A General Route to Water Soluble Nanocrystals.* Nano Letters, 2004. **4**(4): p. 703-707.
10. Soo Choi, H., W. Liu, P. Misra, E. Tanaka, J.P. Zimmer, B. Itty Ipe, M.G. Bawendi, and J.V. Frangioni, *Renal clearance of quantum dots.* Nature Biotechnology, 2007. **25**(10): p. 1165-1170.
11. Liu, W., H.S. Choi, J.P. Zimmer, E. Tanaka, J.V. Frangioni, and M. Bawendi, *Compact Cysteine-Coated CdSe(ZnCdS) Quantum Dots for in Vivo Applications.* Journal of the American Chemical Society, 2007. **129**(47): p. 14530-14531.
12. Pinaud, F., S. Clarke, A. Sittner, and M. Dahan, *Probing cellular events, one quantum dot at a time.* Nature Method. **7**(4): p. 275-285.
13. Zimmer, J.P., S.-W. Kim, S. Ohnishi, E. Tanaka, J.V. Frangioni, and M.G. Bawendi, *Size Series of Small Indium Arsenideâˆ'Zinc Selenide Coreâˆ'Shell Nanocrystals and Their Application to In Vivo Imaging.* Journal of the American Chemical Society, 2006. **128**(8): p. 2526-2527.
14. Breus, V.V., C.D. Heyes, and G.U. Nienhaus, *Quenching of CdSeâˆ'ZnS Coreâˆ'Shell Quantum Dot Luminescence by Water-Soluble Thiolated Ligands.* The Journal of Physical Chemistry C, 2007. **111**(50): p. 18589-18594.
15. Yong, K.-T., H. Ding, I. Roy, W.-C. Law, E.J. Bergey, A. Maitra, and P.N. Prasad, *Imaging Pancreatic Cancer Using Bioconjugated InP Quantum Dots.* ACS Nano, 2009. **3**(3): p. 502-510.
16. Peng, X., M.C. Schlamp, A.V. Kadavanich, and A.P. Alivisatos, *Epitaxial Growth of Highly Luminescent CdSe/CdS Core/Shell Nanocrystals with Photostability and Electronic Accessibility.* Journal of the American Chemical Society, 1997. **119**(30): p. 7019-7029.
17. Reiss, P., J.l. Bleuse, and A. Pron, *Highly Luminescent CdSe/ZnSe Core/Shell Nanocrystals of Low Size Dispersion.* Nano Letters, 2002. **2**(7): p. 781-784.
18. Mekis, I., D.V. Talapin, A. Kornowski, M. Haase, and H. Weller, *One-Pot Synthesis of Highly Luminescent CdSe/CdS Core-Shell Nanocrystals via Organometallic and "Greener" Chemical Approaches* The Journal of Physical Chemistry B, 2003. **107**(30): p. 7454-7462.
19. Schapotschnikow, P., B. Hommersom, and T.J.H. Vlugt, *Adsorption and Binding of Ligands to CdSe Nanocrystals.* The Journal of Physical Chemistry C, 2009. **113**(29): p. 12690-12698.

20. Pong, B.-K., B.L. Trout, and J.-Y. Lee, *Modified Ligand-Exchange for Efficient Solubilization of CdSe/ZnS Quantum Dots in Water: A Procedure Guided by Computational Studies.* Langmuir, 2008. **24**(10): p. 5270-5276.
21. Li, C., M. Ando, H. Enomoto, and N. Murase, *Highly Luminescent Water-Soluble InP/ZnS Nanocrystals Prepared via Reactive Phase Transfer and Photochemical Processing.* The Journal of Physical Chemistry C, 2008. **112**(51): p. 20190-20199.
22. Dollefeld, H., K. Hoppe, J. Kolny, K. Schilling, H. Weller, and A. Eychmuller, *Investigations on the stability of thiol stabilized semiconductor nanoparticles.* Physical Chemistry Chemical Physics, 2002. **4**(19): p. 4747-4753.
23. Reiss, P., M. Protière, and L. Li, *Core/Shell Semiconductor Nanocrystals.* Small, 2009. **5**(2): p. 154-168.
24. Uyeda, H.T., I.L. Medintz, J.K. Jaiswal, S.M. Simon, and H. Mattoussi, *Synthesis of Compact Multidentate Ligands to Prepare Stable Hydrophilic Quantum Dot Fluorophores.* Journal of the American Chemical Society, 2005. **127**(11): p. 3870-3878.
25. Pinaud, F., D. King, H.-P. Moore, and S. Weiss, *Bioactivation and Cell Targeting of Semiconductor CdSe/ZnS Nanocrystals with Phytochelatin-Related Peptides.* Journal of the American Chemical Society, 2004. **126**(19): p. 6115-6123.
26. Thuy, U.T.D., N.Q. Liem, D.X. Thanh, M. Protiere, and P. Reiss, *Optical transitions in polarized CdSe, CdSe/ZnSe, and CdSe/CdS/ZnS quantum dots dispersed in various polar solvents.* Applied Physics Letters, 2007. **91**(24): p. 241908-3.
27. McPherson, T., A. Kidane, I. Szleifer, and K. Park, *Prevention of Protein Adsorption by Tethered Poly(ethylene oxide) Layers: Experiments and Single-Chain Mean-Field Analysis.* Langmuir, 1998. **14**(1): p. 176-186.
28. Muro, E., T. Pons, N. Lequeux, A. Fragola, N. Sanson, Z. Lenkei, and B. Dubertret, *Small and Stable Sulfobetaine Zwitterionic Quantum Dots for Functional Live-Cell Imaging.* Journal of the American Chemical Society. 2010, **132**(13): p. 4556-4557.
29. Breus, V.V., C.D. Heyes, K. Tron, and G.U. Nienhaus, *Zwitterionic Biocompatible Quantum Dots for Wide pH Stability and Weak Nonspecific Binding to Cells.* ACS Nano, 2009. **3**(9): p. 2573-2580.
30. Qiu, W., T. Li, L. Zhang, Y. Yang, Y.-T. Kao, L. Wang, and D. Zhong, *Ultrafast quenching of tryptophan fluorescence in proteins: Interresidue and intrahelical electron transfer.* Chemical Physics, 2008. **350**(1-3): p. 154-164.
31. Arian, S., M. Benjamini, J. Feitelson, and G. Stein, *Interaction between tyrosine and divalent sulfur inn fluorescence quenching and in the photochemistry of ribonuclease*. Photochemistry and Photobiology, 1970. **12**(6): p. 481-487.
32. Xia, Y.-S. and C.-Q. Zhu, *Interaction of CdTe nanocrystals with thiol-containing amino acids at different pH: a fluorimetric study.* Microchimica Acta, 2009. **164**(1): p. 29-34.
33. Burns, J.A., J.C. Butler, J. Moran, and G.M. Whitesides, *Selective reduction of disulfides by tris(2-carboxyethyl)phosphine.* The Journal of Organic Chemistry, 1991. **56**(8): p. 2648-2650.
34. Guzelian, A.A., J.E.B. Katari, A.V. Kadavanich, U. Banin, K. Hamad, E. Juban, A.P. Alivisatos, R.H. Wolters, C.C. Arnold, and J.R. Heath, *Synthesis of Size-Selected, Surface-Passivated InP Nanocrystals.* The Journal of Physical Chemistry, 1996. **100**(17): p. 7212-7219.
35. Wuister, S.F., C. de Mello Donegá, and A. Meijerink, *Influence of Thiol Capping on the Exciton Luminescence and Decay Kinetics of CdTe and CdSe Quantum Dots.* The Journal of Physical Chemistry B, 2004. **108**(45): p. 17393-17397.

36. Crawhall, J.C. and C.J. Thompson, *Cystinuria: Effect of D-Penicillamine on Plasma and Urinary Cystine Concentrations.* Science, 1965. **147**(3664): p. 1459-1460.
37. Moloney, M.A.c.P., Y.K. Gun'ko, and J.M. Kelly, *Chiral highly luminescent CdS quantum dots.* Chemical Communications, 2007(38): p. 3900-3902.
38. Gautier, C. and T. Bürgi, *Chiral Gold Nanoparticles.* ChemPhysChem, 2009. **10**(3): p. 483-492.
39. Shemer, G., O. Krichevski, G. Markovich, T. Molotsky, I. Lubitz, and A.B. Kotlyar, *Chirality of Silver Nanoparticles Synthesized on DNA.* Journal of the American Chemical Society, 2006. **128**(34): p. 11006-11007.
40. Govan, J.E., E. Jan, A. Querejeta, N.A. Kotov, and Y.K. Gun'ko, *Chiral luminescent CdS nano-tetrapods.* Chemical Communications. **46**(33): p. 6072-6074.
41. Kitaev, V., *Chiral nanoscale building blocks-from understanding to applications.* Journal of Materials Chemistry, 2008. **18**(40): p. 4745-4749.
42. Elliott, S.D., M.c.l.P. Moloney, and Y.K. Gun'ko, *Chiral Shells and Achiral Cores in CdS Quantum Dots.* Nano Letters, 2008. **8**(8): p. 2452-2457.
43. Nakashima, T., Y. Kobayashi, and T. Kawai, *Optical Activity and Chiral Memory of Thiol-Capped CdTe Nanocrystals.* Journal of the American Chemical Society, 2009. **131**(30): p. 10342-10343.
44. Li, L., T.J. Daou, I. Texier, T.T. Kim Chi, N.Q. Liem, and P. Reiss, *Highly Luminescent CuInS2/ZnS Core/Shell Nanocrystals: Cadmium-Free Quantum Dots for In Vivo Imaging.* Chemistry of Materials, 2009. **21**(12): p. 2422-2429.
45. Xu, S., J. Ziegler, and T. Nann, *Rapid synthesis of highly luminescent InP and InP/ZnS nanocrystals.* Journal of Materials Chemistry, 2008. **18**(23): p. 2653-2656.
46. Carbone, L., C. Nobile, M. De Giorgi, F.D. Sala, G. Morello, P. Pompa, M. Hytch, E. Snoeck, A. Fiore, I.R. Franchini, M. Nadasan, A.F. Silvestre, L. Chiodo, S. Kudera, R. Cingolani, R. Krahne, and L. Manna, *Synthesis and Micrometer-Scale Assembly of Colloidal CdSe/CdS Nanorods Prepared by a Seeded Growth Approach.* Nano Letters, 2007. **7**(10): p. 2942-2950.
47. Shieh, F., A.E. Saunders, and B.A. Korgel, *General Shape Control of Colloidal CdS, CdSe, CdTe Quantum Rods and Quantum Rod Heterostructures.* The Journal of Physical Chemistry B, 2005. **109**(18): p. 8538-8542.
48. Talapin, D.V., I. Mekis, S. Goetzinger, A. Kornowski, O. Benson, and H. Weller, *CdSe/CdS/ZnS and CdSe/ZnSe/ZnS Core—Shell—Shell Nanocrystals.* ChemInform, 2005. **36**(10): p. no-no.
49. Koo, B., R.N. Patel, and B.A. Korgel, *Synthesis of CuInSe2 Nanocrystals with Trigonal Pyramidal Shape.* Journal of the American Chemical Society, 2009. **131**(9): p. 3134-3135.
50. Dif, A. l.; Boulmedais, F.; Pinot, M.; Roullier, V.; Baudy-Floc'h, M. l.; Coquelle, F. d. r. M.; Clarke, S.; Neveu, P.; Vignaux, F. o.; Borgne, R. L.; Dahan, M.; Gueroui, Z.; Marchi-Artzner, V. r., Small and Stable Peptidic PEGylated Quantum Dots to Target Polyhistidine-Tagged Proteins with Controlled Stoichiometry. *Journal of the American Chemical Society* **2009,** *131* (41), 14738-14746.
51. Dif, A. l.; Henry, E.; Artzner, F.; Baudy-Floc'h, M. l.; Schmutz, M.; Dahan, M.; Marchi-Artzner, V. r., Interaction between Water-Soluble Peptidic CdSe/ZnS Nanocrystals and Membranes: Formation of Hybrid Vesicles and Condensed Lamellar Phases. *Journal of the American Chemical Society* **2008,** *130* (26), 8289-8296.

Chapter IV

InP/ZnS NCs in biological imaging

4.1 Introduction

This chapter focuses on the application of InP/ZnS NCs in biological imaging. The first section (4.2), presents the *in vitro* and *in vivo* studies performed with the NIR emitting InP/ZnS NCs in aqueous medium following a phase transfer (cf chapter III) from organic medium in which they where synthesized by the phosphine gas method described in chapter II. The second part of this chapter (section 4.3) presents the results from collaborative works on dual modality probes [1] involving InP/ZnS NCs conjugated to gadolinium complexes, which act as magnetic resonance imaging (MRI) contrast agent. The objective is to combine fluorescence imaging and MRI within one probe and to overcome the shortcomings of each separate modality. Finally, in section 4.4 the possibility of functionalizing InP/ZnS NCs with specific copies of straptevidin protein based on their electrophoretic mobility will be discussed. Colloidal nanoparticles (NPs) capped with charged molecules move toward the opposite electrode in gel electrophoresis. It was originally shown by Alivisatos' group that Au NPs conjugated with different numbers of DNA strands moved differently in agarose gel forming discrete bands, which allowed the authors to control the number of DNA per particles by separating the bands formed in agarose gel [2]. This technique has been the basis of various works on CdSe/ZnS functionalized with specific number of proteins and antibodies for targeted single molecule assay [3, 4]. We address the prospect of controlling the functionalization of InP/ZnS NCs with a known number of streptavidin molecules.

4.2 Biological studies of NIR emitting InP/ZnS NCs

4.2.1 Quantum dots preparation

NIR emitting InP/ZnS NCs (emission: 730 nm) were phase transferred into aqueous medium by using penicillamine as the transfer ligand (cf. chapter III). The NCs were thoroughly purified by using centrifugal filters from VWR (MWCO 30-50k) to remove excess ligands and dispersed in PBS (pH 7.4).The hydrodynamic diameter of the NCs in PBS measured by DLS was 7.5±1.7 nm (Fig. 4.1a). The Figure 4.1b shows the UV-Vis and PL spectra of the NCs in water.

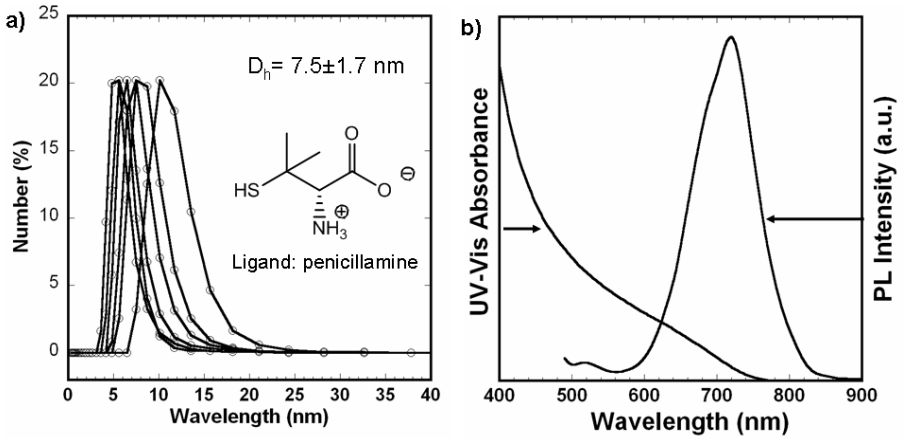

Figure 4.1 a) Hydrodynamic diameter of penicillamine capped InP/ZnS NCs in 1X PBS buffer measured using DLS. Multiple measurements (6 times) were performed and the mean value was calculated. The inset shows the structure of the capping ligand: penicillamine (b) UV-Vis and PL spectra of penicillamine capped InP/ZnS NCs in water.

4.2.2 Cytotoxicity studies of penicillamine-capped InP/ZnS NCs

The cytotoxicity of the penicillamine capped InP/ZnS NCs in 1 X PBS buffer (pH 7.4) was assessed for Chinese hamster ovary (CHO) cells. The MTT assay was used to evaluate cytotoxicity after incubating the cells (60000/well) in presence of the quantum dots for 24 hours. 3-(4, 5-dimethylthiazol-2-yl)-2, 5-diphenyl-tetrazolium bromide (MTT) is reduced to purple colored formazan dye following enzymatic reaction (Scheme 4.1). As this reaction takes place only in the living mitochondria, the amount of formazan formed is proportional to the number of living cells.

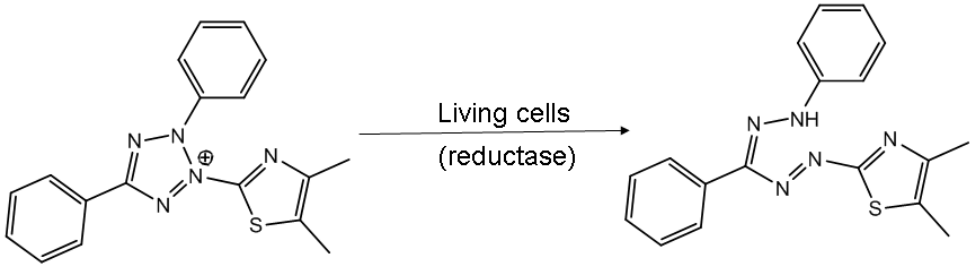

Scheme 4.1 Conversion of the tetrazolium salt MTT into formazan dye in presence of mitochondrial reductase.

Fig. 4.2 shows the cell viablility in presence of different amounts of penicillamine capped InP/ZnS NCs. Even after 24h of exposure (Temperature: 37°C) at a concentration of 20 nmol QDs/10^6 cells (1µM QD concentration) a significant mitochondrial metabolic activity with >90% cell viability was observed. Increasing the concentration to 100 nmol/10^6 cells (5µM QD concentration) reduced the cell viability to about 80%. The cell viability with saponin (Fig. 4.3) a molecule which is highly toxic to CHO cells [5] is plotted for comparison.

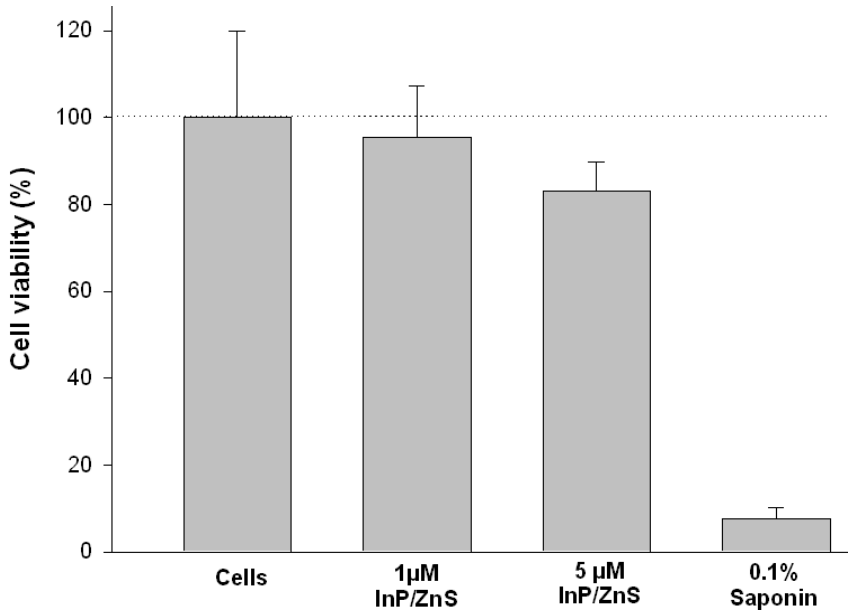

Figure 4.2 MTT assay: cell viability after 24 hrs of incubation with 1 µM and 5 µM of penicillamine capped InP/ZnS NCs and 0.1% (w/v) saponin.

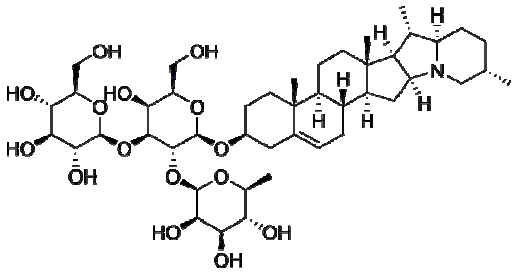

Figure 4.3 Chemical structure of saponin.

4.2.3 Functionalisation of penicillamine-capped InP/ZnS NCs with maurocalcine and *in vitro* studies.

4.2.3.1 Cell penetrating peptide: maurocalcine

Cell penetrating peptides (CPPs) [6] have special properties to penetrate cell membranes and transport different cargoes ranging from small drug molecules to polymers and nanoparticles into cells [7]. There is a growing interest in transporting nanoparticles into cell by means of a cell penetrating peptide; the reason for this is essentially twofold: first, due to a large surface area and possibility to graft functional biomolecules covalently on to the surface, it is a potential candidate for use as a vector for the intracellular delivery of drugs, genes, contrast agents etc. [8]. Second, due to the unique properties of nanoparticles, especially the fluorescent quantum dots, the CPP-QD conjugate serves as an imaging and sensing tool. Maurocalcine (MCa) is a cell penetrating peptide (CPP) constituted of 33 amino acids (Figure 4.4). It was originally isolated from *Scorpio maurus palmate* [9]. One of its various forms has a free terminal thiol group (N-terminal) coming from cysteine residue, which can be attached to cargoes including nanoparticles.

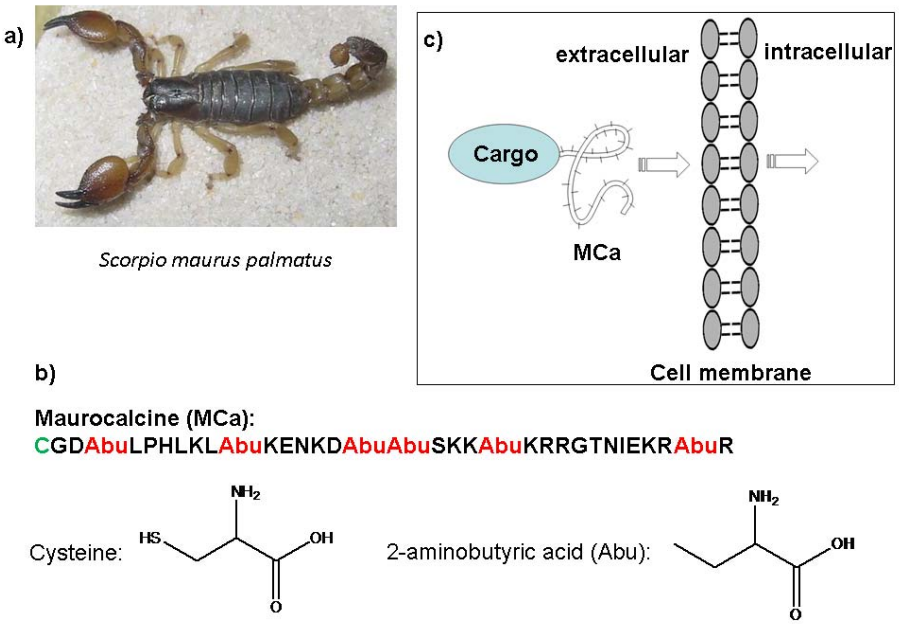

Figure 4.4 (a) A still photograph of Scorpio Maurus palmus [10] (b) Structure of Maurocalcine with terminal cysteine group. (c) MCa translocating a cargo into the cell.

4.2.3.2 *In vitro* studies

MCa conjugation to the nanocrystals' surface was achieved by incubating the quantum dots in a solution containing an approximately 10-fold molar excess of MCa. The grafting of MCa on the NCs was evident in FTIR. The characteristic amide I (at 1665 cm^{-1}) and amide II peaks (at 1522 cm^{-1}) of the peptide bond in maurocalcine were clearly identified (Fig. 4.5) in the purified MCa capped NCs sample. The amide I band arises due to the stretching of peptide C=O bond while the amide II is attributed to the bending of the adjacent N-H bond. The purification using centrifugal filters with a cut-off of 50 kDa (cf. experimental section) assures removal of free MCa (3.8 kDa) and penicillamine (0.15 kDa) molecules. Absorption at 2922 cm^{-1} and 2858 cm^{-1} are attributed to saturated $-CH_3$ stretching which are present in both maurocalcine and penicillamine.

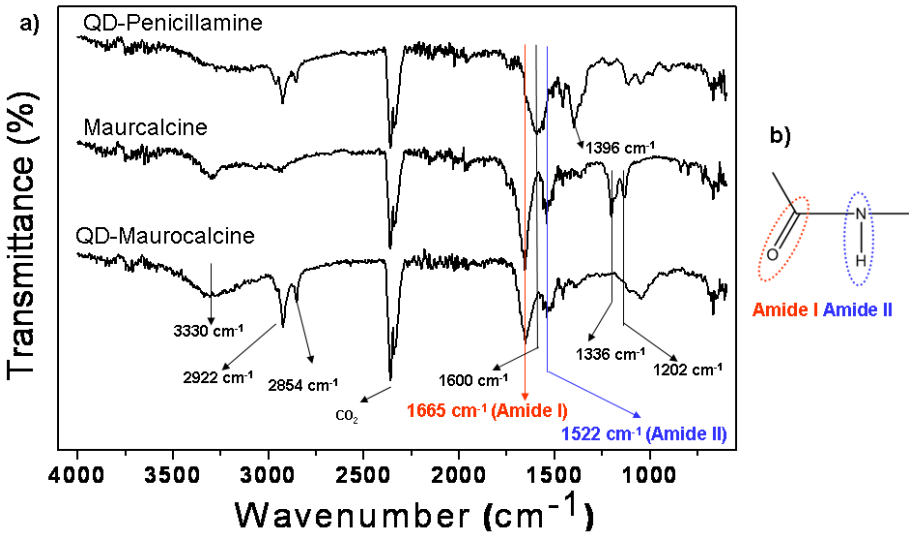

Figure 4.5 a) FTIR spectra of penicillamine capped InP/ZnS NCs, of MCa, and of MCa grafted on InP/ZnS NCs b) Peptide bonds responsible for the characteristic amide I and amide II bands in FTIR spectra.

The purified MCa-functionalized quantum dots (5μM) were used for incubation with CHO cells (~120000 cells/well) in culture (2 hrs). Fig. 4.6 demonstrates successful cell penetration of the MCa-modified quantum dots, whereas no penetration was observed with Pen being the only surface ligand. These results confirm that MCa is indeed bound to the nanocrystals' surface and that it retains its cell-penetration properties upon conjugation.

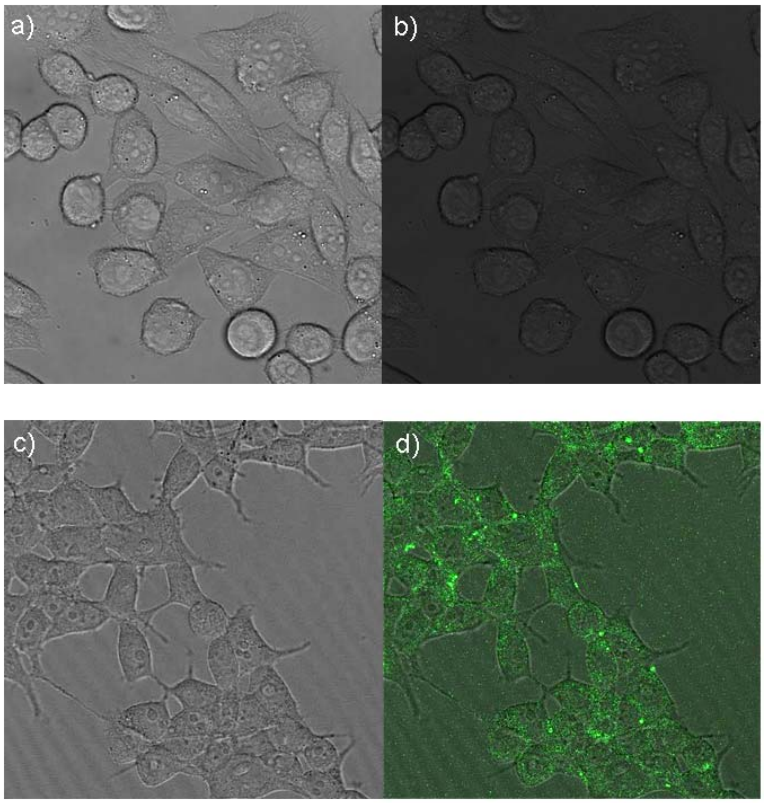

Figure 4.6 Confocal microscopy images of Chinese hamster ovary (CHO) cells showing successful cell penetration of maurocalcine capped InP/ZnS QDs (incubation time: 2 hrs). Image size: 100x100 μM. (a),(b) penicillamine-capped QDs; (c),(d) maurocalcine-functionalized QDs; (a),(c) without excitation; (b),(d) excitation at 480 nm; quantum dots in green (false colors).

The mechanism by which cell translocation occurs has been a subject of debate. There are evidences of both direct membrane translocation [11] and endocytosis [12] in the literature. In addition, a co-existence of both pathways has also been suggested recently [13]. Studies of the fate of NCs cell post-penetration with transmission electron microscopy could

unravel this in our case. Depending upon the mode of internalization the NCs may end up in different compartments of the cell which can be investigated under TEM. For example, if the uptake of the NCs by cells takes place *via* endocytosis, the NCs may end up in late endosomes while the direct translocation of NCs leads to accumulation of NCs in cytoplasm or nucleus [14]. Further, the study of the cell penetration behavior of InP/ZnS NCs functionalized with Maurocalcine in the presence of an inhibitor of endocytosis could be equally interesting for understanding the mechanism of penetration [15]. Another common way to assess the involvement of endocytosis is decreasing the incubation temperature to 0-4°C which inhibits all energy-dependent pathways. Decreasing the incubation temperature could be applied to block the endocytosis process [16] and then study the other forms of translocation taking place, if any. Nonetheless, the observation in our case that only maurocalcine functionalized InP/ZnS NCs was internalized by cell while penicillamine capped InP/ZnS NCs was not strongly suggests that a) maurocalcine is attached to NCs and retains its cell penetrating properties and b) penicillamine capped InP/ZnS NCs alone were not uptaken by cells by any of the internalization modes, be them phagocytotic or non-phagocytotic. This inference is also very interesting because, the phagocytotic uptake of nanoparticles by a cell is highly dependent on cell types, nature of the ligand and size of the particles among other factors. In particular, zwitterionic ligands coated NCs have shown high resistance to endocytotic uptake by cells compared to NCs with charged ligands. For example, the quantities of zwitterionic CdSe/CdZnS QDs adsorbed on or internalized by HeLa cells were comparable to those of the control sample with no QDs whereas high internalization was observed with positively and to a lesser extent with negatively charged QDs [17].

4.2.4 Biodistribution of penicillamine-capped NIR emitting InP/ZnS NCs in mice

There is a growing interest in understanding the pharmacokinetics of the different types of nanoparticles injected intravenously or by other routes of injection as it directly concerns the fate of the nanoparticles in the body and their possible accumulation in organs [18-22]. The biodistribution of the II-IV QDs *in vivo* have been extensively investigated [18, 19, 23], however little is known about III-V QDs, especially InP/ZnS NCs. We studied the biodistribution of InP/ZnS NCs coated with zwitterionic penicillamine in mice after tail

vein injection. By selecting the emission of InP/ZnS in near infrared region (650-900 nm) we sought to minimize the autofluorescence, scattering and absorption of photons by the tissue components. Further, zwitterionic penicillamine is expected reduce the non-specific binding of the NCs with serum proteins which has been recently observed *in vitro* [24]. The non-specific binding of serum proteins leads to increase in hydrodynamic diameter of the NCs complicating the clearance mechanism [25]. Moreover, negatively charged NCs may favor adsorption of plasma opsonins and trigger phagocytosis, a natural response of the immune system when encountering foreign bodies such as nanoparticles [26]. The phagocytosis-mediated uptake by macrophages, white blood cells, may end up in the organs of the reticulo-endothelial system (RES) such as the liver, spleen, and bone marrow [27]. 100 µL of the QDs solution (12 µM) was injected intravenously (IV) into the tail of nude female mice of 4-5 weeks of age and the biodistribution was followed directly by fluorescence imaging. Fluorescence imaging provides qualitative and semi-quantitative information of the quantum dots *in vivo* and can be applied to study the biodistribution of quantum dots in animals by directly exploiting their fluorescence properties [19, 20, 27]. Figure 4.7a shows the temporal evolution of the fluorescence signal emanating from the injected InP/ZnS NCs during 24 hrs. Within 1-3 hrs of injection, the fluorescence signals were detected in kidney and liver. Even after 24h of injection high fluorescence signal was observed in mice indicating the excellent stability of these NCs. The dominant signals in kidney and liver were also observed in the organs after dissection (Fig. 4.7b). As already mentioned, it was previously shown that only small (< 6 nm) zwitterionic-coated QDs could be efficiently eliminated by renal clearance, while larger nanoparticles are known to accumulate in the organs of the RES [28]. Taking into account the hydrodynamic diameter and the size distribution of the QDs used here (7.5±1.7 nm), our results suggest those with smaller hydrodynamic size ended up in the kidneys while the larger ones were uptaken by the RES and accumulated in liver and spleen. Besides, weak fluorescence was also detected in the lungs of *one of the two mice investigated*. The nanoparticles uptaken by the RES are known to enter intestine after hepatobiliary processing (HB) [22]. However, in our case the fluorescence signal detected in the stomach and intestine was similar to that of the healthy Nude mice without injection. This comes from the standard mouse feed *alfalfa*, which fluoresces in the near infrared part of the spectrum. No fluorescence was detected in other organs such as the heart and the brain. Based on fluorescence signals of the organs, an image treatment using ImageJ software resulted in the histogram presented in Figure 4.7c.

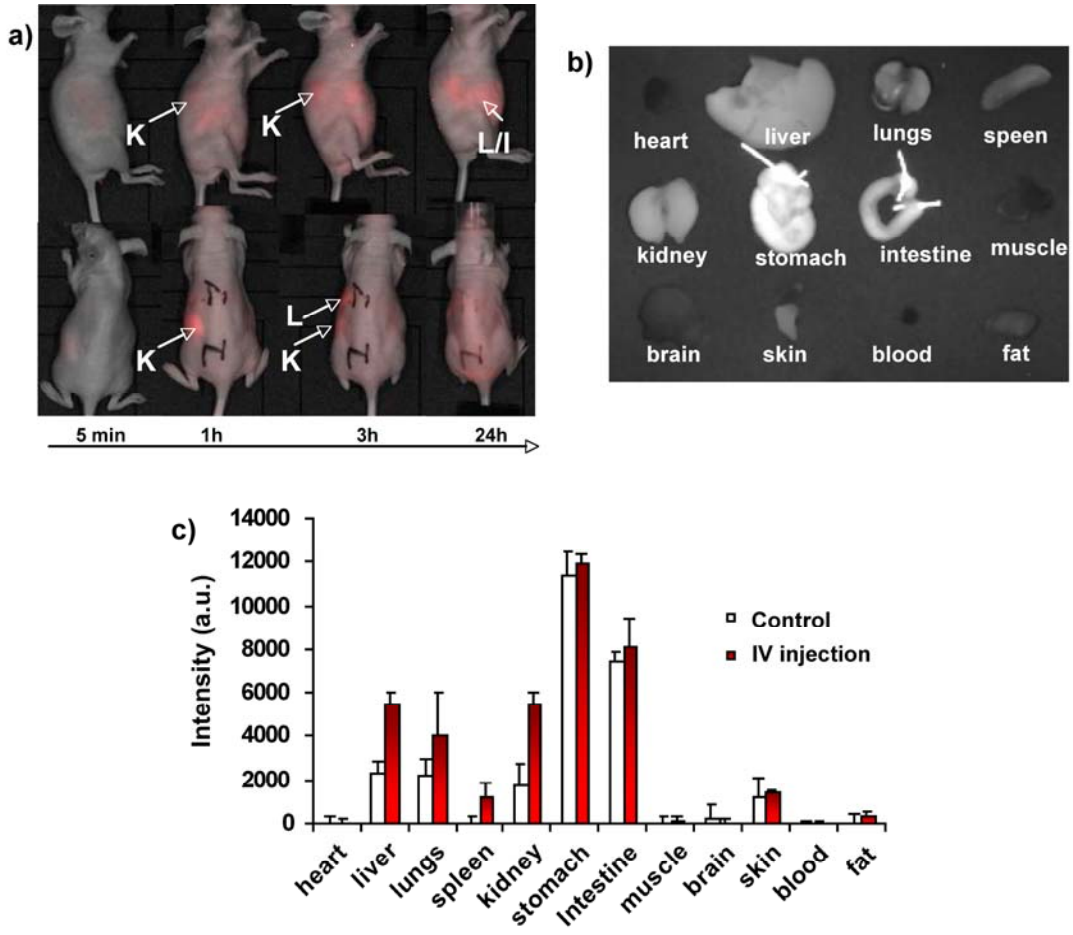

Figure 4.7 (a) Evolution of the fluorescence signal in a nude mouse after the injection of 730 nm emitting penicillamine coated InP/ZnS NCs in 1x PBS buffer. Excitation 640 nm, Exposure time: 10 ms (K=kidney, L=liver, I=intestine). (b) Ex vivo fluorescence analysis of the organs 24h after tail vein injection. Excitation wavelength: 640 nm, Exposure time: 200 ms. (c) Histogram showing the comparative fluorescence signals in organs without injection (control) and after intravenous (IV) injection. The error bars represent the standard deviation for the two animals.

4.2.5 Conclusion

NIR emitting InP/ZnS NCs coated with penicillamine in 1X PBS buffer (pH 7.4) show low cytotoxicity for CHO cells with a cell viability of over 90% for a concentration of 20 nmol per 10^6 cells and about 80% at QD/cells concentration 100 nmol per 10^6. Due to high affinity of ZnS surface to thiolated ions, these QDs could be easily functionalized with maurocalcine, a cell penetrating peptide containing terminal cysteine group. The InP/ZnS NCs attached to the MCa show excellent cell penetration behavior in CHO cells in direct

contrast to pencillamine capped InP/ZnS NCS. Finally, the NIR emitting penicillamine capped InP/ZnS NCs were injected in mice intravenously and their biodistribution was followed by fluorescence imaging. The fluorescence detected in the kidneys, liver and spleen suggests that the NCs may have been partially uptaken by the RES (bigger particles), while the smaller particles accumulated in the kidneys enabling renal clearance.

4.3 Dual modality probes: grafting of MRI contrast agent to fluorescent InP/ZnS NCs

4.3.1 Introduction

A new class of imaging agents called dual modality probes combines two different types of imaging techniques yielding more information than can be harnessed using each method separately. For example, magnetic resonance imaging (MRI) has excellent anatomical resolution; however, it suffers on the molecular level from its intrinsic low sensitivity [1]. Fluorescent based probes on the other hand with excellent molecular level sensitivities have generally poor spatial resolution and penetration depth. To address this issue we combine the two modalities in a single imaging agent. In this section, grafting of this *MRI contrast agent* on the surface of *fluorescent* InP/ZnS NCs and MRI studies in mice are presented.

4.3.2 MRI Contrast Agent

Lanthanide ions are used in a wide range of biomedical applications as contrast agents. The high spin paramagnetism (S=7/2) and the slow electronic relaxation of gadolinium (Gd) ions make them ideal candidate for use as contrast agents in magnetic resonance imaging (MRI). Gd(II) complexes are often favored over iron oxide particles as the former increases both the longitudinal (denoted by $1/T_1$) and transverse relaxation ($1/T_2$) rates of water molecules present in the vicinity to a differing extent depending on the nature of the ligand and the magnetic field compared Iron oxide particles which generally increases $1/T_2$ relaxivity. In addition, Gd complex affect bulk magnetic susceptibility of the tissues to a lesser extent, thereby minimizing the artifacts [29]. In our studies a picolinate based Gd complex was used. This complex containing two picolinate arms and one acetate arm

appended to 1,4,7-tri-azacyclononane core have greater stability (logK_{GdL}=15.8) as compared to Gd complex of analogous ligands such as 1,4,7-triazacyclononane-N,N',N"-triacetic acid (logK_{GdL}=13.7) [29]. Moreover, higher selectivity of the complex to Gd ions over Ca ions (logK_{CaL}=8.18) makes them suitable for biological studies [30]. The complex (Gd-2) whose molecular structure is presented in Fig. 4.8 was prepared by Graeme Stasiuk and Marco Giardello in collaboration with Marinella Mazzanti and Daniel Imbert from CEA/INAC/SCIB/RICC.

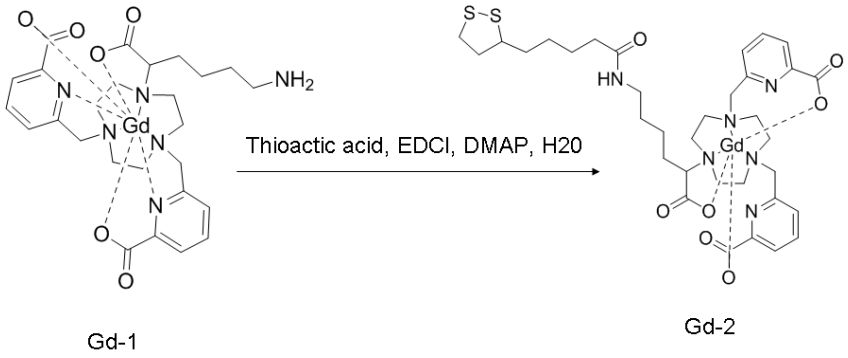

Figure 4.8 Gd complex (GD-2) used for grafting on InP/ZnS NCs. GD-2 was synthesized by a coupling reaction between GD-1 and thioactic acid, using the coupling agent 1-ethyl-3-(3-dimethylaminopropyl) carbodiimide (EDCI) and a catalyst 4-Dimethylaminopyridine (DMAP).

4.3.3 Grafting of Gd complex with InP/ZnS NCs

The grafting of the Gd complex (Gd-2) on the InP/ZnS-pen NCs was achieved by anchoring the complex *via* dithiol group from thioactic acid substituent. Tris(carboxyethyl) phosphine (TCEP) is used to cleave the disulfide bond directly *in situ*. As the reducing ability of TCEP is compromised at higher pHs, only slightly basic pH (~9) was maintained to facilitate thiolate formation and drive the ligand exchange process. To a mixture containing the QDs and 200 fold molar excess of Gd complex, a 9000 fold molar excess of TCEP is added and followed by vortexing (800 rpm) for 12 hrs at room temperature. The large amount of TCEP ensures the cleavage of the disulfide bond facilitating the grafting of dithiols on the ZnS shell.

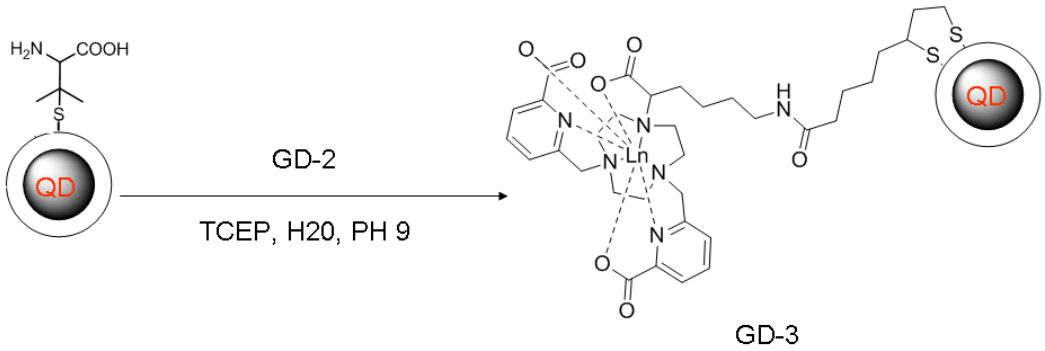

Figure 4.9 Grafting of the Gd complex (GD-2) on penicillamine capped InP/ZnS NCs via in situ generated dithiol groups.

The first evidence of successful grafting comes from the increase of the mean hydrodynamic diameters from 6.9±1.3 nm for the penicilamine capped InP/ZnS NCs (610 nm emitting) to 8.6±1.5 nm for the Gd complex functionalised InP/ZnS NCs. Second, the nuclear magnetic resonance dispersion (NMRD) profile of the purified sample showed a marked increase in relaxivity, r_1 at around 35 MHz as compared to the free Gd complexes (Figure 4.10). The Gd complexes (GD-1 and GD-2) follow a classic profile for mono aqua chelates, with high relaxation rate (r_1) at low fields 0.01 to 1 MHz, showing a decrease in r_1 between 1- 10 MHz until a plateau is reached (10 - 35 MHz). The Gd complex grafted to QD shows intriguingly different profile, with an increase in r_1 from 3 to 35 MHz of 10 to 13 mM^{-1} $s^{-1.}$ The intensity of MRI signal depends on the relaxivity of water protons. For example with increase in r_1 the MRI signal increases [29]. The presence of Gd-complexes improves the MRI signal by increasing the relaxivity (r_1) of the surrounding water molecules. The increase in r_1 in presence of a Gd(III) complex essentially depends on both the properties of the complex as well as the applied magnetic field. In NMRD experiments we measure the dependency of the relaxity with magnetic field; however the profile will also be affected by the changes in the properties of the complex in the presence of QDs. The properties of complex that affect relaxivity (r_1) of water protons which are either directly coordinated to the Gd ions (called inner coordination sphere) or away in the outer coordination sphere or beyond that (called bulk solvent) are (a) hydration number, q (b) the distance between the water proton and the unpaired electron spin of the Gd(III) ions, r (c) the rotational correlation time, τ_R (d) the water exchange rate, τ_m i.e. the rate of water exchange between the water molecule directly coordinated to the Gd(III) ions and the water present in the bulk solvent and (e) the electronic relaxation time, T .The significant

increase in r_1 is attributed to the slower rotation of the complex in the presence of QDs. This effect have been observed when Gd (III) chelates bound to proteins, such as Human serum albumin (HSA) shown by caravan *et a*l. [29]. The increase in r_1 indicates that a Gd (III) chelate is bound to a large particle such as the QD; confirming its grafting. From 35 - 200 MHz there is a loss of r_1 from 13 – 4 $mM^{-1}s^{-1}$, this is standard for T_1 contrast agents at higher field. At 200 MHz the effect of increased mass is lost so the grafted QD appears to have a similar relaxation rate per Gd molecule to that of the Gd complex alone. The relaxivity (r_1) for Gd complex grafted on the QDs at 35 MHz is 12.64 mM^{-1} s^{-1} (Table 4.1). It is interesting to note that this is only the relaxivity per Gd complex. By determining the concentrations of QDs and Gd complex in solutions respectively by UV-Vis spectroscopy and magnetic susceptibity measurements the number of Gd complexes per QD was calculated to be around 70. Consequently, the relaxivity per QD is calculated to be around 900 mM^{-1} s^{-1}.

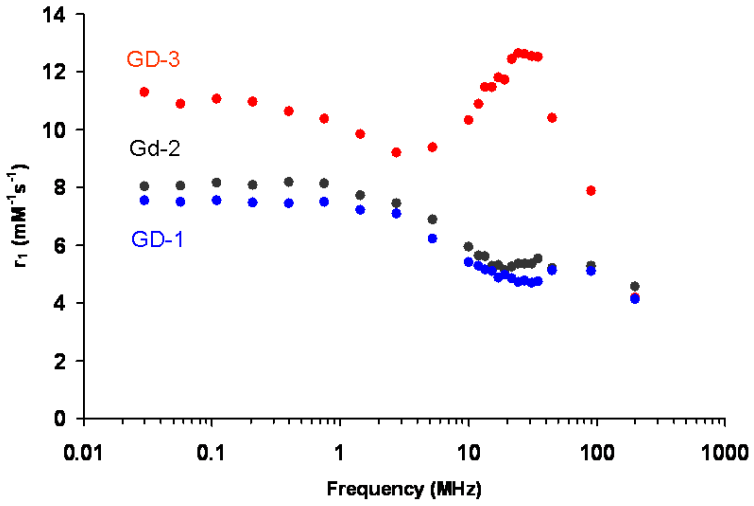

Figure 4.10. NMRD profile for GD-1(blue), GD-2 (black) and GD-3 (red) measured at 298K on a Spinmaster FFC (fast field cycling) NMR relaxometer.

Sample	Relaxivity (r_1 at 35 MHz)
Gd1	4.13 mM^{-1} s^{-1}
Gd2	4.58 mM^{-1} s^{-1}
Gd3	12.64 mM^{-1} s^{-1}

Table 4.1: relaxivity at 35 MHz

4.3.4 MRI studies with Gd picolinate grafted to InP/ZnS NCs

Figure 4.11a-b compares the MRI images of rat brain injected with Gd-1 (left hemisphere) and the Gadolinium complex 1,4,7,10-tetraazacyclododecane-N,N',N'',N'''-tetraacetic acid, Gd-DOTA (right hemisphere) at 30 minutes and 282 minutes. Gd-DOTA is a class of macrocyclic MRI contrast agents used in clinical practice. Gd-1 on the left shows an increased tissue retention time up to 280 minutes compared to Gd-DOTA (about 60 min), which is a major advantage for obtaining better resolved images over a prolonged period of time. Figure 4.11c-d shows the MRI images obtained under the same conditions with Gd-2 grafted on InP/ZnS NCs (Gd-3). As in the case of Gd-1 alone, we can see that GD-3 has also a long tissue retention time, as it can be easily detected after 282 min. Figure 4.11e directly compares the MRI signal vs. time for the free Gd-complex (Gd-1) and the Gd-complex grafted to QDs (Gd-3). These images have been taken at high field (7T), showing that the attachment to the QD provides excellent contrast as a high field agent. In addition, the fluorescence properties of the InP/ZnS NCs (emission: 610 nm) grafted with Gd complex make them an attractive dual modal contrast agent. Figure 4.11f shows the fluorescence excitation and emission spectra of the Gd-complex functionalised InP/ZnS NCs.

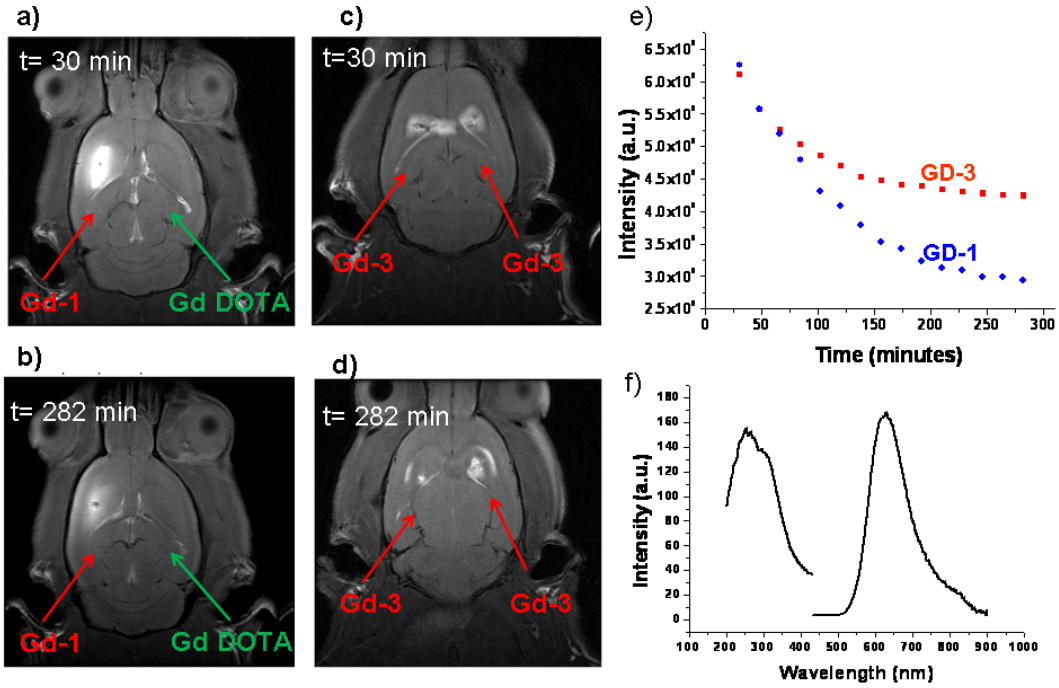

Figure 4.11 MRI images of a rat brain acquired at 7 Tesla a) Gd-1 at 30 minutes, b) Gd-1 at 282 minutes, injected into the left hemisphere of the brain, coinjected with Gd DOTA in the right hemisphere. C) Gd-3 at 30 minutes, d) Gd-3 at 282 minutes, injected into both hemispheres of the brain. e) Graph showing the MRI signal vs. time (retention time), (7T) f) excitation (left) and fluorescence spectra of InP/ZnS NCs functionalised with the Gd-complex (Gd-3). For the PL spectrum, the excitation wavelength is 320 nm.

4.3.5 Conclusion

It has been shown that picolinate based lanthanide chelates bearing a dithiol group can be grafted to InP/ZnS NCs, creating a dual mode contrast agent with r_1=900 $mM^{-1}s^{-1}$ per QD and the PL emission at 610 nm. MRI studies performed on rat brains with Gd functionalized InP/ZnS QDs show a significantly increased retention time.

4.4 Functionalisation of InP/ZnS NCs with a controlled number of protein molecules.

4.4.1 Introduction

The fluorescence properties of InP/ZnS QDs coupled with the possibility to graft biomoleucles on their surface makes these NCs excellent candidates for various biological applications including single-molecule imaging in living cells [31]. However, the lack of the precise control of the number of functional molecules results in undesirable effects such as increased hydrodynamic diameter, multivalency and nonspecificity [3]. One way of controlling functionalisation is based on the movement of gold nanoparticles or QDs conjugated with high molecular weight functional molecules such as proteins [4], oligonucleaotides [2] and polyethylene glycols [32]. For examples, it has been shown that if the molecular weight of the molecule (e.g. polyethylene glycols) is roughly ≥ 5000 g mol^{-1}, the difference between monofunctional and bi or higher functional gold nanoparticles can be detected as discrete bands on the agarose gel [32], which can be isolated. Similar observations have been reported for nanocrystals/DNA conjugates [2]. The electrophoretic separation has been recently applied to conjugate only one copy of straptevidin with single biotin binding site (monovalent) to QDs [3]. While literature examples are available for CdSe/ZnS QDs, gold nanoparticles, no studies have been reported for InP/ZnS NCs. Here we present functionalisation of InP/ZnS NCs with maleimide-activated straptevidin (SAV-mal), by combining conjugation with gel purification. This work has been carried out in collaboration with Samuel Clarke and Maxime Dahan at Laboratory Kastler Brossel (ENS Paris), who brought in their expertise in peptide and protein functionalisation of QDs.

The functionasation of InP/ZnS QDs can be divided into the following three steps:
Step I: Functionalisation of InP/ZnS NCs with a thiol rich peptide to form peptide coated NCs (pQDs)
Step II functionalisation of the pQDs with streptavidin (SAV) and
Step III Electrophoretic separation of SAV conjugated pQDs by analyzing the discrete bands formed on the agarose gel based on stoichiometries of SAV and pQDs

4.4.2 Step I: Functionalisation of InP/ZnS QDs with peptides

Phytochelatin-based peptides with 20 amino acids units were selected for this study following literature reports of their use as a capping peptide, especially with CdSe/ZnS NCs [4, 33]. The chosen peptide is rich in thiol groups due to the presence of 6 cysteine residues. The reason for this choice is two fold: first, the thiol group can be used for binding the peptide covalently with NCs surface and secondly, the free thiol groups present on the surface can be further utilized for attaching other functional molecules by using cross linkers such as succinimidyl 4-(N-maleimidomethyl) cyclohexane-1-carboxylate (SMCC) which contains a thiol reactive maleimide group and an amine-reactive N-hydroxysuccinimide (NHS). The peptide also has a short polyethylene glycol (PEG) segment to reduce nonspecific interactions. The hydrophobic InP/ZnS NCs in toluene are directly coated with peptides using a standard protocol [33]. InP/ZnS NCs in toluene are mixed with a large excess of peptides in a pyridine/dimethyl sulfoxide (DMSO) co-solvent and increased the pH of the medium to initiate the ligand exchange reaction. The column purified pQDs were highly soluble in distilled water and common physiological buffers. However, a drawback of this approach is the strongly reduced fluorescence intensity of the InP/ZnS QDs upon treatment with pyridine and DMSO. Therefore, we explored an alternative to the aforementioned method. It consists of the phase transfer of the InP/ZnS NCs to the aqueous medium (cf. Chapter 3) and subsequent incubation of the water soluble NCs with the peptide in basic pH as in the case of the functionalisation with MCa and Gd-picolinate. Fig. 4.12a shows the gel electrophoresis (GE) of the InP/ZnS NCs phase transferred with three different ligands namely penicillamine (Sample A), thioglycolic acid (B) and 11-mercaptoundecanoic acid, MUA (C). As the method of monofunctionalisation is based on the migration of bands in gel electrophoresis, it is important that the starting QDs have a well defined single band. NCs with a high zeta potential such as MUA coated ones were found to be suitable as confirmed by gel electrophoresis after peptide functionaliation (Fig. 4.12c).

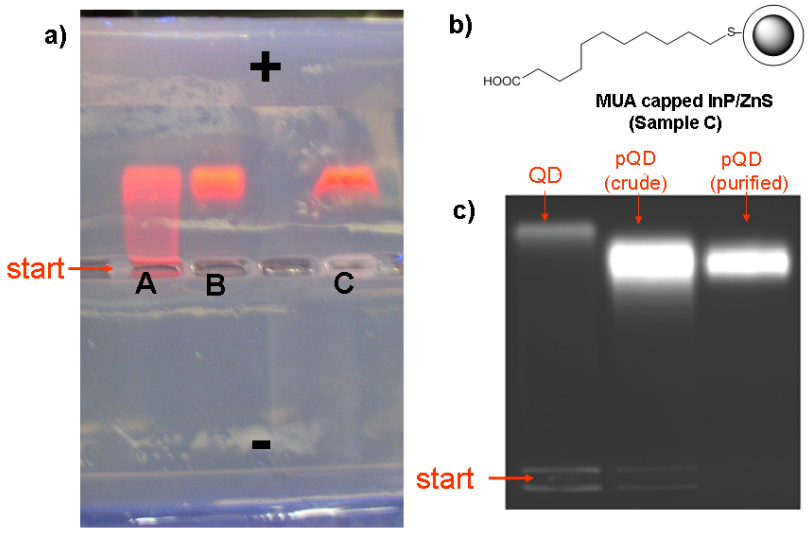

Figure 4.12: Migration of (a) Penicillamine capped InP/ZnS NCs, sample A, thioglycolic capped InP/ZnS NCs , sample B and 11-Mercaptoundecanoic capped InP/ZnS NCs, sample C after 5 minute. b) MUA capped InP/ZnS NCs c) The GE of the MUA capped InP/ZnS NCs (QD), MUA capped InP/ZnS NCs after incubation with peptide at basic pH (pQD crude) and purified peptide coated InP/ZnS NCs (pQD purified).

4.4.3 Step II: functionalisation of InP/ZnS pQDs with streptavidin

We selected streptavidin (SAV) protein because of its very high affinity for biotin. The selective streptavidin - biotin interaction is one of the strongest non-covalent interactions known and have been employed in a large number of nanoparticle related works. As shown in Figure 4.13, when SAV is reacted with four fold excess of the cross linker (SMCC), a fraction of its amino groups reacts with the succinimide groups of SMCC to form maleimide activated SAV (SAV-mal). In a second step, the SAV-mal is grafted on the pQDs *via* reaction between free thiol groups of the pQDs and the thiol-reactive part of the maleimide to form SAV coated InP/ZnS NCs (InP/ZnS-SAV).

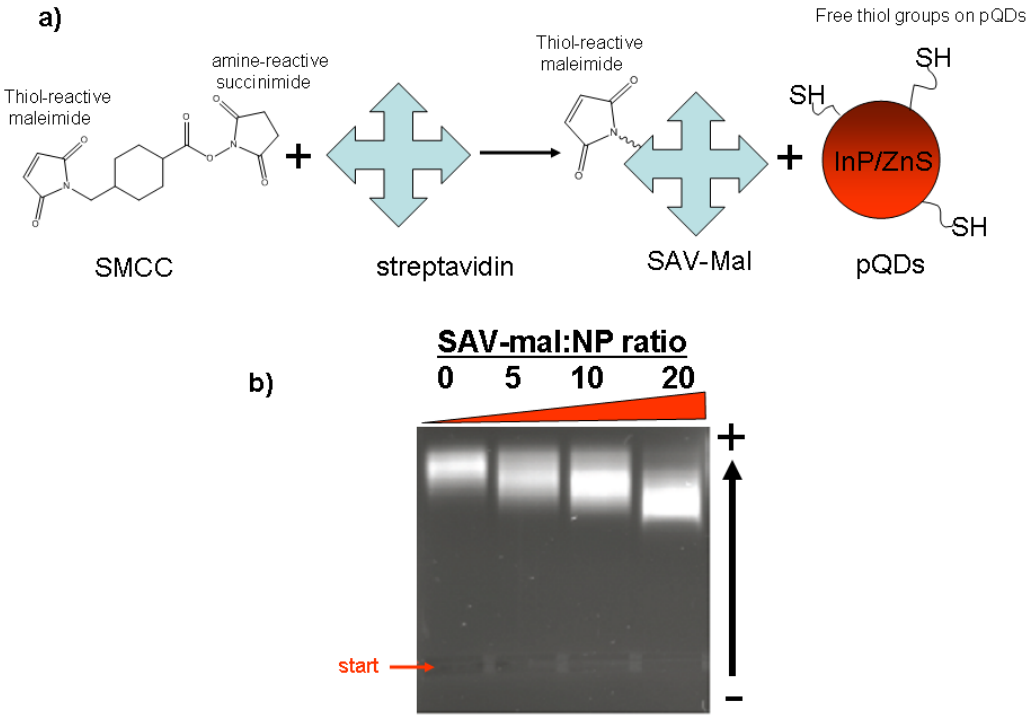

Figure 4.13: a) Scheme for the conjugation of the biomolecules to pQDs. Maleimide-activated streptavidin (SAV-mal) is formed by reaction of SMCC with streptavidin. In a second step, SAV-mal is covalently conjugated to the pQDs by reaction of free thiol groups in the cysteine residues. (b) Gel electrophoresis (GE) of pQDs conjugated to increasing amounts of SAV.

4.4.4 Step III: Electrophoretic separation

The ratio SAV-mal:pQDs is varied from 0 to 20 and the conjugates (InP/ZnS-SAV) migrate correspondingly to the different obtained stoichiometries in agarose gel (Fig. 4.14). InP/ZnS-SAV1 containing one SAV protein are isolated by cutting the gel. Size exclusion chromatography (SEC) is used to confirm the monofunctionality. The SEC was calibrated using a set of protein standards of known molecular weight and hydrodynamic diameter. For the 600 nm emitting InP/ZnS, the hydrodynamic diameters of the InP/ZnS pQDs and InP/ZnS-SAV1 are respectively 9.4 and 10.5 nm. Similarly for the 650 nm emitting QDs the diameters are 12.5 to 13.3 nm confirming the monofuntionality as well as the compact nature of the obtained conjugates.

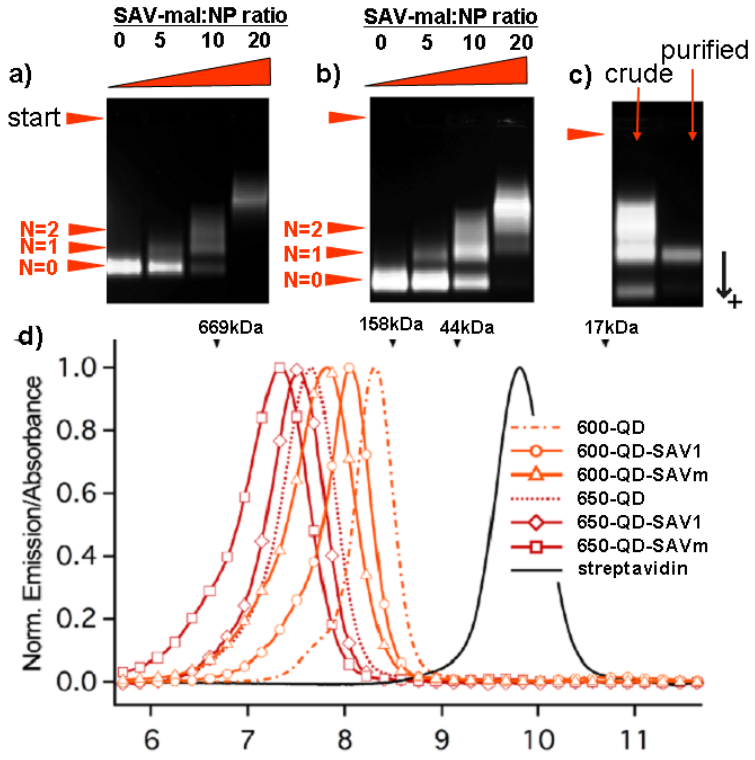

Figure 4.14: a) Gel electrophoresis (GE) of 650 nm emitting InP/ZnS pQDs conjugated to increasing amounts of SAV. Discrete bands represent pQDs with N=O, 1 or ≥2 copies of SAV. B) GE of 600 nm emitting InP/ZnS pQDs conjugated to increasing amounts of SAV c) GE of monofunctional, SAV-conjugated pQDs (InP/ZnS-SAV1) after their purification from the crude mixture. The monofunctional pQDs retain the N=1 position in the gel, indicating good stability of the isolated conjugate. d) Size exclusion chromatography (SEC) of streptavidin (SAV) (elution at 9.8 ml, D_h=4.8 nm), 600 nm emitting monofunctional InP/ZnS SAV1 (8.1 ml, 10.5 nm), multifunctional InP/ZnS-SAV (7.8 ml, 11.7 nm), 650 nm emitting InP/ZnS-SAV1 (7.5 ml, 13.3 nm) and InP/ZnS-SAVm (7.3 ml, 14.5 nm)

4.4.5 Conclusion

This section demonstrates that by employing a simple concept that nanoparticles coated with different stoichiometries of high molecular weight molecules such as streptavidin, monofunctionalised InP/ZnS NCs can be prepared. These monofunctional NCs with compact size and controlled number of active sites have potential application in various biological imaging experiments, including single molecule imaging.

4.5 Experimental

4.5.1 MTT assay

4.5.1.1 Preparation of 3-(4, 5-dimethylthiazol-2-yl)-2, 5-diphenyl-tetrazolium bromide (MTT) stock solution

The 12 mM MTT stock solution was prepared by a standard procedure. 5 mg of MTT was dissolved in sterile PBS (pH 7.4) by sonication and then the clear solution is stored at 4^{o}C in dark.

4.5.1.2 Cell viability

Primary cultures of Chinese hamster ovary (CHO) cells were seeded into 96 well micro for 24h. The next day, the culture with CHO cell density of approximately 60000 cells/well were incubated for 24 hrs at 37°C with 100 µL of 1 µM QDs, 5 µM QDs and 0.1% (w/v) saponin. Control wells containing cell culture medium with cells, without QDs addition, were included in each experiment. The medium in the well is removed and replaced with 100 µL of fresh culture medium. 10 µL of stock solution of 3-(4, 5-dimethylthiazol-2-yl)-2, 5-diphenyl-tetrazolium bromide (MTT) was added to each well and incubated for 4 hours. The formed formazan crystals were dissolved by adding 50 µL of DMSO to each well and the optical density of the colored solution was measured at 540 nm using a microplate reader (Biotek ELx- 800, Mandel Scientific Inc.) for quantification of the living cells

4.5.2 Functionalisation of penicillamine capped InP/ZnS NCs with Maurocalcine

300 µL (0.5µM) of QDs in distilled water are mixed with 2 mg of MCa in 400 µL of borate buffer. pH is adjusted to ~9 by addition of NaOH. The mixture is allowed to incubate for 12h at room temperature. The sample is then thoroughly been purified with centrifugal filters from VWR (MWCO 50kDa) *via* centrifugation at 2,800 g (2 times) for 4 minutes.

4.5.3 Cell penetration experiment

200 μL (5 μM) of the MCa-functionalized quantum dots and penicillamine capped InP/ZnS NCs were used for incubation with CHO cells (120000 cells/well) in culture (2 hrs). After two hours the cells were washed with 1X PBS for 3 time and the cells were imaged using a confocal microscope.

4.5.4 Biodistribution of InP/ZnS NCs in mice

Two healthy mice (female swiss nu/nu, 2 months old) were anesthetized and each was injected intravenously with 100 μL of 12 mM penicillamine capped InP/ZnS NCs (emission: 730 nm) in 1 X PBS (pH 7.4). The injected mice were placed on a warm chamber (37.5 °C) connected to an anesthesia mask (isoflurane/air 1.5%) and imaged with a Xenogen IVIS Lumma at 5 minutes, 1 hour, 3 hours and 24 hours. The software used to drive the set up was Living Image® 3.0. For the mouse imaging excitation wavelength of 640 nm was used with exposure time set at 10 ms. After 24 hours the mice were sacrificed and the organs were imaged under the same condition, except the exposure time was set at 200 ms. All the animal experiments were performed in agreement with the EEC guidelines and the "Principles of Laboratory Animal Care" (NIH publication no. 86-23, revised 1985). Semiquantitative data for the biodistribution was obtained using imageJ software from the fluorescence images by drawing regions of interest (ROI) on the area to be quantified. For calculations, the lower and upper intensities were set at 250 and 14000 counts respectively.

4.5.5 Functionalisation of InP/ZnS NCs with Gd-complex

QD dispersions (0.5 mL, 5.2 x 10^{-6}M), Gd-2(0.247 mL, 2.1 x 10^{-3}M) and TCEP (0.046 mL, 0.5 M) in degassed water, is combined and the pH adjusted to 9 by adding NaOH (0.5 M). The mixture is shaken at 800 rpm overnight at room temperature. 200 μL of the QDs in water are centrifuged in a Millipore centrifugal filter from VWR (MWCO 30k) at 11,200 g for 2 min. 200 μL of 1X PBS buffer (pH 7.4) or MilliQ water are added to the pellet and

the QDs are redispersed in 200 µL of 1X PBS buffer or MilliQ water (pH ~7) and stored in a fridge (~4°C).

4.5.6 *In vivo* MRI studies

MRI experiments were performed in collaboration with Cathy Poillot and Michael Dewaard at Neurosciences institute. All the experiments were conducted in agreement with the "Principles of Laboratory Animal Care" (NIH publication no. 86-23, revised 1985). The guidelines of the French Ministry of Agriculture (87/848) and of the European community (86/609/EEC) were also respected. The protocol was submitted for approval to the local Neuroscience institute committee to minimize animal suffering and abusive use of animal numbers. OFA 7 week-old rats were anesthesized by 5% isoflurane inhalation in a mixture air/O2 30%, and maintained in anaesthesia in 2% isoflurane. Rats were then injected with 10 µM of 1 mM Dotarem or GD-3 or GD-1 in the striatum using a stereotaxic frame (coordinates: 0 mm frontal, 3.5 mm lateral, and 5.5 mm in depth) and at a rate of 2mL/min. T1 images of the rat brain were acquired 15 min after striatum injection and after placing the rats in a 7T magnet (Bruker BioSpec 70/20 USR AVIII). Sequences of 16 images of slice depths of 1 mm each over a period of 15 min were taken. This sequence was repeated over 4 hrs period, thus leading to the total acquisition of 16 sets of 16 images. The temperature was maintained at 37°C throughout the experiments.

4.5.7 Monofunctionalisation of InP/ZnS NCs

4.5.7.1 Synthesis of peptide coated NPs

Method 1

200 µL of the 1 mg/mL QD stock solution in toluene is heated to remove the solvent and redispersed in 450 µL of pyridine. Separately, 4 mg of the peptides (New England peptides) were dissolved in 50 µL of dimethyl sulfoxide (DMSO) at the ratio 60% Nterm-KGSESGGSESGFCCFCCFCCF-Cterm and 40% Nterm-PEG_{12}-FCCFCCFCCF-Cterm. Peptides and QDs solutions are mixed and 10 mL of tetramethyl ammonium hydroxide (TMAH, 25% w/v in methanol) was added (pH ~11). The solution immediately becomes

turbid and the QDs precipitate. Following centrifugation, the supernatant is discarded and the resulting peptide coated QDs are redissolved in 50 μL of distilled water.

Method 2

InP/ZnS NCs, phase transferred with 11-mercaptoundecanoic acid (cf. chapter III), were purified by the centrifugation method over 10 kD filter (2800 g). ~1 mg/ml stock solution of MUA capped InP/ZnS NCs was prepared. Separately, 4 mg of peptides (New England peptides) were dissolved in 300 μL in water at the ratio 60% Nterm-KGSESGGSESGFCCFCCFCCF-Cterm and 40% Nterm-PEG_{12}-FCCFCCFCCF-Cterm at pH 11. The peptides are added to the QDs solution and incubated at room temperature for 48 hours. The quantum dots are purified using centrifugal filters from VWR (MWCO 30k) at 10,000 rpm for 2 minutes (two times).

4.5.7.2 Monofuntionalisation of peptide coated NPs with streptavidin

Maleimide-activated SAV (SAV-mal) was prepared by adding a four fold excess of succinimidyl 4-(N-maleimidomethyl) cyclohexane-1-carboxylate (SMCC) to 20 mM of streptavidin in HEPES buffered saline (HBS, 20 mM HEPES, 50 mM NaCl, pH 7.2) and then incubating for 30 minutes at RT. Next, SAV-mal is added to the InP/ZnS NCs coated with peptide (pQDs, section: 4.5.6.1) at the molar ratio of 5, 10 and 20 and incubated for further 30 minutes at RT (Concentrations: 1mM for pQDs and 10 mM of SAV-mal). Gel electrophoresis was employed to separate the pQDs conjugated with different stoichiometries of the SAV.

4.6 References

1. Jennings, L.E. and N.J. Long, *'Two is better than one'-probes for dual-modality molecular imaging.* Chemical Communications, 2009(24): p. 3511-3524.
2. Zanchet, D., C.M. Micheel, W.J. Parak, D. Gerion, and A.P. Alivisatos, *Electrophoretic Isolation of Discrete Au Nanocrystal/DNA Conjugates.* Nano Letters, 2000. **1**(1): p. 32-35.
3. Howarth, M., W. Liu, S. Puthenveetil, Y. Zheng, L.F. Marshall, M.M. Schmidt, K.D. Wittrup, M.G. Bawendi, and A.Y. Ting, *Monovalent, reduced-size quantum dots for imaging receptors on living cells.* Nature Method, 2008. **5**(5): p. 397-399.
4. Clarke, S., F. Pinaud, O. Beutel, C. You, J. Piehler, and M. Dahan, *Covalent Monofunctionalization of Peptide-Coated Quantum Dots for Single-Molecule Assays.* Nano Letters. **10**(6): p. 2147-2154.
5. Brevig, T., U. Kruhne, R. Kahn, T. Ahl, M. Beyer, and L. Pedersen, *Hydrodynamic guiding for addressing subsets of immobilized cells and molecules in microfluidic systems.* BMC Biotechnology, 2003. **3**(1): p. 10.
6. Zorko, M. and Ü. Langel, *Cell-penetrating peptides: mechanism and kinetics of cargo delivery.* Advanced Drug Delivery Reviews, 2005. **57**(4): p. 529-545.
7. Medintz, I.L., T. Pons, J.B. Delehanty, K. Susumu, F.M. Brunel, P.E. Dawson, and H. Mattoussi, *Intracellular Delivery of Quantum Dot-Protein Cargos Mediated by Cell Penetrating Peptides.* Bioconjugate Chemistry, 2008. **19**(9): p. 1785-1795.
8. Emerich, D.F. and C.G. Thanos, *The pinpoint promise of nanoparticle-based drug delivery and molecular diagnosis.* Biomolecular Engineering, 2006. **23**(4): p. 171-184.
9. Estève, E., K. Mabrouk, A. Dupuis, S. Smida-Rezgui, X. Altafaj, D. Grunwald, J.-C. Platel, N. Andreotti, I. Marty, J.-M. Sabatier, M. Ronjat, and M. De Waard, *Transduction of the Scorpion Toxin Maurocalcine into Cells.* Journal of Biological Chemistry, 2005. **280**(13): p. 12833-12839.
10. Boisseau, S., K. Mabrouk, N. Ram, N. Garmy, V. Collin, A. Tadmouri, M. Mikati, J.-M. Sabatier, M. Ronjat, J. Fantini, and M. De Waard, *Cell penetration properties of maurocalcine, a natural venom peptide active on the intracellular ryanodine receptor.* Biochimica et Biophysica Acta (BBA) - Biomembranes, 2006. **1758**(3): p. 308-319.
11. Derossi, D., A.H. Joliot, G. Chassaing, and A. Prochiantz, *The third helix of the Antennapedia homeodomain translocates through biological membranes.* Journal of Biological Chemistry, 1994. **269**(14): p. 10444-10450.
12. Leifert, J.A. and J.L. Whitton, *"Translocatory proteins" and "protein transduction domains": A critical analysis of their biological effects and the underlying mechanisms.* Molecular Therapy, 2003. **8**(1): p. 13-20.
13. Patel, L., J. Zaro, and W.-C. Shen, *Cell Penetrating Peptides: Intracellular Pathways and Pharmaceutical Perspectives.* Pharmaceutical Research, 2007. **24**(11): p. 1977-1992.
14. Cathy Poillot, K.D., Hicham Bichraoui, Julien Pêcher, Sebastien Alphonse, Badreddine Douzi, Michel Ronjat, Hervé Darbon and Michel De Waard,, *d-Maurocalcine, a Pharmacologically Inert Efficient Cell-penetrating Peptide* Journal of Biological Chemistry, 2010 **285**: p. 34168-34180.
15. Vivès, E., P. Brodin, and B. Lebleu, *A Truncated HIV-1 Tat Protein Basic Domain Rapidly Translocates through the Plasma Membrane and Accumulates in the Cell Nucleus.* Journal of Biological Chemistry, 1997. **272**(25): p. 16010-16017.

16. Jaiswal, J.K., H. Mattoussi, J.M. Mauro, and S.M. Simon, *Long-term multiple color imaging of live cells using quantum dot bioconjugates.* Nature Biotechnology, 2003. **21**(1): p. 47-51.
17. Park, J., J. Nam, N. Won, H. Jin, S. Jung, S. Jung, S.-H. Cho, and S. Kim, *Compact and Stable Quantum Dots with Positive, Negative, or Zwitterionic Surface: Specific Cell Interactions and Non-Specific Adsorptions by the Surface Charges.* Advanced Functional Materials. **21**(9): p. 1558-1566.
18. Ballou, B., B.C. Lagerholm, L.A. Ernst, M.P. Bruchez, and A.S. Waggoner, *Noninvasive Imaging of Quantum Dots in Mice.* Bioconjugate Chemistry, 2003. **15**(1): p. 79-86.
19. Soo Choi, H., W. Liu, P. Misra, E. Tanaka, J.P. Zimmer, B. Itty Ipe, M.G. Bawendi, and J.V. Frangioni, *Renal clearance of quantum dots.* Nature Biotechnology, 2007. **25**(10): p. 1165-1170.
20. Li, L., T.J. Daou, I. Texier, T.T. Kim Chi, N.Q. Liem, and P. Reiss, *Highly Luminescent CuInS2/ZnS Core/Shell Nanocrystals: Cadmium-Free Quantum Dots for In Vivo Imaging.* Chemistry of Materials, 2009. **21**(12): p. 2422-2429.
21. Khlebtsov, N. and L. Dykman, *Biodistribution and toxicity of engineered gold nanoparticles: a review of in vitro and in vivo studies.* Chemical Society reviews. **40**(3): p. 1647-71.
22. Tu, C., X. Ma, A. House, S.M. Kauzlarich, and A.Y. Louie, *PET Imaging and Biodistribution of Silicon Quantum Dots in Mice.* ACS Medicinal Chemistry Letters. **2**(4): p. 285-288.
23. Fischer, H.C., L. Liu, K.S. Pang, and W.C.W. Chan, *Pharmacokinetics of Nanoscale Quantum Dots: In Vivo Distribution, Sequestration, and Clearance in the Rat.* Advanced Functional Materials, 2006. **16**(10): p. 1299-1305.
24. Breus, V.V., C.D. Heyes, K. Tron, and G.U. Nienhaus, *Zwitterionic Biocompatible Quantum Dots for Wide pH Stability and Weak Nonspecific Binding to Cells.* ACS Nano, 2009. **3**(9): p. 2573-2580.
25. Liu, W., H.S. Choi, J.P. Zimmer, E. Tanaka, J.V. Frangioni, and M. Bawendi, *Compact Cysteine-Coated CdSe(ZnCdS) Quantum Dots for in Vivo Applications.* Journal of the American Chemical Society, 2007. **129**(47): p. 14530-14531.
26. Smith, A.M., H. Duan, A.M. Mohs, and S. Nie, *Bioconjugated quantum dots for in vivo molecular and cellular imaging.* Advanced Drug Delivery Reviews, 2008. **60**(11): p. 1226-1240.
27. Daou, T.J., L. Li, P. Reiss, V.r. Josserand, and I. Texier, *Effect of Poly(ethylene glycol) Length on the in Vivo Behavior of Coated Quantum Dots.* Langmuir, 2009. **25**(5): p. 3040-3044.
28. Choi, H.S., W. Liu, P. Misra, E. Tanaka, J.P. Zimmer, B.I. Ipe, M.G. Bawendi, and J.V. Frangioni, *Renal clearance of quantum dots.* Nature Biotechnology, 2007. **25**(10): p. 1165-1170.
29. Caravan, P., J.J. Ellison, T.J. McMurry, and R.B. Lauffer, *Gadolinium(III) Chelates as MRI Contrast Agents: Structure, Dynamics, and Applications.* Chemical Reviews, 1999. **99**(9): p. 2293-2352.
30. Nonat, A., C. Gateau, P.H. Fries, and M. Mazzanti, *Lanthanide Complexes of a Picolinate Ligand Derived from 1,4,7-Triazacyclononane with Potential Application in Magnetic Resonance Imaging and Time-Resolved Luminescence Imaging.* Chemistry – A European Journal, 2006. **12**(27): p. 7133-7150.
31. Dahan, M., S. Lévi, C. Luccardini, P. Rostaing, B.a. Riveau, and A. Triller, *Diffusion Dynamics of Glycine Receptors Revealed by Single-Quantum Dot Tracking.* Science, 2003. **302**(5644): p. 442-445.

32. Sperling, R.A., T. Pellegrino, J.K. Li, W.H. Chang, and W.J. Parak, *Electrophoretic Separation of Nanoparticles with a Discrete Number of Functional Groups.* Advanced Functional Materials, 2006. **16**(7): p. 943-948.
33. Pinaud, F., D. King, H.-P. Moore, and S. Weiss, *Bioactivation and Cell Targeting of Semiconductor CdSe/ZnS Nanocrystals with Phytochelatin-Related Peptides.* Journal of the American Chemical Society, 2004. **126**(19): p. 6115-6123.

General conclusion

We presented a method of producing near infrared (NIR) emitting InP/ZnS core/shell NCs for biological imaging. Using phosphine gas as a precursor and controlling the reaction parameters such as temperature and the amount of precursor larger sized InP NCs (> 4 nm) with photoluminescence in the NIR region (720-750 nm) can be reproducibly synthesized. In addition, as phosphine gas generation involves relatively less expensive precursors such as Zn_2P_3 (rodenticide) and sulfuric acid, this synthetic scheme is more economical than existing routes involving $P(TMS)_3$. The fluorescence quantum yield of these NIR emitting InP NCs (<1 %) could be increased up to 18% by overcoating them with 1-2 monolayers of ZnS shell. Moreover, absence of the toxic elements such as Cd, As, Hg, Se etc. make these InP/ZnS NCs highly attractive for biological imaging applications.

Phase transfer of InP/ZnS NCs to aqueous medium was studied with various thiol groups containing ligand. The deprotonation of the thiol function by an appropriate adjustment of the pH of the aqueous phase to slightly basic values is important to obtain strong binding of the ligand molecules to the NCs' surface. Cysteine and penicillamine capped NCs prepared using this approach were stable for several weeks in water or buffer solution. They combine a low hydrodynamic diameter (<10nm) and low non-specific binding in biological environment due to their zwitterionic coating. The developed strategy can be applied for a large variety of QDs and NPs whose surface atoms have an affinity for thiolates. Strong fluorescence quenching was observed in the case of cysteine capped InP/ZnS NCs which is attributed to the formation of cysteine dimer, cystine. The problem has been addressed by either using the reducing agent TCEP during the transfer reaction or by substituting the molecule penicillamine which is more resistant to oxidation. NIR emitting InP/ZnS NCs coated with penicillamine in 1X PBS buffer (pH 7.4) show low cytotoxicity for CHO cells with a cell viability of over 90% for a concentration of 20 nmol per 10^6 cells and about 80% at QD/cells concentration of 100 nmol per 10^6. Due to high affinity of the ZnS surface for thiolated ions, these QDs could be further functionalized with maurocalcine, a cell penetrating peptide containing terminal cysteine group. The InP/ZnS NCs attached to the MCa show excellent cell penetration behavior in CHO cells in direct contrast to pencillamine capped InP/ZnS NCS. The NIR emitting properties of penicillamine capped InP/ZnS NCs were exploited by injecting in mice intravenously and following their biodistribution using fluorescence imaging. These QDs can be potentially used as fluorescence probes for sensitive, multiplexed detection of surface markers on tumour cells. A gadolinium picolinate bearing a dithiol group were grafted on to the InP/ZnS NCs surface, creating a dual mode

contrast agent with high rexalivity (r_1=900 $mM^{-1}s^{-1}$ per QD) and photoluminescent properties. MRI studies performed on rat brains showed a significantly increased in retention time, allowing for a non-invasive and prolonged monitoring of the area of interest. Finally, it was demonstrated that the number of protein molecules grafted on the QDs can be controlled by employing a simple concept that nanoparticles coated with different stoichiometries of high molecular weight molecules such as streptavidin. These monofunctional NCs with compact size and controlled number of active sites have potential application in various biological imaging experiments, including single molecule imaging.

ANNEXE : Instruments and techniques

A.1 Ultraviolet-visible (UV-Vis) spectroscopy

UV-Vis spectroscopy was performed on a HP 8452A spectrophotometer. It is a single beam spectrophotometer operating in the wavelength range 190-820 nm using a diode array for detection. The background run and the sample acquisition are performed in series on the same cuvette holder. In the absorption spectra absorbance (dimensionless) is plotted against wavelength (nm). UV-visible ChemStation has been used as operating software. For all the measurements, a quartz cuvette of 1 cm width has been used. UV-Vis spectroscopy forms the basis of quantum dot characterisation because the fundamental aspect of fluorescence is the absorption of photons. They have characteristic absorption onset called excitonic peak. The position of this peak depends on the band gap of the material and thus the size of the NCs.

The change of intensity of light passing through a sample can be expressed in terms of optical density or absorbance *(A)* as follows:

$$A=log_{10}(I_o/I) \qquad \text{E-A1}$$

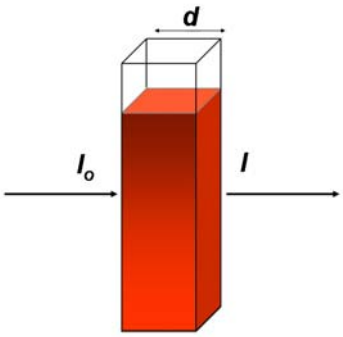

Figure A.1. Absorption of light

where I_0 is the intensity of the light at a given wavelength λ before it enters the sample and I is the intensity of light that has passed through a sample (transmitted intensity). By applying Lambert-Beer's law concentration of the absorbing species in the solution can be quantitatively determined as follows:

$$c = \frac{A}{\varepsilon \times l} \qquad \text{E-A2}$$

where ε is molar extinction coefficient and ε is the path length (cm) of the sample (cuvette)

For colloidal semiconductor NCs the molar extinction coefficient in the equation A.2 is a size dependent variable. For example, the ε of InP quantum dots is given by

$$\varepsilon = 3046.1(D)^3 - 76532(D)^2 + (5.5137 \times 10^5)(D) - (8.9839 \times 10^5) \qquad \text{E-A3}$$

where D is the diameter (nm) of the NCs. D can be obtained either directly from TEM micrographs or by measuring the first excitonic peak in the UV-VIS spectrum. The relation between the first excitonic peak and the diameter is given by the equation A4 [1]

$$D = (-3.7707 \times 10^{-12})\lambda^5 + (1.0262 \times 10^{-8})\lambda^4 - (1.0781 \times 10^{-5})\lambda^3 + (5.4550 \times 10^{-3})\lambda^2 - (1.3122 \times 10^{-12})\lambda +$$

A.2 Photoluminescence (PL) spectroscopy

Fluorescence spectra were obtained on a F-4500 spectrofluorometer **(**Hitachi**)** with a quartz cell of 1 cm by dispersing quantum dots in suitable solution. Except otherwise noted, all the measurements were performed with Instrument Parameters:

Parameters	**Set**
Scan mode:	Emission
Data mode:	Fluorescence
Scan speed:	1200 nm/min
Delay:	0 s
EX Slit:	5.0 nm
EM Slit:	5.0 nm
PMT Voltage:	700 V
Response:	2.0 s

Table A.1 Instrument parameters used for PL spectroscopy

The excitation wavelengths used for the measurements have been mentioned in the legend of the spectra. The light absorbed by quantum dots is emitted within a few nanoseconds (10-30 ns) at a lower energy (higher wavelength). Monochromatic light of certain wavelength is passed through the sample. As the proportion of the incident light is absorbed by the sample, the light of higher wavelength is emitted. This fluorescent light then passes through a monochromator and reaches a detector, which is usually placed at 90° to the incident light

beam to minimize the risk of transmitted incident light reaching the detector. The intensity vs. wavelength plot obtained is referred to as the PL emission spectrum.

A3 Quantum yield calculation

The fluorescence quantum yield (QY) is the ratio of the number of photons emitted to the number absorbed.

$$QY = \frac{photons_{em}}{photons_{abs}} \qquad \text{E-A.4}$$

One way to determine the relative quantum yield of an unknown sample (QY_S) is by comparing the integrated photoluminescence of the sample with that of a standard dye of known quantum yield (QY_R) using the equation:

$$QY_S = QY_R \times \frac{I_S \times A_R \times {n_S}^2}{I_R \times A_S \times {n_R}^2} \qquad \text{E-A.5}$$

Where *I is* the integrated PL intensity, n is the refractive index, and *A* is the absorbance.

The above equation can be written a follows

$$QY_S = QY_R \times \frac{\frac{I_S}{A_S}}{\frac{I_R}{A_R}} \times \frac{{n_S}^2}{{n_S}^2} \qquad \text{E-A.6}$$

If we take the multiple measurements and obtain the gradient of I vs. A. Then above equation E-A.6 can be written as

$$QY_S = QY_R \times \frac{Gradient_S}{Gradient_R} \times \frac{{n_S}^2}{{n_S}^2} \qquad \text{E-A.7}$$

Using equation E-A.7, the QY of the obtained InP//ZnS NCs were determined by comparing with Rhodamine 6G in ethanol (QY = 95%). Both the sample and the reference were excited at 480 nm and the room temperature solvent refractive indices of hexane (1.36), water (1.33) and ethanol (1.375) were taken into consideration. We plotted the integrated fluorescence intensity vs. optical density (see example in Figure A.2) and compared the slopes of the linear fit for the sample and the standard.

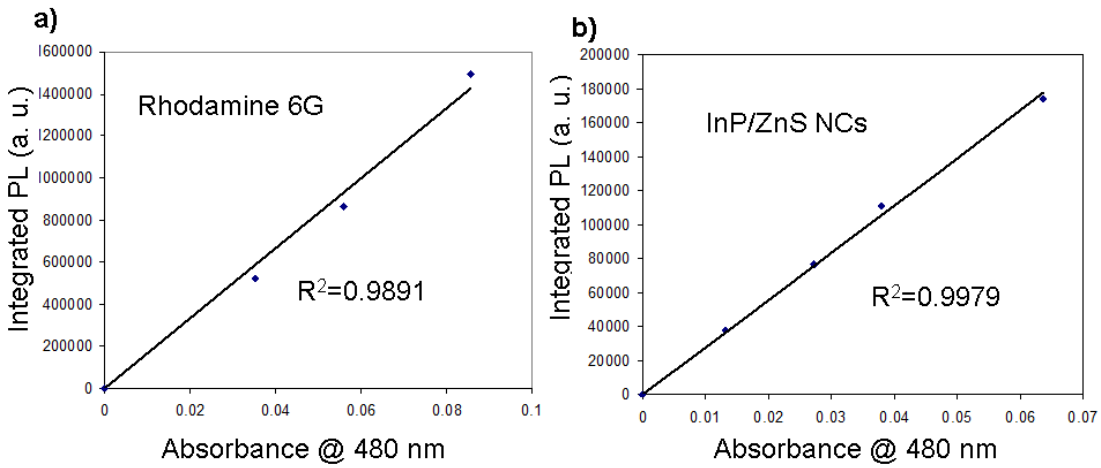

Fig. A.2 a) Integrated PL vs. absorbance plot for a) Rhodamine 6G (QY=95 %) and b) InP/ZnS NCs (calculated QY=18%)

A4 X-ray diffraction (XRD)

Powder X-ray diffraction was carried out using Philips X'Pert diffractometer with z Co source (λ = 1.789 Å, 50 kV/35 mA). Disoriented silicon was used as the substrate for the measurements. Rietveld refinement was performed on X'pert highscore software operated in semi-automatic mode. The fit had the following agreement indices:

R expected	3.21573
R profile	6.0679
Weight R profile	6.85054
D-statistics	0.48079
Goodness of fit	4.53817

The crystallite size calculated using Scherrer's equation

$$D = \frac{K\lambda}{B\cos\theta} \qquad \text{E-A.7}$$

where K is the shape factor, λ is the wavelength of the X-ray, B is the full width at half maximum (FWHM) in radians, and θ is the Bragg angle. For our calculation, we use the shape factor of 1.1 which is a theoretical value for a perfect sphere [2]. The Scherrer formula

provides a lower bound on the crystallite size due to contribution of other factors (e.g. inhomogeneous strain and instrumental effects) to the width of a diffraction peak besides crystallite size.

A.5 Transmission electron microscopy (TEM)

TEM measurements were performed with JEOL 4000EX electron microscopy operated at 400 kV. The samples were thoroughly purified prior to drop casting onto a Cu grid. Size distribution was analyzed using imageJ software.

A.6 Energy dispersive X-ray spectroscopy (EDX)

EDX experiments were performed on a JOEL JSM-840A scanning electron microscope (SEM) equipped with an Oxford Instrument energy dispersive X-ray (EDX) analyzer. The instrument was operated at 20 KeV. For sample preparation, a highly concentrated colloidal solution (~10^{-2} M) of colloidal NCs in chloroform was obtained. The solution was drop cast on a conducting silicon wafer. For better signal, thick (at least 0.5 mm) deposits were made on the wafer. Multiple runs (>10) were performed at various positions of the grid and the data are expressed as mean value with standard deviations. In EDX spectroscopy a sample is bombarded with a high-energy beam of charged particles such as electrons or protons or X-rays. These charged particles may eject an electron from the inner shell of a sample atom such as K, L, M creating an electron hole. An electron from any of the outer shell then fills the hole, releasing an energy corresponding to the differences between the two shells. In EDX this energy released is detected. As the energy difference between the electronic shell of the materials is characteristic for the nature of the atoms and hence the element. Thus, the presence of different elements in the sample can be detected quantitatively.

A.7 Dynamic light scattering (DLS)

Dynamic light scattering (DLS) is a technique for measuring what is known as hydrodynamic diameter of particles usually in colloidal suspension. It is based on the Brownian motion of colloidal particles in solution and calculated from the translational diffusion coefficient using Stokes-Einstein equation:

$$D_h = \frac{kT}{3\pi\eta D} \qquad \text{E-A.8}$$

Where

k = Boltzmann constant

T = absolute temperature

η =viscosity

D = translational diffusion coefficient

The hydrodynamic diameter is always bigger than the particle size measured by TEM or other similar techniques due to the contribution of the surrounding molecules or ions in the translational motion of the particles in a liquid. Further in the case of quantum dots, the presence of capping ligands contributes to the slowing of the Brownian motion significantly and hence the increase in hydrodynamic diameter. The latter can be measured as intensity distribution, volume distribution, number distribution or sometimes also expressed in mass distribution. Unfortunately, the obtained values differ significantly from one method to another, especially intensity distribution gives larger hydrodynamic diameter than the others as scattering intensity is proportional to $(D_h)^6$ and the size obtained is more weighed towards larger sized particles. However, for comparing size with microscopy techniques such as TEM, the number distribution is recommended [3]. The hydrodynamic diameter of the water-soluble NCs dispersed in water was measured by dynamic light scattering (DLS), using a Malvern Zeta Sizer (NanoZS). The samples have been thoroughly purified with centrifugal filters from VWR (MWCO 30k) and dispersed in MilliQ water (18 mΩ) prior to the measurements. Given the sensitivity of the instrument, multiple runs (> 3) were performed to avoid erroneous results. The spectra have been corrected by the instrument software for viscosity (0.882 mPa.s at 25°C), absorption (at 532 nm), solvent (water) refractive index (1.33) and material (InP) refractive index (3.1). The data is collected in automatic mode and is expressed in number-percent.

A.8 Nuclear magnetic resonance (NMR)

Proton and carbon NMR spectra were recorded on Brüker DPX200 instruments using standard Brüker software. The $1/T_1$ measurements were performed by Graeme Statiuk at CEA/INAC Grenoble on a Brucker Avance 200 spectrometer (200MHz). The NMRD profiles were measured at 298K in the range 0.1 and 35Mz, by using a Spinmaster FFC (fast field cycling) NMR relaxometer.

A.9 Circular dichroism

Chirality measurements were performed in Chirascan CD spectropolarimeter. Penicillamine capped InP/ZnS NCs were passed through Nap 5 size exclusion columns from GE-biosciences and dispersed in 1X PBS buffer prior to measurements.

A.10 Size exclusion chromatography

SEC of the peptide coated InP/ZnS QDs (pQDs) was performed by Samuel Clarke at LKB/ENS Paris on an Agilent 1200 series HPLC system with a TSKG4000SW colum (Tosoh Bioscience) and a mobile phase of borate buffer (10 mM borate, 50 mM NaCL, pH 7.5). (Flow rate: 0.5 mL/min). Following injection of 20 mL of sample, the absorption and fluorescence were detected online during the elusion. The hydrodynamic diameter (D_h) of the pNPs was determined from their peak elution volume and comparison with a standard curve, which was obtainedfrom a set of protein standards (Biorad) of known molecular weight and D_h: thyroglobulin (669 kDa, 17 nm), gammaglobulin (158 kDa, 11 nm), ovalbumin (44 kDa, 55 nm), myoglobin (17 kDa, 3.8 nm) and vitamin B-12 (1.4 kDa, 1.5 nm)

A.11 Gel electrophoresis (GE)

GE was performed on 1% agarose (sigma) gels in 0.25X TAE buffer (10mM Tris, 10 mM acetate, 0.25 μM EDTA, pH 8.3), 25 μL of pNPs (and pNPs conjugated with SAVs) were mixed with 2 % glycerol and then loaded into the wells of the gel. 10 V cm^{-1} electric field was applied for 30 minutes. The band was extracted using a razor and loaded into a 0.2 μm centrifugation filter (Pall). After centrifugation at 5000 g for 5 minutes, the pure QDs were eluted with 0.25 TAE and stirred at 4°C.

1. Reiss, P., M. Protière, and L. Li, *Core/Shell Semiconductor Nanocrystals.* Small, 2009. **5**(2): p. 154-168.
2. Patterson, A.L., *The Diffraction of X-Rays by Small Crystalline Particles.* Physical Review, 1939. **56**(10): p. 972.
3. Nobbmann, U. and A. Morfesis, *Light scattering and nanoparticles.* Materials Today, 2009. **12**(5): p. 52-54.

Abbreviations

CD: circular dichroism

CHO: Chinese hamster ovary (cells)

CIS: copper indium sulphide

CPP: cell penetrating peptide

Cys: cysteine

D_h: hydrodynamic diameter

DHLA: dihydrolipoic acid

DMAP: 4-Dimethylaminopyridine

DMF: dimethylformamide DLS: dynamic light scattering

DMSO: dimethyl sulfoxide

DNA: Deoxyribonucleic acid

DOTA: 1,4,7,10-tetraazacyclododecane-N,N',N'',N'''-tetraacetic acid

DTT: dithiothreitol

EDCI: 1-ethyl-3-(3-dimethylaminopropyl) carbodiimide

EDX: energy dispersive X-ray spectroscopy

FTIR : Fourier transform infrared (spectroscopy)

FWHM: full width at half maximum

Gd-DOTA: 1,4,7,10-tetraazacyclododecane-N,N',N'',N'''-tetraacetic acid

HB: hepatobiliary processing

HDA: hexadecylamine

HAS: human serum albumin

^{1}H NMR: proton nuclear magnetic resonance

HOMO: highest occupied molecular orbital

InP: indium phosphide

kDa: kiloDalton

MA: myristic acid

MCa: maurocalcine

MPA: 3-mercaptopropanoic acid

MRI: magnetic resonance imaging

MTT: 3-(4, 5-dimethylthiazol-2-yl)-2, 5-diphenyl-tetrazolium bromide

MUA: 11-mercaptoundecanoic acid

NCs: nanocrystals

NHS: N-hydroxysuccinimide

NIR: near infrared

NMR: nuclear magnetic resonance

NMRD: nuclear magnetic resonance dispersion

NPs: nanoparticles

ODE : 1-octadecene

PBS : phosphate buffer saline

PEG: polyethylene glycol

Pen: penicillamine

PL : photoluminescence

$P(TMS)_3$: tris**(**trimethylsilyl)phosphine

pH : potentia hydrogenii

PEG : polyethylene glycol

QDs: quantum dots

QY : quantum yield

RES: reticulo-endothelial system

rpm: rotaion per minute

SAMs: self assembled monolayers

SAV: streptavidin

SEC: size exclusion chromatography

SMCC: 4-(N-maleimidomethyl) cyclohexane-1-carboxylate

TCEP : tris(2-carboxyethyl) phosphine hydrochloride

TEM : transmission electron microscopy

TGA : thioglycolic acid

TMAH: tetramethylammonium hydroxide

UV : ultra violet

UV-Vis : ultra violet-visible

XRD: X-ray diffraction

Title: Synthesis and functionalisation of near infrared emitting nanocrystals for biological imaging.

Summary

This thesis concerns the development of near infrared (NIR) emitting InP/ZnS core/shell nanocrystals for biological imaging. *In situ* generated phosphine gas was used as the phosphorous precursor, indium myristate as the In precursor and 1-Ocadecene as the solvent to produce InP NCs with emission in the range of 720-750 nm. Growth of 1-2 monolayers of a ZnS shell on the surface of the InP NCs strongly improves their quantum yield. Next, we studied the phase transfer of the obtained InP/ZnS NCs to aqueous medium with various thiol group containing ligands. Emphasis is put on the colloidal stability and the retention of fluorescence quantum efficiency during the transfer. Zwitterionic ligands such as pencillaime and cysteine have been studied in view of their biological interest in providing compact size and reduced non-specific interaction with cells.

The cytotoxicity of pencillamine capped InP/ZnS NCs has been evaluated in cell culture. The NIR emitting properties of the QDs have been exploited to their study bio-distribution in mice by fluorescence imaging. In addition, functionalisation of the InP/ZnS NCs with a cell penetrating peptide, with a MRI contrast agent (gadolinium complex) and with a controlled number of streptavidin molecules have been explored to demonstrate the large interest of InP/ZnS NCs in biology.

Key words: Indium phosphide, quantum dots, near infrared fluorescence imaging, phase transfer, surface functionalisation

Titre: Synthèse et fonctionnalisation de nanocristaux émettant dans le proche infrarouge pour l'imagerie biologique

Résumé :

Cette thèse concerne le développement de nanocristaux (NCs) cœur/coquille d'InP/ZnS émettant dans le proche infrarouge pour l'imagerie biologique. Dans la synthèse chimique des NCs cœur d'InP, nous avons utilisé la phosphine générée *in situ* comme précurseur de phosphore en combinaison avec le myristate d'indium comme précuseur d'indium et l'1-octadécène comme solvant. Les NCs obtenus sont hautement cristallins et présentent une fluorescence dans la gamme 720-750 nm, selon leur taille. La croissance d'une ou deux monocouches (coquille) de ZnS sur la surface des NCs d'InP a considérablement amélioré leur rendement quantique de fluorescence.

Nous avons de plus étudié le transfert de phase de ces NCs InP/ZnS du milieu organique au milieu aqueux en utilisant diverses molécules hydrophiles contenant un groupe thiol. En particulier, nous nous sommes intéressés au transfert de phase avec des molécules zwitterioniques tels que la penicillamine et la cystéine afin d'obtenir une taille hydrodynamique compacte, et de réduire les interactions non-spécifiques en milieu biologique. Dans l'étude du transfert de phase, l'accent a été mis sur la stabilité colloïdale des NCs et sur la préservation de leur efficacité de fluorescence en milieu aqueux.

La cytotoxicité des NCs InP/ZnS fonctionnalisés avec la pencillamine a été évaluée en culture cellulaire. Puis la bio-distribution de ces NCs a été étudiée dans des souris vivantes par imagerie de fluorescence grâce à leur émission dans le proche infrarouge. Pour finir, les fonctionnalisations de NCs InP/ZnS d'une part avec un peptide de pénétration cellulaire, d'autre part avec des agents de contraste IRM (complexes de gadolinium) et enfin avec un nombre contrôlé de molécules streptavidine ont été explorées, démontrant le grand intérêt de ces NCs pour l'imagerie biologique.

Mots clés: phosphure d'indium, boîtes quantiques, nanocristaux, imagerie biologique de fluorescence, infrarouge, transfert de phase, fonctionnalisation de surface